

**INVESTIGATION OF RHEOLOGICAL IMPLICATIONS OF THE
CRUSTAL REFLECTIVITY IN THE SEA OF MARMARA**

**PhD Thesis by
Arlhan ŞAPAŞ**

Department : Geophysical Engineering

Programme : Geophysical Engineering

FEBRUARY 2010

**INVESTIGATION OF RHEOLOGICAL IMPLICATIONS OF THE
CRUSTAL REFLECTIVITY IN THE SEA OF MARMARA**

**PhD Thesis by
Arlhan ŞAPAŞ
(505012086)**

**Date of submission : 23 July 2009
Date of defence examination: 03 February 2010**

**Supervisor (Chairman) : Prof. Dr. Aysun GÜNEY (İTU)
Members of the Examining Committee : Prof. Dr. Emin DEMİRBAĞ (İTU)
Prof. Dr. Bedri ALPAR (İU)
Prof. Dr. Ruhi Saatçılar (SU)
Prof. Dr. Aral Okay (İTU)**

FEBRUARY 2010

İSTANBUL TEKNİK ÜNİVERSİTESİ ★ FEN BİLİMLERİ ENSTİTÜSÜ

**MARMARA DENİZİ'NDE KABUĞA AİT YANSITILABİLİRLİĞİN
REOLOJİK ANLAMLARININ ARAŞTIRILMASI**

DOKTORA TEZİ
Aslihan ŞAPAŞ
(505012086)

Tezin Enstitüye Verildiği Tarih : 23 Temmuz 2009
Tezin Savunulduğu Tarih : 03 Şubat 2010

Tez Danışmanı : Prof. Dr. Aysun GÜNEY (İTÜ)
Diğer Jüri Üyeleri : Prof. Dr. Emin DEMİRBAĞ (İTÜ)
Prof. Dr. Bedri ALPAR (İÜ)
Prof. Dr. Ruhi Saatçılar (SÜ)
Prof. Dr. Aral Okay (İTÜ)

ŞUBAT 2010

FOREWORD

This Ph.D. thesis is supported by İstanbul Technical University, Institute of Science and Technology post-graduate theses support project (project number:2044). I would like to thank Institute of Science and Technology for financial support for the thesis.

I would like to thank Vehbi Koç Foundation for awarding me with grant in 2005-2006 academic year.

I would like to thank TUBITAK-Marmara Research Center for providing multi-channel deep seismic reflection data from SEISMARMARA 2001 project. I also thank to KOERI-NEMC and IRIS for providing earthquake data for SKS splitting analysis.

I am grateful to Prof. Dr. Paul Silver, Prof. Dr. Marian Ivan and Dr. Nick Teanby for providing splitting analysis software and help during using the softwares.

I would like to express my appreciation and thanks for my advisor Prof. Dr. Aysun Güney for her support.

I would like to thank my Ph.D. thesis committee and Ph.D. thesis examination members; Prof. Dr. Emin Demirbağ, Prof Dr Bedri Alpar, Prof. Dr. Ruhi Saatçılar and Prof.Dr. Aral Okay for their review and helpful contributions to my thesis.

I am grateful to Dr. Onur Tan, Dr. Seda Yolsal, Ahmet Ökeler and Assist. Prof. Dr. Turgay İşseven for their friendship and help, Assist. Prof. Dr. Neslihan Ocakoğlu Gökaşan, Assist. Prof. Dr. Caner İmren and Assoc. Prof. Dr. Hülya Kurt for fruitful discussions and all department members for support through my education.

I would like to thank and express my deep appreciation to my parents, my sister and my brother for their intengible and material support, endless patience and inspiration during the study and every step of my life.

I would like to thank to my collique and husband for his patience, encouragement, and never ending help in every aspect since the beginning of my education at İTÜ.

February 2010

Aslıhan ŞAPAŞ
Geophysical Engineer, M.Sc.

TABLE OF CONTENTS

	<u>Page</u>
FOREWORD.....	v
TABLE OF CONTENTS.....	viix
ABBREVIATIONS	ixx
LIST OF TABLES	xi
LIST OF FIGURES	xiii
SUMMARY	xvii
ÖZET.....	xxi
1. INTRODUCTION.....	1
1.1 Velocity-Depth Models of the Sea of Marmara	4
1.2 Gravity and Magnetic Studies in the Sea of Marmara	6
1.3 Heat Flow Studies in the Sea of Marmara.....	9
1.4 Seismicity of the Sea of Marmara	13
1.5 GPS Measurements in the Sea of Marmara.....	17
1.6 Electrical Conductivity Studies around the Sea of Marmara	18
2. TECTONICS OF THE SEA OF MARMARA.... Error! Bookmark not defined.1	Error! Bookmark not defined.1
2.1 The North Anatolian Fault in the Sea of Marmara.....	Error! Bookmark not defined.1
2.2 Deep Basins in the Sea of Marmara	30
2.2.1 The Çınarcık Basin.....	30
2.2.2 The Central Basin.....	31
2.2.3 The Tekirdağ Basin	32
3. METHOD and DATA.....	33
3.1 Seismic Reflection Method	33
3.2 Data Acquisition and Resolution.....	35
3.2.1 SEISMARMARA 2001 Project, deep seismic reflection data acquisition	35
3.2.2 Data resolution	39
3.2.2.1 Vertical resolution	39
3.2.2.2 Lateral resolution.....	40
3.3 Data Processing Steps	41
3.3.1 Editing.....	43
3.3.2 Mute	44
3.3.3 Gain.....	44
3.3.4 Statics correction.....	44
3.3.5 Frequency filtering.....	44
3.3.6 F-K filtering	45
3.3.7 Geometry definition	47
3.3.8 Sort	47
3.3.9 Velocity analysis	47
3.3.10 NMO and stack	48
3.3.11 Attribute analysis	48

3.4 Rheological Implications of Obtained Crustal Reflection Patterns and Comparison for Three Basins of the Sea of Marmara	49
3.4.1 The Tekirdağ Basin	49
3.4.2 The Central Basin.....	54
3.4.3 The Çınarcık Basin.....	60
4. SKS SPLITTING ANALYSIS	65
4.1 Shear Wave Splitting.....	65
4.2 Method and Data	68
5. DISCUSSION and CONCLUSIONS.....	79
REFERENCES	91
APPENDICES	105
CURRICULUM VITA.....	129

ABBREVIATIONS

ANTO	: Ankara Broad-Band Station
AP	: Armutlu Peninsula
BFZ	: Bornova Flysch Zone
CB	: Central Basin
CPD	: Curie Point Depth
CH	: Central High
cu. in.	: cubic inch
ÇB	: Çınarcık Basin
EAF	: East Anatolian Fault
f-k	: frequency-wavenumber
GPS	: Global Positioning System
Hz	: Hertz
IRIS	: Incorporated Research Institutions for Seismology
ISK	: Istanbul Broad-Band Station
ISP	: Isparta Broad-Band Station
KOERI-NEMC	: Kandilli Observatory Earthquake Research Institute National Earthquake Monitoring Center
MMF	: Main Marmara Fault
MTA	: General Directorate of the Mineral Research and Exploration Institute of Turkey
NAF	: North Anatolian Fault
NBF	: Northern Boundary Fault
NMFS	: North Marmara Fault System
OBS	: Ocean Bottom Seismometers
PDZ	: Principal Deformation Zone
R(t)	: Radial Component
SAC	: Seismic Analysis Code
SBF	: Southern Boundary Fault
SHOD	: Department of Navigation, Hydrography and Oceanography
TB	: Tekirdağ Basin
TUBITAK-MAM	: Scientific and Technological Research Council of Turkey- Marmara Research Center
T(t)	: Transverse Component
tw	: two-way travel time

LIST OF TABLES

	<u>Page</u>
Table 1.1: Composite focal mechanism solutions of microearthquakes in the Sea of Marmara (Sato et al., 2004).....	17
Table 3.1: Acquisition parameters of multi-channel seismic reflection data acquired in the Sea of Marmara between 1997-2000 (İmren, 2003; Demirbağ et al., 2007).	36
Table 3.2: SEISMARMARA 2001 project, Leg 1 and Leg 2 data acquisition parameters.	36
Table 3.3: Threshold values for vertical resolution (Yılmaz, 1987).	40
Table 3.4: Deep seismic reflectivity patterns of the three deep basins of the Sea of Marmara.	64
Table 4.1: Origin of anisotropy and related seismic observations for the different depths of the Earth (Babuska and Cara, 1991).....	66
Table 4.2: Selected earthquakes for İstanbul broad-band station (ISK). (-) latitudes represent south direction, (-) longitudes represent west direction.	70
Table 4.3: Selected earthquakes for Ankara broad-band station (ANTO).....	70
Table 4.4: Selected earthquakes for Isparta broad-band station (ISP).	71
Table 5.1: Variation of different physical parameters in the three deep basins of the Sea of Marmara.	87
Table B.1: List of Earthquakes Studied for SKS Splitting Analysis. (-) latitudes represent south direction, (-) longitudes represent west direction.	121

LIST OF FIGURES

	<u>Page</u>
Figure 1.1 : TOPO (GTOPO-30) and bathy (USGS-NIMA) map of Turkey (Smith and Sandwell, 1997). Abbreviations; NAF: North Anatolian Fault, EAF: East Anatolian Fault	1
Figure 1.2 : Depth level classification of deep crustal reflections, SKS anisotropy and Pn anisotropy with respect to the information they provide (Babuska and Cara, 1991).....	4
Figure 1.3 : Aeromagnetic map of the Sea of Marmara (Ateş et al., 2003 and 2008)	8
Figure 1.4 : Heat flow distribution map of Turkey (Tezcan, 1995).....	11
Figure 1.5 : Curie Point Depth (CPD) map of Turkey (Aydın et al., 2005)	12
Figure 1.6 : Seismicity of the Sea of Marmara between 1973 and 2008 (USGS-NEIC)	15
Figure 1.7 : Focal mechanism solutions, obtained from cluster analyses. Open circles in each mechanism show dilatations; solid circles show compressions. Compressional quadrants are shaded in gray (Sato et al., 2004). Abbreviations; MMF: Main Marmara Fault (Le Pichon et al., 2001), CH: Central High	16
Figure 1.8 : GPS vectors in the Marmara region (McClusky et al., 2000), including multi-beam bathymetry, faults in the Sea of Marmara (Le Pichon et al., 2001) and land faults (Şaroğlu et al., 1992). Abbreviations: NAF: North Anatolian Fault; TB: Tekirdağ Basin; CB: Central Basin; ÇB: Çınarcık Basin.....	18
Figure 1.9 : Interpretive cross-section of electric resistivity study (Tank et al., 2005)	19
Figure 2.1 : Active tectonic map of the Eastern Mediterranean showing the geological setting of the Sea of Marmara lines with filled triangles show active subduction zones, lines with open triangles are active thrust faults at continental collision zones. The large solid arrows indicate approximate senses of motion of the lithospheric plates relative to Eurasia. EAF, East Anatolian Fault. Tectonic lines are redrawn from Okay et al. (2004).....	22
Figure 2.2 : Tectonic map of northeastern Mediterranean region showing the major sutures and continental blocks. Sutures are shown by heavy lines with the polarity of former subduction zones indicated by filled triangles. Heavy lines with open triangles represent active subduction zones. Small open triangles indicate the vergence of the major fold and thrust belts. BFZ denotes the Bornova Flysch Zone (Şengör, 1984; Okay, 1989; Okay et al., 1994; 1996, Okay and Tüysüz, 1999) (url-1).....	23
Figure 2.3 : Fault map of the Sea of Marmara; en-echelon segments model, redrawn from Parke et al. (1999). Abbreviations: NBF: Northern Boundary Fault; TB: Tekirdağ Basin; CB: Central Basin; ÇB: Çınarcık Basin; GF: Ganos Fault	25

Figure 2.4 : Faults in the Sea of Marmara; pull-apart basins model (Armijo et al., 2002). Abbreviations: MMF: Main Marmara Fault; ÇB: Çınarcık Basin; CB: Central Basin; TB: Tekirdağ Basin; GF: Ganos Fault.	27
Figure 2.5 : Faults in the Sea of Marmara; single master fault model (Le Pichon et al., 2001). Abbreviations: İF: İzmit Fault, MMF: Main Marmara Fault; ÇB: Çınarcık Basin; CB: Central Basin; TB: Tekirdağ Basin; GF: Ganos Fault.	29
Figure 3.1 : An example of deep crustal seismic reflections from DEKORP2 project from an area of thin-skinned tectonics (DEKORP Res. Group, 1985)	34
Figure 3.2 : Location map for the SEISMARMARA 2001 lines (url-2)	37
Figure 3.3 : Location map for the processed SEISMARMARA 2001 lines in the Sea of Marmara including topography (NASA-SRTM) and bathymetry (Le Pichon et al., 2001) data. Processed parts are shown in square brackets. Abbreviations are : TB: Tekirdağ Basin; CB: Central Basin; ÇB: Çınarcık Basin	38
Figure 3.4 : Wavelength values for different frequencies as a function of velocity (Yılmaz, 1987)	40
Figure 3.5 : Fresnel Zone AA' in (x, z) space (Yılmaz, 1987)	41
Figure 3.6 : Flow diagram of data processing steps applied to the data used in the thesis.....	42
Figure 3.7 : An example of edited traces in the processed data.....	43
Figure 3.8 : Raw data with noise (Line 22b in the Tekirdağ Basin)	45
Figure 3.9 : Application of f-k filter to the data: a) f-k spectrum of the data before filtering, b) data in (x-t) domain before filtering, c) f-k spectrum of the data after filtering, d) data in (x-t) domain after filtering (before filtering, mute is also performed).....	46
Figure 3.10 : a) Stacked and b) interpreted stacked section of Line 22b in the Tekirdağ Basin	50
Figure 3.11 : Reflection strength section of a part of Line 22b in the Tekirdağ Basin (square area in Figure 3.10 a).....	51
Figure 3.12 : Stacked section of Line 11c in the Tekirdağ Basin	52
Figure 3.13 : Interpreted stacked section of Line 11c in the Tekirdağ Basin	53
Figure 3.14 : Stacked section of Line 40a in the Central Basin.....	55
Figure 3.15 : Interpreted stacked section of Line 40a in the Central Basin	56
Figure 3.16 : Magnified image from the stacked section of Line 40a in the Central Basin between ~4.3 and 8.3 s twt.....	57
Figure 3.17 : a) Magnified image from the stacked section of Line 40a in the Central Basin between ~8 and 10 s twt and b) reflection strength of the area between ~8 and 10 s twt.....	57
Figure 3.18 : Stacked section of Line 11b in the Central Basin.....	58
Figure 3.19 : Interpreted stacked section of Line 11b in the Central Basin.....	59
Figure 3.20 : Reflection strength section of a ~10 km area of stacked section (rectangle area in Figure 3.18) of Line 11b, between ~10.5 and 12 s twt of Line 11b	60
Figure 3.21 : Stacked section of a) Line 130 and b) Line 143, interpreted stacked section of c) Line 130 and d) Line 143 in the Çınarcık Basin	61
Figure 3.22 : Stacked section of Line 11a in the Çınarcık Basin.....	62
Figure 3.23 : Interpreted and stacked section of Line 11a in the Çınarcık Basin	63

Figure 3.24 : a) Magnified image from the stacked section of Figure 3.22 (area in square), b) reflection strength image from the stacked section of Figure 3.22 (area in square).....	64
Figure 4.1 : Schematic illustration of shear wave splitting in anisotropic media (url-3)	65
Figure 4.2 : SKS wave results from P to S conversion at the core-mantle boundary (url-4)	67
Figure 4.3 : Evaluation of shear-wave splitting in the ray-coordinate LQT (L: longitudinal; Q: radial, normal to the (L–T) plane) system (Vecsey et al., 2008). The fast polarization direction F lies in the plane (Q–T) perpendicular to the ray path and its orientation in the plane is given by angle ϕ measured from axis Q. The fast polarization direction F can be also defined by two Euler angles: azimuth ϕ angle (measured from the N axis in the horizontal plane) and inclination θ angle (measured from the Z axis oriented downward in the vertical plane).....	68
Figure 4.4 : ISK, ANTO, ISP broad band stations used in the thesis and GPS displacement vectors of Turkey (McClusky et al., 2000)	69
Figure 4.5 : An example of the processed data using ASS.f. a) Radial (R) and transverse (T) components. b) Corrected radial and transverse components. S: start of the SKS phase; F: end of the SKS phase; A: start of the analysis window	72
Figure 4.6 : Fast (dashed line) and slow (bold line) waveforms a) before and b) after the correction (upper diagrams). Particle motion diagram, a) before and b) after the correction (lower diagrams).....	73
Figure 4.7 : Contour diagram with the best pair of splitting parameters ϕ - δt (“+” symbol) after a grid search is performed.....	73
Figure 4.8 : Rose diagrams of SKS splitting parameters for three broad-band stations ISK, ANTO, and ISP calculated in this study. In the rose diagrams black lines point to the fast polarization direction (ϕ) and length of the lines indicates the duration of the delay time (δt) in second. GPS vectors are from Mc Clusky et al. (2000).....	74
Figure 4.9 : Azimuthal distribution of the earthquakes used in the analysis. Green squares, red squares, blue stars indicate earthquakes recorded at ISK, ANTO, ISP broad-band stations, respectively	75
Figure 4.10 : Backazimuthal distribution of SKS splitting parameters ϕ and δt for a) ISK and b) for ANTO stations	76
Figure 4.11 : a) Delay times (δt), and b) fast polarization directions (ϕ) versus back-azimuths for the ISP station. Calculated delay times (a) and polarization directions (b) are marked by filled triangles together with their error bars. Delay times δt (a) and polarization directions ϕ (b) obtained from the model study ($\phi=40^\circ$, $\delta t=1$ s for upper layer), $\phi=150^\circ$, $\delta t=2$ s for lower layer) for two-layer anisotropy models are plotted with the curved lines	77
Figure 4.12 : Pn anisotropy map of Turkey comparing GPS vectors and SKS splitting measurements in the the Eastern Turkey (Al-Lazki et al., 2004)	78
Figure 5.1 : Seismic reflections of three laterally different Moho velocity models at three different frequencies (Braile and Chiang, 1986).....	81

Figure 5.2 : Classification of seismic reflectivity patterns: a) lamellae, b) bands of reflections, c) diffractions, d) diffractions accompanied with upper crustal reflections, e) seismic crocodiles, f) decreasing reflectivity with depth, g) deep reaching, steeply dipping reflection zones, h) ramp and flat structure, i) seismic duplex (Sadowiak et al., 1991).....	83
Figure 5.3 : Keel-like structure from Iapetus suture (Freeman et al., 1998).....	84
Figure 5.4 : Strength-depth models for different heat flow regions (Meissner, 1996).....	85
Figure 5.5 : Different models of varying views of the rheological properties distribution and strength in the Earth. a) Jelly Sandwich Model, b) Cream Brulee Model, c) Banana Split Model (Bürgmann and Dresen, 2008)	88
Figure 5.6 : Schematic model for proposed rheological models for the Sea of Marmara including faults and bathymetry data (Le Pichon et al., 2001). Solid lines represent the results obtained from processed SEISMARMARA 2001 lines, dashed lines represent interpolation between obtained results	89
Figure A.1 : Location map for the processed SEISMARMARA2001 lines	107
Figure A.2 : Tekirdağ Basin lines stack sections	109
Figure A.3 : Tekirdağ Basin lines interpreted stack sections.....	111
Figure A.4 : Central Basin lines stack sections.....	113
Figure A.5 : Central Basin lines interpreted stack sections	115
Figure A.6 : Çınarcık Basin lines stack sections.....	117
Figure A.7 : Çınarcık Basin lines interpreted stack sections	119

INVESTIGATION OF RHEOLOGICAL IMPLICATIONS OF THE CRUSTAL REFLECTIVITY IN THE SEA OF MARMARA

SUMMARY

The Sea of Marmara (northwest Turkey) is a marine basin, which is situated at the western termination of the right lateral strike slip North Anatolian Fault Zone (NAFZ), as a transition area from strike slip regime of the NAFZ to extensional regime of Aegean. Due to its complicated structure, it has been focus of earth scientists especially, after two devastating 1999 earthquakes ($M_w=7.4$, İzmit; $M_w=7.2$, Düzce). In spite of numerous geological and geophysical surveys, there is still debate related to the detailed crustal and mantle structure, tectonic history and active tectonics of the region. In this thesis, rheological models of the crust and mantle beneath the three main basins of the Sea of Marmara (the Tekirdağ, the Central and the Çınarcık Basins) based on multi-channel deep seismic reflection and teleseismic earthquake data are investigated. Present results of Pn velocity and anisotropy, GPS, heat flow studies are used to provide additional constraints for the derived rheological models.

All of the marine seismic reflection data acquired in the Sea of Marmara until 2001 were shallow data. The first deep seismic reflection data of the Sea of Marmara were acquired in a multidisciplinary project, the SEISMARMARA. The project was a combination of seismic refraction, deep seismic reflection and OBS studies. SEISMARMARA project was conducted with the collaboration of Turkish and French Teams in July-October 2001. French N/O Le Nadir acquired 4000 km of multi-channel seismic reflection data using a 4.5 km long streamer with 360 channels. As a source, 8100 cu.in. and 2900 cu.in. single-bubble mode 12-air gun array was used. Survey consisted of two parts: Leg 1 with 45 seismic profiles crossing the whole northern Sea of Marmara and Leg 2 with a dense grid of seismic profiles (~2200 km with 600-900 m spacing) across the Çınarcık Basin and its margins. Also 37 ocean bottom seismometers (OBS) and 30 land stations were deployed to record regional earthquakes and airgun shots. In this thesis, selected parts of 7 deep seismic reflection lines (~142 km); Line 11c and Line 22b in the Tekirdağ Basin; Line 11b and Line 40a in the Central Basin; Line 11a, Line 143 and Line 130 in the Çınarcık Basin are processed.

EMSI-TUBITAK-MAM (Earth and Marine Sciences Institute of Scientific and Technological Research Council of Turkey- Marmara Research Center) provided the SEISMARMARA data used in the thesis. The data are processed in the Nezihi Canitez Data Processing Laboratory of İstanbul Technical University using Disco-Focus data processing package running on a Sun-Solaris platform. Main seismic data processing steps applied to the data are as follows:

- Data editing,
- Mute,

- Shot-receiver statics correction,
- Gain (spherical divergence),
- Band-pass filtering,
- f-k filtering,
- Geometry definition,
- Sort,
- Velocity analysis,
- Normal move-out (NMO) correction,
- Stack,
- f-k filtering,
- Mute,
- Attribute analysis (reflection strength).

Lower crustal seismic reflections are significant on Line 11b (the Central Basin) and Line 11a (the Çınarcık Basin). Beneath the Tekirdağ Basin (Line 11c), the base of the lower crustal reflections is only identified around 7 s twt on the western part of the section, where reflections from the western slopes of the basin are not severe. On the stack section of Line 11b (the Central Basin), the base of lower crustal reflections is around 7-8 s twt. Nature of lower crustal reflections change beneath the Çınarcık Basin (Line 11a). They are in the form of multiple-band seismic reflections disappearing after 8 s twt.

Moho reflections exist on the stack section of the Line 22b (the Tekirdağ Basin), which are visible between 10-12 s twt as dipping reflections. Beneath the Central Basin (Line 40a) similar dipping and discontinuous Moho reflections are distinguishable after 9 s twt. No clear Moho reflections are visible on the seismic stack sections of Line 143 and Line 130 (the Çınarcık Basin).

Deep seismic reflection patterns of Line 22b (the Tekirdağ Basin) and Line 40a (the Central Basin) might be correlated with the traces of the Intra-Pontid suture zone but it is difficult to attain a definite conclusion without 3-D deep seismic reflection and multi-disciplinary data.

In this thesis, the control of mantle processes upon deep crustal geologic features is also investigated by studying shear wave anisotropy in the upper mantle. Teleseismic earthquake data from selected ~450 events with magnitude greater than 5.0 and focal depth greater than 100 km are analyzed to obtain the shear wave splitting parameters, fast polarization direction (ϕ°) and delay time (δt) in second. Automated Shear Wave Splitting Analysis code Ass.f is used on Linux platform to calculate the parameters. Obtained shear wave splitting parameters are correlated with the existing results of Pn anisotropy and velocity studies since they convey information from the upper levels of the mantle.

SKS anisotropy direction, which is analyzed for the east of the Sea of Marmara (Şapaş and Boztepe-Güney, 2009), is not consistent with the results of Pn anisotropy studies. For the west of the Sea of the Marmara, SKS, Pn anisotropy GPS and strain directions are coherent. High Pn velocities, consistent strain, Pn and SKS anisotropy

directions suggest a strong mantle for the western Sea of the Marmara beneath the Tekirdağ Basin. Correlated data indicates a weak mantle for the east of the Sea of Marmara (The Çınarcık Basin) due to highly reflective lower crust and probably hot region under extension beneath the basin, different GPS, SKS and Pn anisotropy orientations, low Pn velocities and thinner crust. Differing strength of the mantle requires two different rheological models to explain the mechanical behaviour of the region. In the light of the classified parameters, investigated region is expressed in terms of two different rheological models, cream brulee for the east (beneath the Çınarcık Basin) and jelly sandwich for the west of the Sea of Marmara (beneath the Tekirdağ Basin) considering the fact that rheology and deformation mechanisms may vary over short spatial (shear zone) scales. The Central Basin reflects the features of a transition area with moderate physical parameters evaluated in the comparison of the basins.

This study provides a rheological model for the three deep basins of the Sea of Marmara based on the deep seismic and seismological data sets. Detailed heat flow, magnetotelluric and gravity data focused in the Sea of Marmara would provide improved rheological models of the crust and mantle beneath the Sea of Marmara in the future.

MARMARA DENİZİ'NDE KABUĞA AİT YANSITILABİLİRLİĞİN REOLOJİK BELİRTİLERİNİN ARAŞTIRILMASI

ÖZET

Marmara Denizi (kuzeybatı Türkiye) sağ yanal atımlı Kuzey Anadolu Fay Zonu'nun batı ucunda yer alan ve Kuzey Anadolu Fay Zonu'nun doğrultu atım rejimi ile Ege'nin gerilme rejimi arasında geçiş bölgesi niteliğinde bulunan denizel bir havzadır. Karmaşık yapısı nedeniyle bilim insanlarının odak merkezi olan bölgeye olan ilgi 1999 yılında meydana gelen iki yıkıcı depremin ardından ($M_w=7.4$, İzmit; $M_w=7.2$, Düzce) daha da artmıştır. Yürütülen birçok çalışma bulunmasına rağmen, bölgenin detayı kabuk ve manto yapısı, tektonik geçmişi ve aktif tektoniği ile ilgili tartışmalar sürmektedir. Bu tezde, Marmara Denizi'nin üç ana havzası olan Tekirdağ, Orta ve Çınarcık Havzalarının altındaki kabuk ve mantoya ait reolojik modeller, çok kanallı sismik yansıma verisi ve telesismik deprem verileri kullanılarak araştırılmıştır. Bölge için mevcut bulunan Pn hızı ve anizotropisi, GPS ve ısı akısına ilişkin çalışmaların sonuçlarından da reolojik modellerin oluşturulmasında faydalanılmıştır.

Marmara Denizi'nde 2001 yılına kadar toplanmış olan bütün deniz sismik yansıma verileri sığ veriler olmuştur. Marmara Denizi'nde ilk derin yansıma verisi, çok-disiplinli bir proje olan SEISMARMARA projesi kapsamında toplanmıştır. Proje sismik kırılma, derin sismik yansıma ve OBS çalışmalarından oluşmuştur. SEISMARMARA projesi Türk ve Fransız ekiplerinin ortak çalışmasıyla 2001 yılının Temmuz-Ekim ayları arasında yürütülmüştür. Fransız Le Nadir gemisi ile 360 kanallı, 4.5 km uzunluğunda streamer kullanarak 4000 km boyunca çok-kanallı sismik yansıma verisi toplanmıştır. Kaynak olarak 8100 cu. in. ve 2900 cu. in. single-bubble modundaki 12 hava tabancası düzeni kullanılmıştır. Çalışma iki bölümden oluşmuştur: bütün kuzey Marmara Denizi'ni kesen 45 sismik profili kapsayan birinci aşama ve Çınarcık Havzası ve sınırları boyunca, yoğun grid şeklinde toplanmış (600 –900 m aralıklı yaklaşık 2200 km) ikinci aşama. Ayrıca bölgesel depremleri ve hava tabancası atışlarını kaydetmek üzere, 37 okyanus tabanı sismometresi (OBS) ve 30 kara istasyonu kurulmuştur. Bu tez kapsamında Tekirdağ Havzası içinde toplanmış olan Hat 11c ve Hat 22 b, Orta Havzada toplanmış olan Hat 11b ve Hat 40a, Çınarcık Havzası'nda toplanmış olan Hat 11a, Hat 143 ve Hat 130 dan oluşan (yaklaşık 142 km) 7 derin sismik profilin seçilen kısımları işlenmiştir.

Tezde kullanılan SEISMARMARA projesi verileri TÜBİTAK-MAM YDBAE (Türkiye Bilimsel Araştırma Kurumu, Marmara Araştırma Merkezi, Yer ve Deniz Bilimleri Araştırma Enstitüsü) tarafından sağlanmıştır. Veriler, İstanbul Teknik Üniversitesi Nezihi Canitez Veri İşlem Laboratuvarında Sun-Solaris platformunda çalışan Disco-Focus veri işlem paketi kullanılarak işlenmiştir. Uygulanan ana veri işlem adımları izleyen şekildedir:

- Verilerin ayıklanması,
- Doğrudan ve kırılma atışlarının giderilmesi,

- Atış-alıcı statik düzeltmesi,
- Kazanç uygulaması (küresel açılıma),
- Band geçiren süzgeçleme,
- f-k filtresi,
- Geometri tanımlanması,
- Atış düzeninden ortak yansıma düzenine geçiş,
- Hız analizi,
- Dik yola kaydırma düzeltmesi,
- Yığma,
- F-k filtresi,
- Mute,
- Nitelik analizi (yansıma gücü).

Hat 11b (Orta havza) ve Hat 11a (Çınarcık Havzası) da belirgin alt kabuk yansımaları gözlemlenmiştir. Tekirdağ Havzası altında (Hat 11c) alt kabuk yansımaları sadece kesitin batı kısmında havzanın dalan yamaçlarından gelen yansımaların etkisinin fazla olmadığı 7 s gidiş-geliş zamanında görülmüştür. Alt kabuk yansımalarının tipi, Çınarcık Havzası altında değişim göstermektedir. Bu bölgede alt kabuk yansımaları, 8 s gidiş-geliş zamanından sonra kaybolan, çok bantlı sismik yansımalar şeklinde gözlemlenmiştir.

Hat 22b (Tekirdağ Havzası) ve Hat 40a (Orta Havza)'nın işlenmesiyle elde edilen derin yansıma paternleri Intra-Pontid suture zone'uyla ilişkili olabilir. 3 boyutlu derin sismik yansıma verisi ve diğer disiplinlerden veri olmaksızın bu ilişkinin kesinliği konusunda karara varmak güçtür.

Bu tez kapsamında mantodaki jeodinamik süreçlerin derin jeolojik yapılar üzerindeki kontrolü de, üst mantodaki SKS ayrımlanması analizi ile araştırılmıştır. Büyüklüğü 5.0 den fazla ve odak derinliği 100 km'den büyük olan yaklaşık 450 deprem, kesme dalgası ayrımlanması parametreleri olan hızlı polarlanma açısı (ϕ °) ve gecikme zamanını (δt s) elde etmek üzere analiz edilmiştir. Elde edilen kesme dalgası ayrımlanması parametreleri mantonun üst seviyelerinden bilgi taşıyan, mevcut Pn hızı ve anizotropisi çalışmalarının sonuçlarıyla ilişkilendirilerek değerlendirilmiştir.

Marmara Denizi'nin doğusu için elde edilen SKS anizotropi doğrultusu, Pn anizotropisi çalışmalarından elde edilen sonuçlarla uyumlu değildir. Marmara Denizi'nin batı kısmı için, SKS, Pn anizotropisi, GPS ve yamulma doğrultuları uyumludur. İlişkilendirilen veriler Marmara Denizi'nin doğu kısmı için (Çınarcık Havzası) yüksek yansıtıcılık özelliği gösteren alt kabuk nedeniyle zayıf mantonun varlığını ve farklı GPS, SKS, Pn anizotropi yönleri ile düşük Pn hızı ve incelen kabuk nedeniyle gerilme altındaki göreceli olarak sıcak bir bölgeyi işaret etmektedir. Manto gücünde gözlemlenen değişim, bölgenin mekanik davranışının açıklanması için iki farklı reolojik modelle açıklanmasını gerektirmektedir. Sınıflandırılan fiziksel parametreler ışığında, reoloji ve deformasyon mekanizmalarının küçük ölçeklerde değişebileceği de göz önünde bulundurularak, araştırılan bölge, Marmara Denizi'nin doğusu (Çınarcık Havzası)

iin “cream brulee”, Marmara Denizi’nin batısı (Tekirdağ Havzası) iin “jelly sandwich” olmak zere iki farklı model ile tariflenmiřtir. Orta Havza sınıflandırılan fiziksel parametreler aısından Tekirdağ ve ınarcık Havzalarıyla karşılaştırılınca ortalama deęerler gsterdięi iin, bir geiş blgesi nitelięinde olduęu dřnlmektedir.

Bu alıřmada derin sismik yansıma ve sismolojik veri setlerinin deęerlendirilmeisinden yola ıkılarak, Marmara Denizi’nin derin havzaları iin bir reolojik model retilmiřtir. Blgede yapılacak detaylı ısı akısı, manyetotellurik ve gravite alıřmaları, Marmara Denizi’nin altındaki kabuk ve mantoya reolojik modelin geliřtirilmesine byk katkıda bulunacaktır.

1. INTRODUCTION

The Sea of Marmara is located in NW Turkey, which is a very unique region for earth scientists due to its complicated and unresolved tectonic structure (Figure 1.1). It is a transition zone between right lateral strike slip nature of the North Anatolian Fault (NAF) and N-S extensional regime of the western Aegean region.

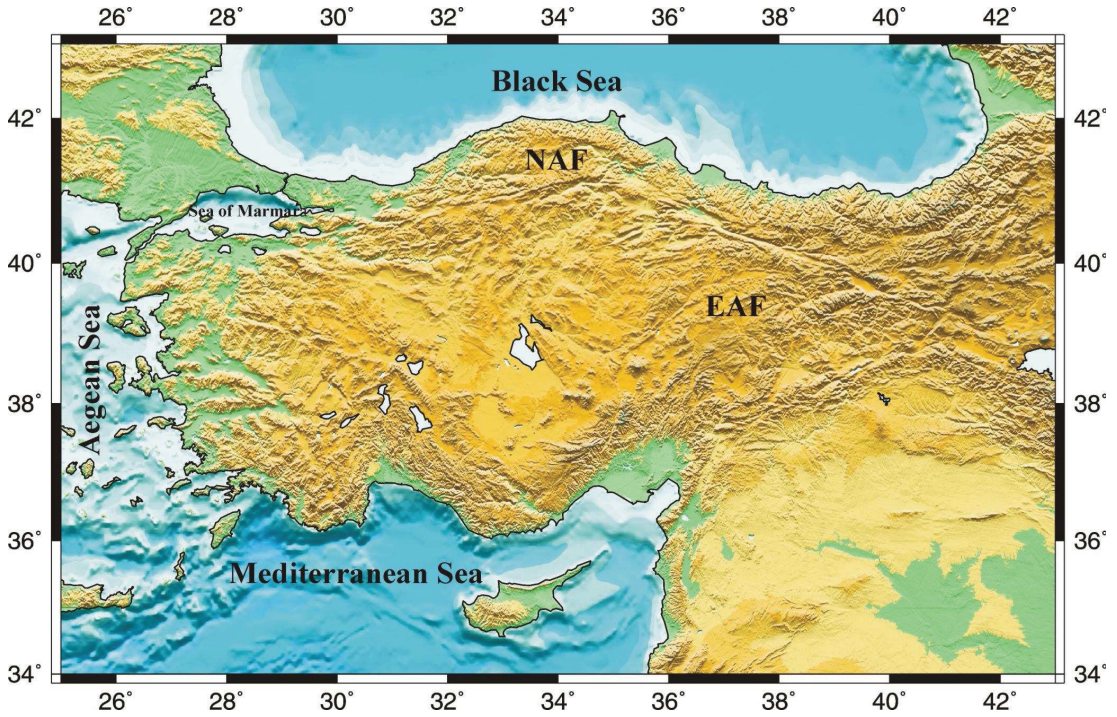


Figure 1.1: TOPO (GTOPO-30) and bathy (USGS-NIMA) map of Turkey (Smith and Sandwell, 1997). Abbreviations; NAF: North Anatolian Fault, EAF: East Anatolian Fault.

Between 1939 and 1999, eleven major earthquakes with magnitude $M_w > 6.7$ have occurred along 1200 km of NAF (Şengör et al., 2005). Especially after destructive İzmit earthquake with magnitude $M_w 7.4$ (~70 km away from İstanbul), the number of investigations related to the geometry of NAF in the Sea of Marmara increased. Since the Sea of Marmara and İstanbul did not experience a large earthquake during XX. century, it has been one of the exceptionally high earthquake risk areas in Turkey (Ambraseys and Jackson, 2000; Parsons et al., 2000; Hubert-Ferrari et al., 2002). Question mark still resides on the matter whether the deformation in the Sea of Marmara could be accommodated on a single fault which is capable of generating

an earthquake with magnitude (M_w) 7.5-8 or on several smaller faults generating earthquakes with magnitude (M_w) 6.5-7.0. Reilinger et al. (2006) suggested that the evolution of Anatolia is associated with the roll back of the Hellenic-Cyprus Trench and back arc extension in the Aegean Sea. Meade et al. (2002) reported that the North Anatolian Fault Zone (NAFZ) in northwestern Turkey carries approximately four times as much right-lateral motion (~ 24 mm/yr) as does the southern strand based on the Global Positioning System (GPS) data. They suggested that both the geometry of the strike-slip faulting in the shallow sedimentary layer and the asymmetric loading along the fault in the Sea of Marmara are controlled by the rheology of the crust. Studies of post seismic deformation following August 17, 1999, İzmit earthquake ($M_w=7.4$) showed that deep rheology differs depending on the local lithosphere structure and tectonics (Hearn et al., 2002). The S-wave quality factors ($Q_s = 1/\text{S-wave attenuation}$) estimated from the earthquake data for five different regions in the Sea of Marmara ranging from $13 \pm 1 f^{1.22 \pm 0.05}$ to $94 \pm 3 f^{0.83 \pm 0.04}$ indicated that the regional differences in the rheology and the tectonic activity of the crust exist (Horasan and Boztepe-Güney, 2004).

In the study area, previous studies based on different data sets (seismology, gravity and magnetic, heat flow, GPS) have been carried on. Objective of them were to investigate the active tectonics and physics of the crust in the study area. The results of those previous studies are summed up in the next sub-sections of this chapter to establish a reliable basis for the interpretation of crustal rheology of the Sea of Marmara. Proposed models for the tectonics and evolution of the Sea of Marmara are adverted in the Chapter 2.

All of the marine seismic reflection data acquired in the Sea of Marmara until 2001 were shallow data. The first deep seismic reflection data of the Sea of Marmara were acquired in a multidisciplinary project, the SEISMARMARA, which is a combination of seismic refraction, deep seismic reflection and OBS studies. SEISMARMARA was conducted with the collaboration of Turkish and French Teams in July-October 2001. The objective of the project was; to investigate the regional tectonics and the recent evolution of the area at crustal scale, to record local earthquakes, to deduce a reliable velocity-depth model to improve the quality of locations and focal mechanism solutions of earthquakes (Carton et al., 2007).

French N/O Le Nadir acquired 4000 km of multichannel deep seismic reflection data using a 4.5 km long streamer with 360 channels. As the source, 8100 cu.in. and 2900 cu.in. single-bubble mode 12-air gun array was used. Seismic survey consisted of two parts: Leg 1 with 45 profiles crossing the whole northern Sea of Marmara and Leg 2 with a dense grid of lines (total ~2200 km with 600-900 km spacing) across the Çınarcık Basin and its margins. Also 37 OBS were deployed and 30 land stations were settled to record regional earthquakes and airgun shots. In the scope of this thesis, short but deep lines from Leg 1 and Leg 2 are processed to reveal the deep reflection patterns and rheological implications of those patterns from the three major basins of the Sea of Marmara (the Tekirdağ, the Central and the Çınarcık Basins) as comparative to each other for the first time. Details of the applied method, data processing steps and interpreted seismic sections are given in the Chapter 3.

Shear wave splitting method is used to investigate seismic anisotropy in the upper mantle. It is one of the most widely used methods to relate the surface tectonic processes and deformations with mantle dynamics. Deformations in the upper mantle and the crust have influence on each other (Rudnick, 1996). Therefore it is benefited while interpreting deep seismic reflection patterns of the crust and their rheological implications since shear wave splitting assists to build a connection between the upper mantle and the crust. SKS splitting analysis is performed for İstanbul broad-band station (ISK) and compared with the results from Ankara (ANTO) and Isparta (ISP) broad-band stations. Details and results of the analysis are given in the Chapter 4.

In the Chapter 5, detailed interpretation of the processed seismic reflection data provided. Different physical parameters from different methods (deep seismic reflections, Pn and SKS anisotropy) for different levels of the crust and mantle are used to derive the rheological models for the crust and the mantle beneath the Sea of Marmara (Figure 1.2). Previously studied focal mechanism solutions, heat flow, gravity-magnetic studies are also combined. The results of those studies are classified for the Tekirdağ Basin, the Central Basin and the Çınarcık Basin to provide a basis for comparison. Rheological implications of the presented data are evaluated together to build preliminary rheological models for the crust and the mantle beneath the deep basins of the Sea of Marmara. Derived rheological models and recommendations for related future studies are also provided in the thesis.

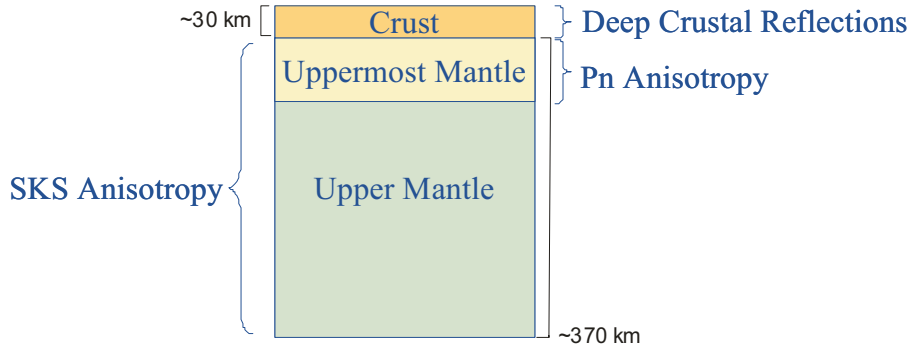


Figure 1.2: Depth level classification of deep crustal reflections, SKS anisotropy and Pn anisotropy with respect to the information they provide (Babuska and Cara, 1991).

1.1 Velocity-Depth Models of the Sea of Marmara

Various studies were performed to deduce the crustal velocity structure of the Sea of Marmara using different data sets and methods (Zor et al., 2006; Barış et al., 2005; Al-Lazki et al., 2004; Karabulut et al., 2003; Nakamura et al., 2002; Horasan et al., 2002; Gürbüz et al., 1980; Crampin and Üçer, 1975).

Barış et al. (2005) investigated 3D velocity structure of the upper crust of the Sea of Marmara using first arrival times of selected 3949 earthquakes recorded between 1985 and 2002. They reported that the western part of the North Anatolian Fault Zone showed strong lateral heterogeneity. They observed low P wave velocities in the sedimentary units such as basins and plains. Low velocity zone in the central and western parts of the Sea of Marmara was reported to continue to the depth of 15 km. They observed one high velocity body at depth of 10 km at longitude 28.0° E. They also estimated high velocities in the vicinity of south of Tekirdağ. They suggested that mafic rocks are characterized by high velocity, whereas sedimentary rocks are characterized by low velocity.

Zor et al. (2006) investigated the crustal structure of the eastern Marmara region using earthquake data from 11 broad-band stations. They applied receiver function method to the data and observed a crustal thickness of 34-35 km for the eastern and 29-32 km for the western part of the eastern Marmara region. They calculated the average thickness for the eastern Marmara as 31 ± 2 km and S wave velocity 3.64 ± 0.15 km/s. Comparing regional heat flow values, extensional features and crustal

thickening from 29 km to 35 km towards east, they concluded that eastern Marmara region seems to be a transition zone between the Sea of Marmara extensional domain and continental Anatolian inland region.

Al-Lazki et al. (2004) studied Pn anisotropy and velocity structure at the junction of Arabian, Eurasian and African plates using 29-station broadband network of the Eastern Turkey Seismic Experiment and a 20-station short period seismic network in Syria. Pn velocities in the continental lithosphere vary from high values (>8 km/s) to low values that are accepted to be the indications of stable mantle lid and partial melt, respectively (Calvert et al., 2000). Al-Lazki et al. (2004) reported that Pn velocities in the west of the Marmara region are higher than those in the east of the Marmara region which indicates partial melting for the Eastern Marmara Region. Pn anisotropy orientations were observed to change along the NAF as NE-SW in the east, E-W, N-S in the central parts and NW-SE in the west close to the Sea of Marmara. In the Sea of Marmara anisotropy orientations were observed to change from NW-SE in the east, NE-SW direction in the west. They noted that more complex crustal and upper mantle processes seem to influence Pn anisotropy orientations in the mantle lid as they contrast with the relatively uniform westward motion of the Anatolian plate deduced from detailed GPS measurements. (McClusky et al., 2000).

Karabulut et al. (2003) obtained 2D seismic image of the Eastern Marmara Region across an E-W directional 120 km long refraction profile over NAF and tectonically active the Çınarcık Basin. Data were acquired during SEISMARMARA project. Deduced P-wave velocity model was confined to the top 7 km of the crust and had clear heterogeneities in the upper crust. In the study, lateral P-wave velocity variations were attributed to surface geology. Beneath Armutlu Peninsula, reported local high P-wave velocities (5.8 – 6.1 km/s) were interpreted as related to the granitic intrusions. In the Gulf of Gemlik, calculated P-wave velocities were 3.1 – 4.5 km/s for the depth of ~ 4 km. Beneath the Çınarcık Basin, they reported a velocity change from 2.5 km/s to 4.5 km/s for the same depth range and also high P-wave velocities (>6 km/s) at a localized zone of 5 km depth. This zone was observed to be around ruptured segment of NAF in 1999 İzmit earthquake and confined with the lower velocity northern branches of NAF. Also, in the Kocaeli Peninsula, high P-wave velocities (5.7-6.0 km/s) were observed under İstanbul Paleozoic units.

Horasan et al. (2002) investigated lithospheric structure of Marmara and Aegean by waveform modeling of three aftershocks of 1999 İzmit earthquake with magnitude $M_w = 7.4$. During modeling, different velocity models were used to determine the crustal structure, which provides the best coherency between synthetic seismograms and observed ones. They estimated 8.0 km/s of Pn wave velocity and 4.6 km/s of S-wave velocity for the upper mantle and 32 km of crustal thickness for the Gulf of İzmit area.

Nakamura et al. (2002) investigated 3D P-wave velocity structure of the 1999 İzmit earthquake hypocentral area. They used tomography method of Zhao et al. (1992) to determine the 3D P-wave velocity structure and observed that aftershocks of 1999 İzmit earthquake built an E-W directional narrow zone of 170 km through the northern branch of NAF. They also observed that distributions of the aftershocks were not homogeneous but clustered in three groups as; near main shock hypocenter, in the Sea of Marmara around longitude 29.2 E°, and in the east of longitude 30.4 E°. According to their results, there is a low-velocity area west of the main shock hypocenter and a high-velocity anomaly east of longitude 30.4 E°. This anomaly was observed to exist under the aftershock cluster in the east of longitude 30.4 E° which extends to the shallow depths of southern branch of NAF (İznik-Mekece Fault).

Gürbüz et al. (1980) investigated crustal thickness and Pn velocities for the southern Sea of the Marmara using quarry blasts. They estimated, a crustal thickness of 28-29 km and Pn wave velocity of 8.1 km/s. They suggested that high velocities in the west and shallow depth to the upper mantle in the southwest of the area could be indication of a dome-like structure.

Crampin and Üçer (1975) investigated crustal seismic velocities beneath the Sea of Marmara using 4 different earthquakes from 35 stations. Crustal P-wave velocities obtained in this study were in the range of 5.8-6.0 km/s.

1.2 Gravity and Magnetic Studies in the Sea of Marmara

A relationship between the Sea of Marmara and NAF was established by Ergün and Özel (1995) combining shallow seismic data with geological and aeromagnetic data. Ates et al. (2003; 2008), studied seismic, aeromagnetic and gravity data in the Sea of Marmara to investigate the extend of the faults identified on the land, into the sea.

Ateş et al. (2003; 2008), used aeromagnetic data provided by the General Directorate of the Mineral Research and Exploration Institute of Turkey (MTA), which were recorded from an altitude of 600 m along flight lines in N-S direction with 500-1000 m spacing. In the produced aeromagnetic map (Figure 1.3) a positive large amplitude anomaly of 150 km in the E-W direction was observed. Regions of the Gulf of Saros, the Dardanelles, the Biga Peninsula also exhibited strong positive anomalies. Those are interpreted as magmatic bodies observed in the extensional provinces as in the southwestern Turkey. Anomalies observed in the southern parts of the Sea of the Marmara, parallel to the NAF, were suggested to represent highly magnetized, two-dimensional dyke-like bodies parallel to the fault elongation (Tunçer et al., 1991). Average depth to those andesitic intrusions were determined to be 100 m. Gravity data used in the investigation were collected by the MTA and were provided as an analogue Bouguer anomaly map (Erden and Oray, 1977). In the gravity profiles, a sharp negative anomaly was observed on the town of Gölcük, which was interpreted as the bifurcation of the NAF with normal component. Strong negative anomalies around the southern shore of the Sea of the Marmara were also observed. Those anomalies were interpreted as the possible western extension of the NAF in the Sea of Marmara.

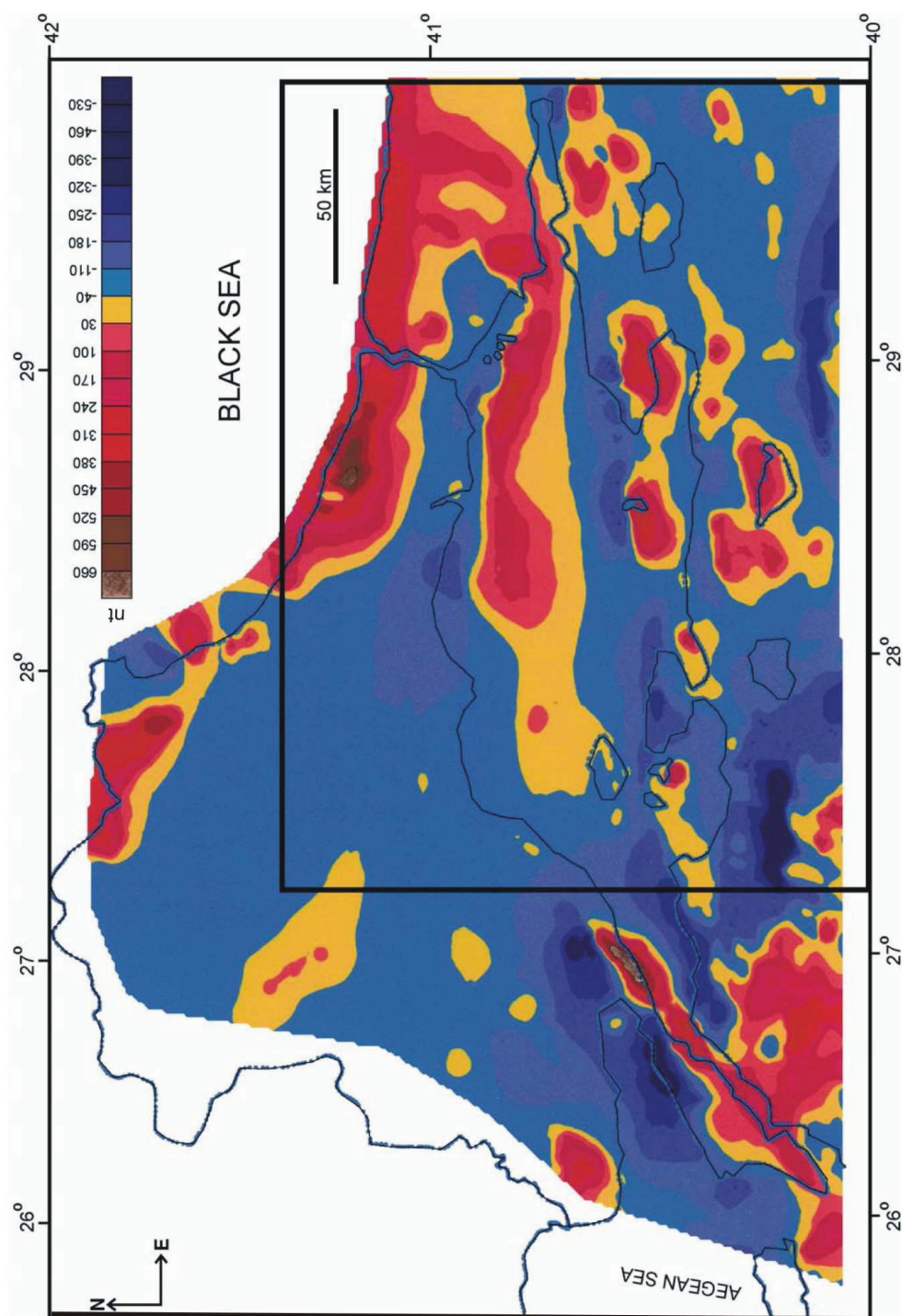


Figure 1.3: Aeromagnetic map of the Sea of Marmara (Ateş et al., 2003 and 2008).

1.3 Heat Flow Studies In the Sea of Marmara

The first detailed heat-flow map of Turkey was prepared by Tezcan (1979) using temperature gradients in the wells. By the addition of new well data, this map was improved by Tezcan (1995) and given in Figure 1.4. Heat-flow determinations in thermal springs in Western Anatolia were also studied by İlkışık et al. (1990; 1995) and İlkışık (1995) and were correlated with crustal structure. According to the heat flow map of Turkey (Tezcan, 1995), heat flow values for the Sea of Marmara range between 40 mW/m² and 140 mW/m². Average heat flow value for the continental crust is 65 ± 1.6 mW/m² (Pollack et al., 1993). Measured values point out that the crust of the region is heater than the average continental crust. Curie Point Depth (CPD) investigations are also a geothermic study area parallel to the heat flow measurements since CPD is also sensitive to the crustal heat variations. CPD is the depth at which temperature reaches the Curie point temperature.

At the Curie point, magnetism of rocks diminishes (~580°C for magnetite). Thus, magnetic bearing rocks do not generate any signatures on the measured geomagnetic field after this temperature. The depth to the Curie point temperature, CPD, is assumed to be the bottom of magnetized bodies in the crust. Magnetic data is analyzed by the most commonly used method given by Vacquier and Affleck (1941), Bhattacharyya and Leu (1975), Shuey et al. (1977), Connard et al., (1983) and Tanaka et al. (1999) to obtain CPDs. Different mineralogical contents and different geologies result in varying CPDs from region to region. Variations of the CPD in the crust reflect variations of the crustal thermal regime. In the regions with geothermal potential, thinned crust and young volcanism, shallow CPDs are expected. CPD map of Turkey (Figure 1.5) was prepared using magnetic data obtained from MTA (Aydın et al., 2005). It was suggested that the shallow CPD patterns depends on the tectonic regime and morphology. It was also observed that the map coincided with the geological (plate) structure and volcanism of the Turkey. It was reported that the deep Curie point anomalies in the southeastern part of Turkey coincide roughly with the subduction of the Arabian plate together with volcanic activity. The easternmost shallow CPDs were interpreted to be related with the volcanoes in the eastern Turkey, which implies that a shallow magma chamber had yielded the volcanic activity or magma plump. In the central part of Eastern Turkey, E-W elongated

moderate CPDs were correlated with the heavily faulted Karlıova depression. Another possible interpretation for the cause of observed depths were upper mantle flow and asthenospheric upwelling. Extensional, thinned nature of the western Turkey with E-W directional grabens was also reflected in the map. Anomalies along the NAF were in the range of middle to deep.

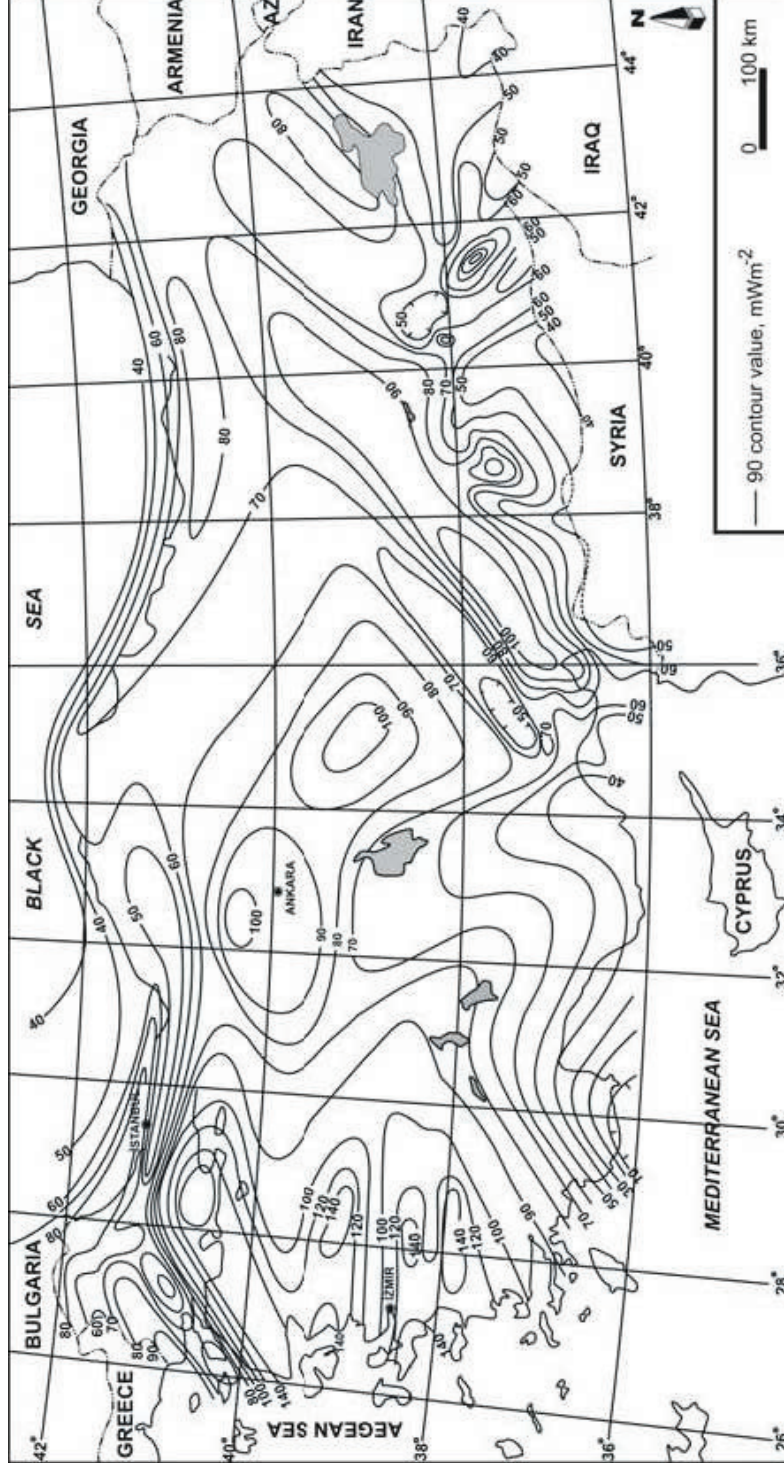


Figure 1.4: Heat flow distribution map of Turkey (Tezcan, 1995).

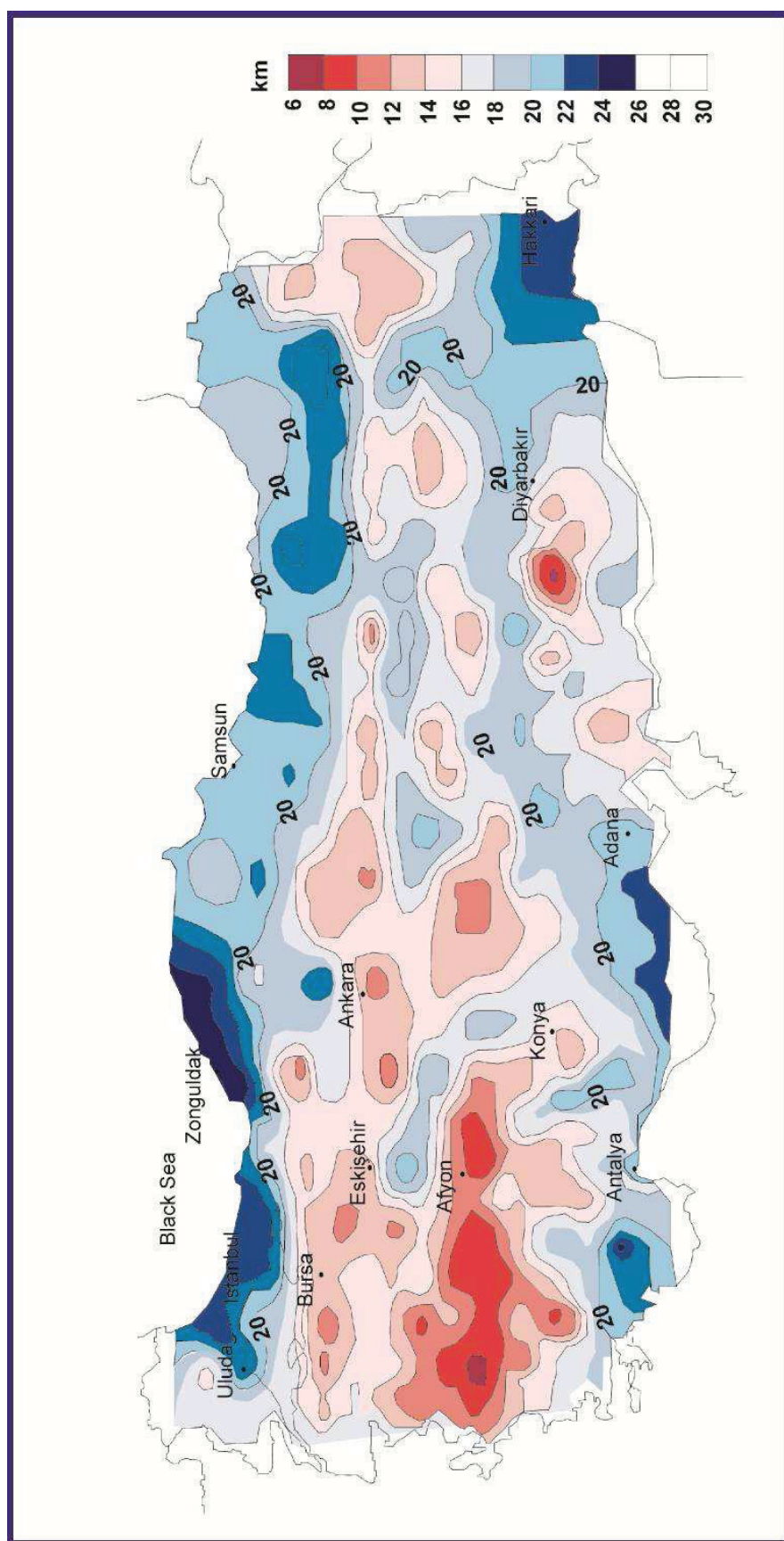


Figure1.5 Curie Point Depth (CPD) map of Turkey (Aydın et al., 2005).

Along the southern Marmara branch of NAF, CPDs were observed to be around 15 km. At the northern edge of the Aegean region and to the south of Marmara Sea, where hot-spring fields with surface temperature of 52-59°C were situated, CDPs were shallower in the range of 10-12 km. For Thrace in NW Turkey, CDP values were higher, around the depth of 17-18 km. They interpreted all those results as follows;

- The depths less than ~10 km occur in the geothermal areas that have the highest heat-flow contribution, orogenic belts with some nappe structure such as Taurus and Pontides,
- Suture zones are the regions with the deepest CPD values more than 20 km,
- Shallow depths in the CPD map of Turkey are well correlated with the young volcanic areas and geothermal potential fields.

1.4 Seismicity of the Sea of Marmara

Seismicity and tectonics of the Marmara region have been studied by different scientists (Crampin and Üçer, 1975; Barka, 1997; Eyidoğan, 1988; Taymaz, 1999; Ambraseys, 2002; Karabulut, 2002; Özalaybey et al., 2002) since 1970's. In this section, results of two recent studies are going to be presented.

Long term seismicity (1973-2008) of the Sea of Marmara is mainly concentrated along the branches of the NAF (Figure 1.6). Installation of a permanent network by Kandilli Observatory and Earthquake Research Institute (KOERI) improved the quality of earthquake monitoring in the region. In order to obtain precise determination of hypocenters of seismic events and to increase the number of well-determined focal mechanisms in the area, Gürbüz et al. (2000) conducted a micro-seismic experiment with 48 stations around the Sea of Marmara. Along the northern branch of the NAF, a linear seismic activity was observed. Obtained stress tensor was compatible with the stress tensor obtained from long-term (1943-1997) seismicity.

Land-based observations were insufficient to determine detailed fault geometries and microearthquake activities within the Sea of Marmara. In the region, the first marine seismological observation was conducted by Sato et al. (2004) to study focal mechanism solutions and microearthquake activity. Ten OBSs were deployed in the

Çınarcık, the Central and the Tekirdağ Basins and provided 350 well-constrained, high-resolution hypocenters and 9 composite focal mechanism solutions. Distribution of the microearthquakes determined in the study (Figure 1.7) was similar to the long-term seismicity pattern given in Figure 1.6. According to the observed hypocenter distributions, it was suggested that most of the earthquakes occurred in the vicinity of the Main Marmara Fault (Le Pichon et al., 2001).

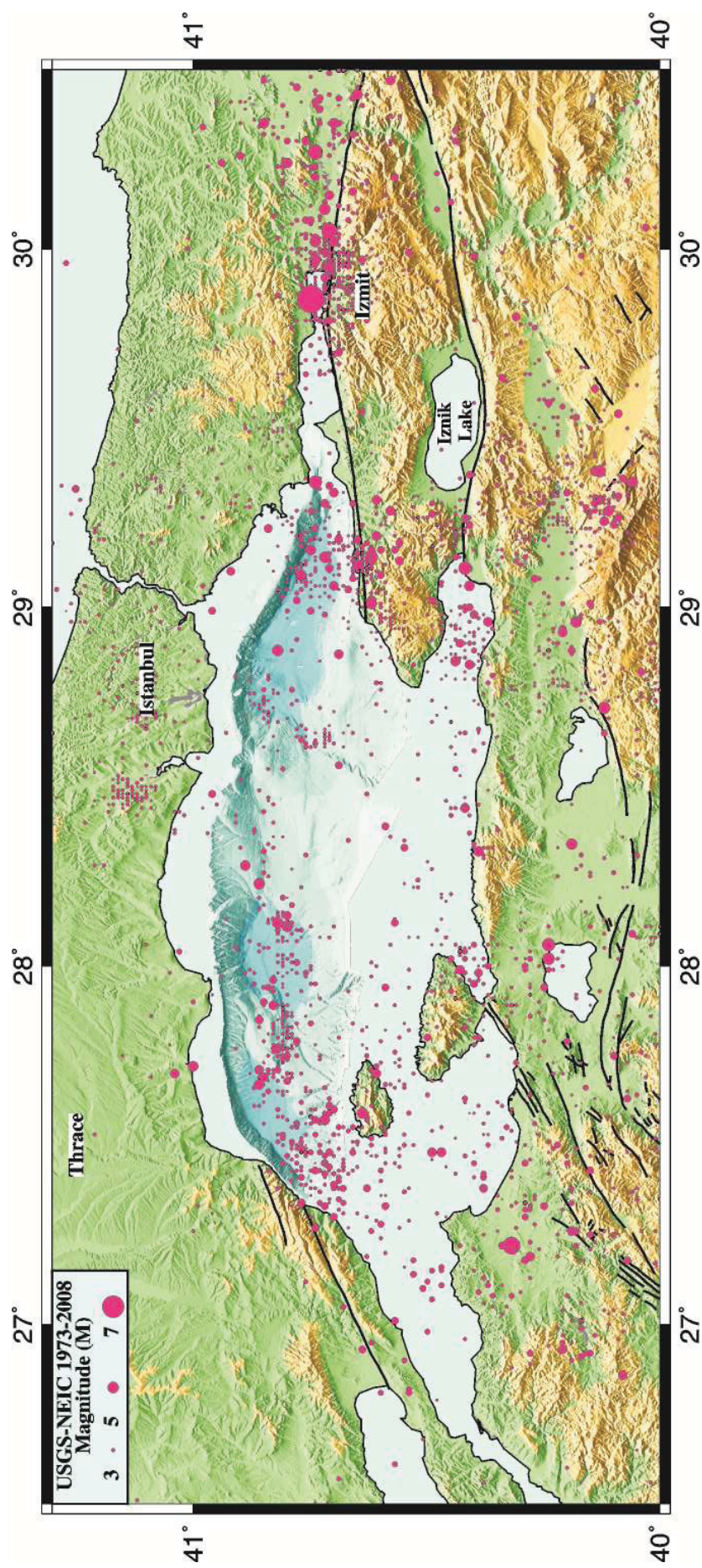


Figure 1.6: Seismicity of the Sea of Marmara between 1973 and 2008 (USGS-NEIC).

In the eastern basin, earthquakes clustered to the south of the MMF whereas fewer earthquakes occurred beneath the MMF, and the Central High (CH) had low seismicity. The depth limits of the events were reported to be 15 km in the eastern and 20 km in the western part of the Sea of Marmara. It was also noted that, occurrence of most of the earthquakes along the western MMF beneath the fault except that the shallowest events indicated that the western MMF was sub vertical.

It was inferred that, only southern half of the structure was relatively active and the fault geometry was sub vertical in the Central Basin. Micro earthquake distribution which dips towards the south at $\sim 45^\circ$ in the eastern part, indicated that the MMF dips south in this area. For the eastern end of the MMF, it was reported that the NAF could be vertical but more data were required to confirm this possibility. Focal mechanism solutions obtained in this study are given in Figure 1.7 and Table 1.1.

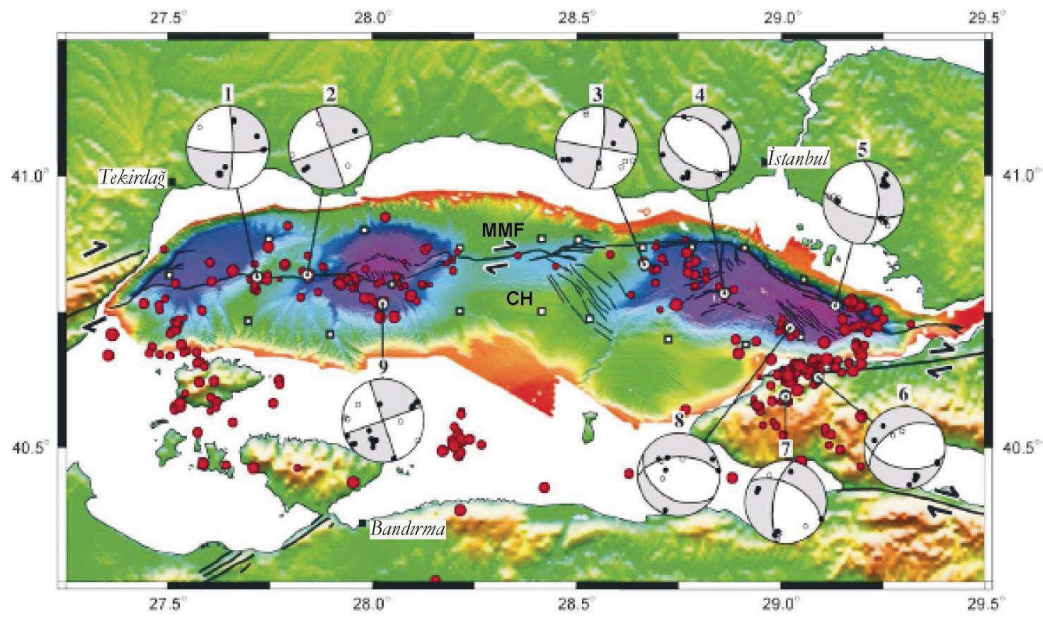


Figure 1.7: Focal mechanism solutions, obtained from cluster analyses. Open circles in each mechanism show dilatations; solid circles show compressions. Compressional quadrants are shaded in gray (Sato et al., 2004). Abbreviations; MMF: Main Marmara Fault (Le Pichon et al., 2001), CH: Central High.

Table 1.1: Composite focal mechanism solutions of microearthquakes in the Sea of Marmara (Sato et al., 2004).

Event no.	Number of events	Average latitude (°N)	Average longitude (°E)	Average Depth (km)	Strike (°)	Dip (°)	Rake (°)
1	9	40.8131	27.7213	10.1	0	80	-10
2	2	40.8169	27.8441	11.2	70	90	-180
3	8	40.8362	28.6669	7.1	280	90	170
4	3	40.7832	28.8606	10.6	120	50	-100
5	10	40.7606	29.1313	9.6	0	60	-30
6	10	40.6297	29.0901	6.5	240	50	-120
7	9	40.5939	29.0109	9.3	190	65	-40
8	4	40.7201	29.0215	5.3	120	40	-65
9	17	40.7642	28.0273	5.4	70	90	-180

On the basis of the obtained pure strike-slip focal mechanisms, a dominant right lateral strike-slip regime was suggested in the western Sea of Marmara. More complex mechanisms consisting strike-slip faulting in the NW and normal faulting in the central part of the Çınarcık Basin were reported. Those were related to the oblique extension to the trend of the MMF in the western Çınarcık Basin. At the eastern end of the basin vertical faults were suggested and strain partition was proposed as also suggested by Le Pichon et al. (2001). They also noted that, their results supported the single localized active through going right-lateral strike-slip fault system in the western Sea of Marmara.

1.5 GPS Measurements in the Sea of Marmara

Many GPS surveys have been carried on to determine interseismic crustal deformations by the means of velocity vectors for the last two decades (Straub et al., 1997; Reilinger et al., 1997; Kahle et al., 2000; McClusky et al., 2000; Meade et al., 2002; McClusky et al., 2003; Allmendinger et al., 2007). The Aegean plate is moving towards the SW at 30 ± 1 mm/yr relative to Eurasia which gives rise to the extension in the western Turkey with motion at 15 ± 1 mm/yr. The NAF is dominated by right-lateral strike slip motion at 24 ± 1 mm/yr with slight compression along the easternmost segment and extension in the Marmara Sea–North Aegean trough (McClusky et al., 2003).

Most of the GPS velocity vectors relative to Eurasia (Figure 1.8) can be explained by rotation of Anatolia and the Aegean around an Euler pole (McClusky et al., 2000). But there are misfits for much of southern Aegean and the Sea of Marmara (Flerit et al., 2003). To obtain a better-fit model, Flerit et al. (2003) proposed a slip-partitioning model between the northern and southern branches of the NAF, where 20 % of the required slip (24 ± 1 mm/yr) is transferred to southern branch, extension increased to the south and decreased across structures within the northern part. It is also reported that, details of the model will be better constrained as more data accumulates.

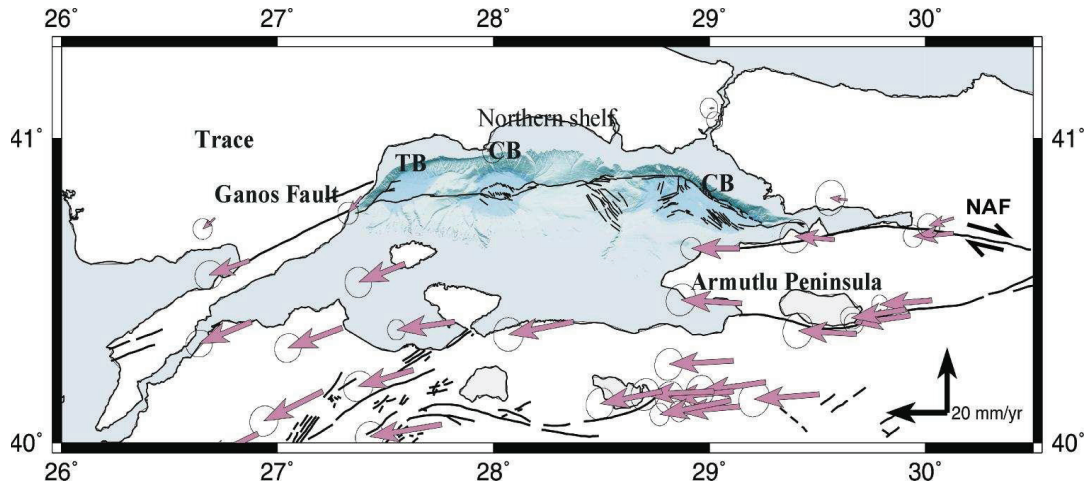


Figure 1.8: GPS vectors in the Marmara region (McClusky et al., 2000), including multi-beam bathymetry, faults in the Sea of Marmara (Le Pichon et al., 2001) and land faults (Şaroğlu et al., 1992). Abbreviations; NAF: North Anatolian Fault TB: Tekirdağ Basin, CB: Central Basin, ÇB: Çınarcık Basin.

1.6 Electrical Conductivity Studies around the Sea of Marmara

Around the western part of the North Anatolian Fault numerous electrical resistivity studies were conducted (Honkura et al., 1985; Gürer, 1996; Tank et al., 2003; Tank, et al., 2005). Tank et al. (2005) used wide-band magnetotelluric data to investigate the fault rupture area of the 1999 İzmit earthquake with $M_w=7.4$ on the NAFZ, in the eastern Marmara region. Their final models indicated that, hypocenters of the main shocks and aftershocks were located on the highly resistive side of a conductive zone. They observed a low conductivity zone extending down to 50 km between two fault branches. They interpreted this deep zone as partial melting which resulted from

the past tectonics in the region. Cartoon model of the interpretation is given in Figure 1.9.

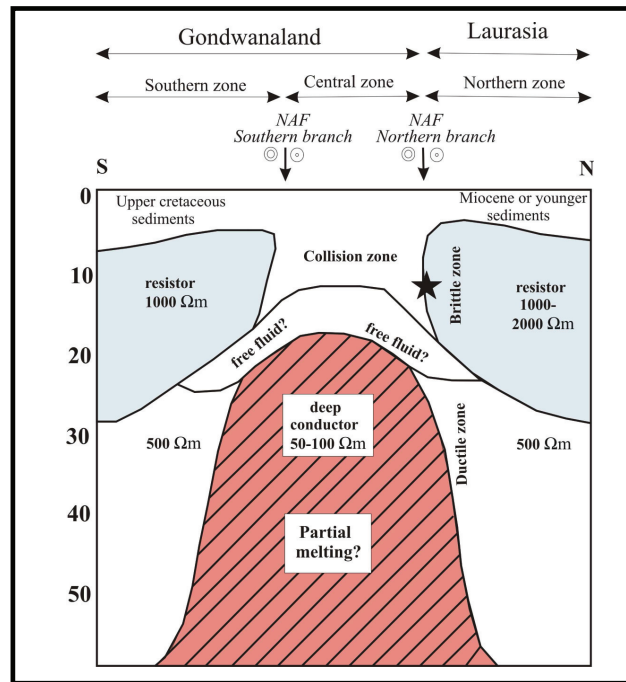


Figure 1.9: Interpretive cross section of electric resistivity study (Tank et al., 2005).

In the Thrace region of Turkey, Bayrak et al. (2004) reported that, large earthquakes occurred around the areas of high electrical resistivity in the upper crust whereas small magnitude earthquakes were observed in the conductive lower crust. The fluid migration from the conductive lower crust to resistive upper crust was suggested as the possible reason for seismicity in resistive areas. It was also reported that, the depth to the lithospheric upper mantle is around 45 km beneath Istranca massif whereas it decreases to 17 km towards southeastern part and interpreted this as the effect of mantle uplifting in the area.

2. TECTONICS of the SEA of MARMARA

2.1. The North Anatolian Fault in the Sea of Marmara

The North Anatolian Fault (NAF) is one of the World's largest active, strike slip systems (Figure 2.1) which extends about 1200 km from Karlıova triple junction, eastern Turkey, to the North Aegean Sea (Ketin, 1969; Ambreseys, 1970; Şengör, 1979; Barka, 1992; Westaway, 1994; Hubert-Ferrari et al., 2002). The Anatolian plate is characterized by collision of Arabia and Africa with the Eurasian plate, which started during the Early Miocene (Yılmaz et al., 1995). The right lateral North Anatolian Fault and the left lateral East Anatolian Fault (EAF) constitute the boundaries of the westward rotating Anatolian plate (Reilinger and Barka, 1997). The NAF accommodates the westward motion and counterclockwise rotation of the Anatolia relative to the Eurasian plate forming a boundary between those two plates (McKenzie, 1972; Dewey and Şengör, 1979). The westward motion of the Anatolian plate along the NAF is about 24 mm/y on the basis of the GPS studies (McClusky et al., 2000). The age of the NAF is controversial but it is commonly accepted that the NAF has become active around the start of the Pliocene (Ketin, 1948; 1969; McKenzie, 1972; Şengör, 1979; Barka, 1992; Barka et al., 2000; Barka and Kadinsky-Cade, 1988; Koçigit, 1988; 1989; 1991; Şaroğlu, 1988; Toprak, 1988; Barka and Gülen, 1989; Bozkurt and Koçiyigit, 1996; Yaltrak, 1996; Okay et al., 1999; 2000; Tüysüz et al., 1998; Yaltrak et al., 2000). According to the recent models, it has become active at the end of the Miocene but recent geometry has developed in the Pliocene (Westaway, 2004). Stratigraphic studies around the Sea of Marmara Sea region suggest an age of 3.5 Ma (Yaltrak et al., 1998; Sakıncı et al., 1999; Alpar and Yaltrak, 2002). It is suggested that the NAF represents a transform margin that follows a pre-existing zone of crustal weakness; Intra Pontid suture given in Figure 2.2 (Şengör and Yılmaz, 1981; Şengör et al., 1985; Okay and Tüysüz, 1999). The Intra Pontid Suture Zone forms a ~400 km long boundary between the İstanbul Zone and the Sakarya Zone and also extends for another ~400 km farther west through the Sea of Marmara (Okay and Tüysüz, 1999). It was formed as a result

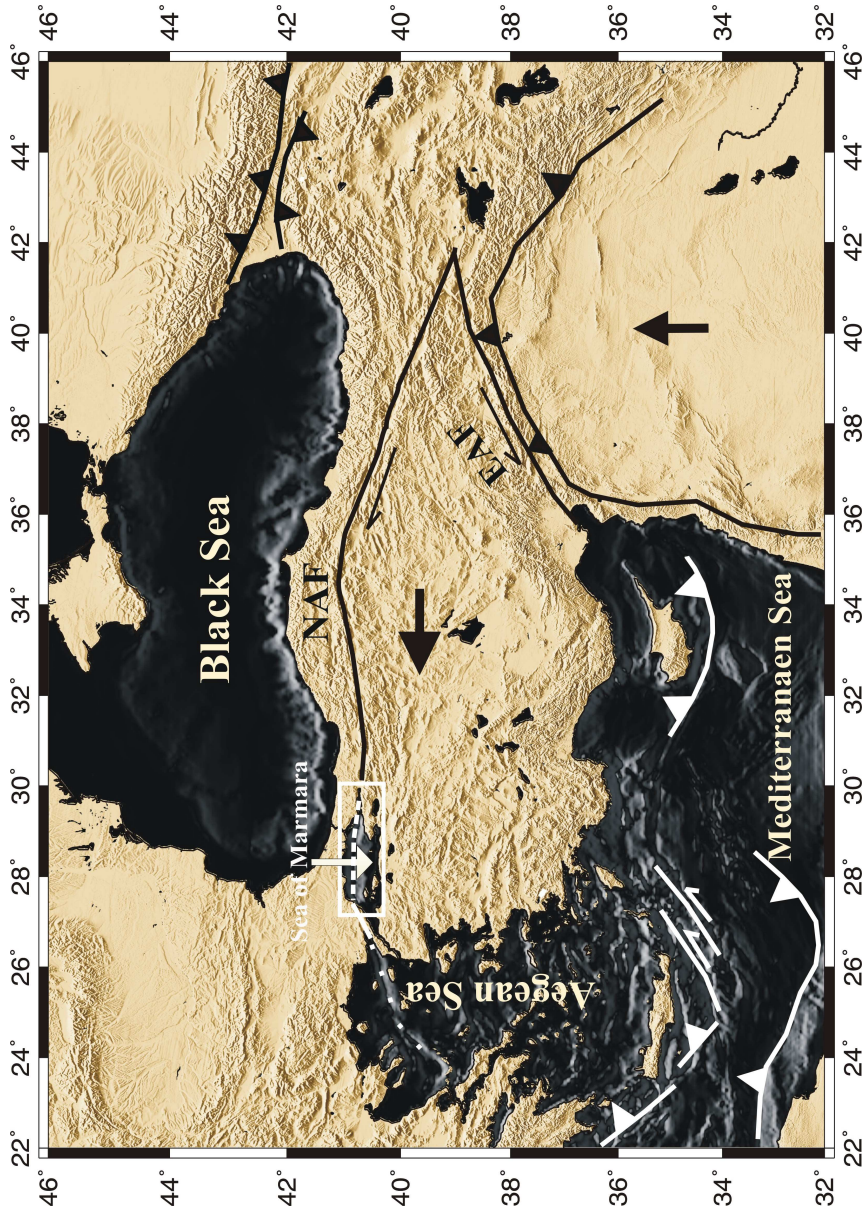


Figure 2.1 : Active tectonic map of the Eastern Mediterranean showing the geological setting of the Sea of Marmara. Lines with filled triangles show active subduction zones, lines with open triangles are active thrust faults at continental collision zones. The large solid arrows indicate approximate senses of motion of the lithospheric plates relative to Eurasia. EAF, East Anatolian Fault. Tectonic lines are redrawn from Okay et al. (2004).

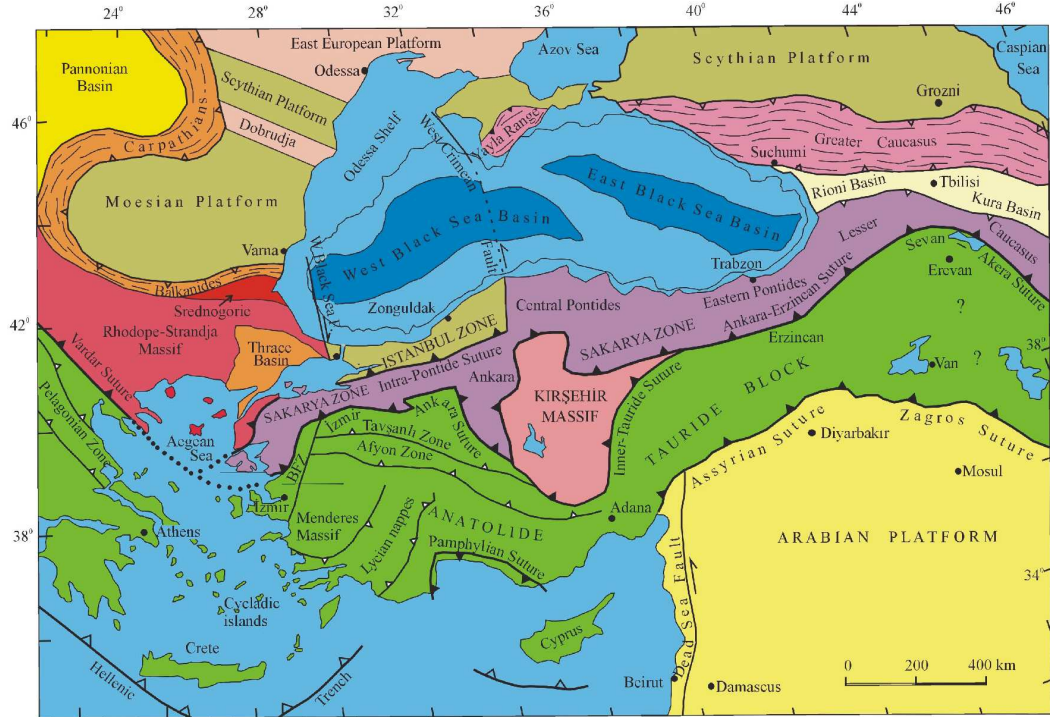


Figure 2.2 : Tectonic map of northeastern Mediterranean region showing the major sutures and continental blocks. Sutures are shown by heavy lines with the polarity of former subduction zones indicated by filled triangles. Heavy lines with open triangles represent active subduction zones. Small open triangles indicate the vergence of the major fold and thrust belts. BFZ denotes the Bornova Flysch Zone (Şengör, 1984; Okay, 1989; Okay et al., 1994; 1996, Okay and Tüysüz, 1999) (url-1).

of closure of a major embayment İzmir-Ankara-Erzincan Ocean. The Intra-Pontide suture consists of an east-west trending segment, used later in some parts by the North Anatolian Fault. The Intra-Pontide suture in the west is disguised under the Sea of Marmara and comes again onshore in the region of Şarköy in Thrace.

Various data including multi-beam bathymetry, multi-channel seismic and deep-towed seismic were acquired and interpreted in order to define the geometry of the North Anatolian Fault within the Sea of Marmara (Okay et al., 1999; 2000; Parke et al, 1999; Aksu et al., 2000; Rangin et al., 2001; İmren et al., 2001; Le Pichon et al., 2001; Armijo et al., 2002; Demirbağ et al., 2003; Carton, et al, 2007; Laigle et al, 2008; Becel et al., 2009). There are different suggestions related to the extension of the NAF to the east of the Marmara region. It was suggested that the NAF splits into three branches in the Marmara region (Barka and Kadinsky-Cade, 1988; Yaltrak, 2002). However, more recent studies (Le Pichon, 2001; Armijo et al., 2002; Meade et al., 2002 and Flerit et al., 2003) indicate two strands. Also different models were

proposed related to the nature of the NAF and formation mechanisms of the active structures under the Sea of Marmara.

Pınar (1943) had first suggested that three deep basins of the Sea of Marmara (Spindler, 1896) had been formed by a single fault between the Gulf of İzmit on the east and the trace of the 1912 earthquake fault on Gelibolu. Since then, several models have been suggested by different scientists (Pfannenstiel, 1944; Egeran, 1947; McKenzie, 1972). The recent proposed models for the extension of the North Anatolian Fault under the Sea of Marmara are:

- En-echelon fault segments models given in Figure 2.3 (Parke et al. 1999; Okay et al., 1999; 2000, Siyako et al., 2000)
- Pull-apart models given in Figure 2.4 (Barka and Kadinsky-Cade, 1988; Barka, 1992; Wong et al., 1995; Ergün and Özel, 1995; Armijo, 2002; Armijo et al., 2005)
- Single master fault models given in Figure 2.5 (Le Pichon et al., 2001; İmren, 2001; Demirbağ et al., 2003; 2007),

According to Wong et al. (1995), three basins of the Sea of Marmara are pull-apart basins and intervening areas are push-up structures originated from transpression. They suggested that the NAF branches into two overlapping, right stepping, oblique master faults at the eastern and western border of the Sea of Marmara. Observed neotectonic and sedimentary regime in the Sea of Marmara is the result of this nature of the NAF together with the compressional movement between Eurasia and Africa. The two major fault systems are called Northern Boundary Fault (NBF) and Southern Boundary Fault (SBF). Seyitoğlu and Scott (1991), and Seyitoğlu et al. (1992) suggested that the N-S extension in the Aegean had developed in the Early Miocene, before the NAF developed, and related this extension to the spreading and thinning of a previously thickened crust in an extensional arc environment. Wong et al. (1995) suggested that this extension inferred with the NAF in the Sea of Marmara and created wedge shaped transtensional pull-apart basins and intervening transpressional push-up structures in the Late Neogene to Quaternary. They explained the tectonic structure of the Sea of Marmara by five fault-bounded, tilted blocks created by en-echelon faults between two master transtensional faults.

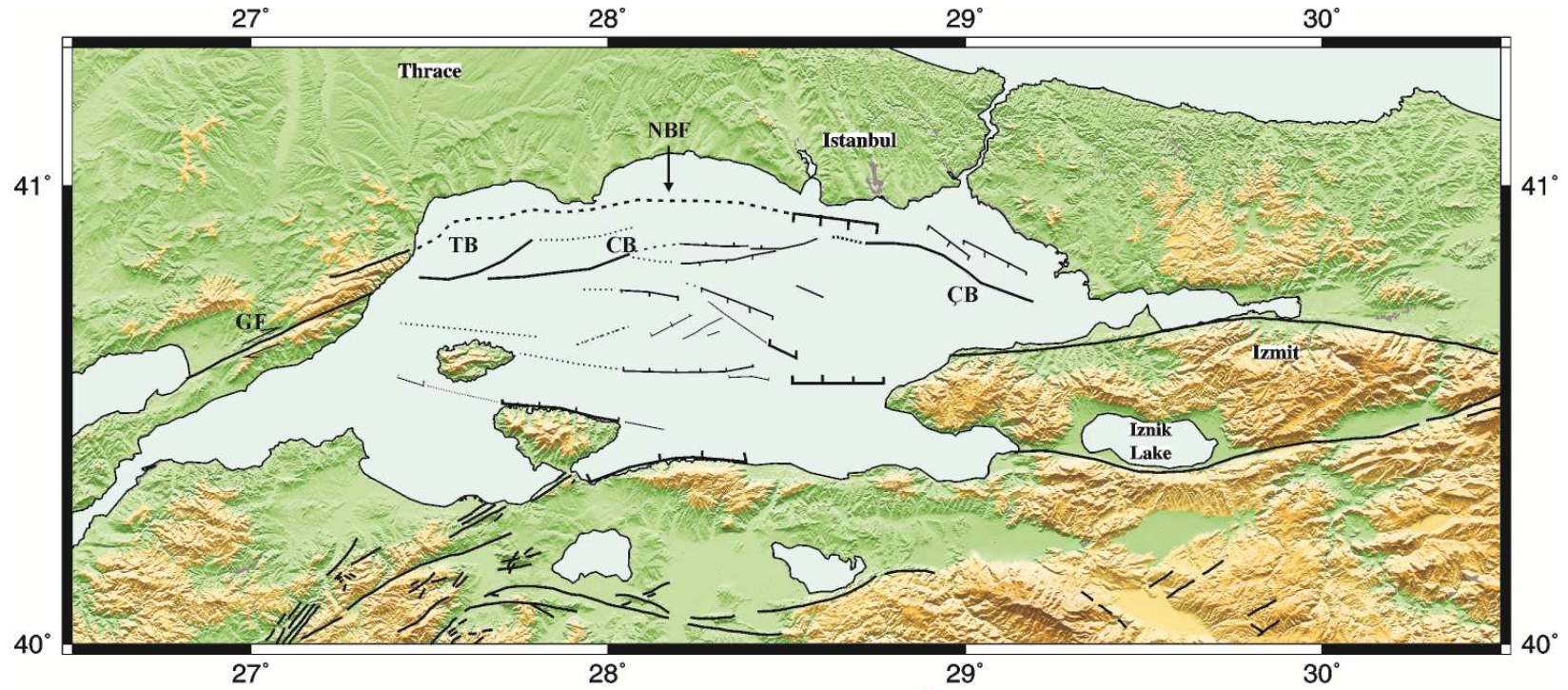


Figure 2.3: Fault map of the Sea of Marmara; en-echelon segments model, redrawn from Parke et al. (1999). Abbreviations: NBF: Northern Boundary Fault; TB: Tekirdağ Basin; CB: Central Basin; ÇB:Çınarcık Basin; GF: Ganos Fault.

But Parke et al, (1999; 2002) reported that, no evidence is found for the existence of a NBF along the Central and Tekirdağ Basins. They interpreted the results of the high-resolution seismic reflection survey conducted in the Sea of Marmara on September 1997 and supported the model that motion steps across the Sea of Marmara on a set of en echelon faults (Figure 2.3). They reported that it is difficult for a single strike-slip fault to account for the different styles of tectonic observation existing in the Sea of Marmara. They also suggested that the presence of the Sea of Marmara on the western end of the of the North Anatolian fault is a direct result of localized N-S extension and it is the consequence of the interaction between the strike slip motion on the North Anatolian fault and the onset of influence of the Hellenic Arc.

According to Armijo et al. (2002) in the Marmara region, the right lateral North Anatolian Fault splays into two branches, which are about 100 km apart, before entering the Aegean (Figure 2.4). They reported that, most of the lateral motion appears to be transferred obliquely northward from the main northern branch, across the large rhomb-shaped basin that the two branches meet. They termed the oblique submarine zone which forms a smaller pull-apart in the larger Marmara pull-apart as the North Marmara Fault System (NMFS). They interpreted the highs and basins in terms of this system. They suggested that, along this system, active faulting is segmented and it interconnects largest pull-apart basins the Çınarcık, the Central and the Tekirdağ Basins with the İzmit and Ganos faults on land.

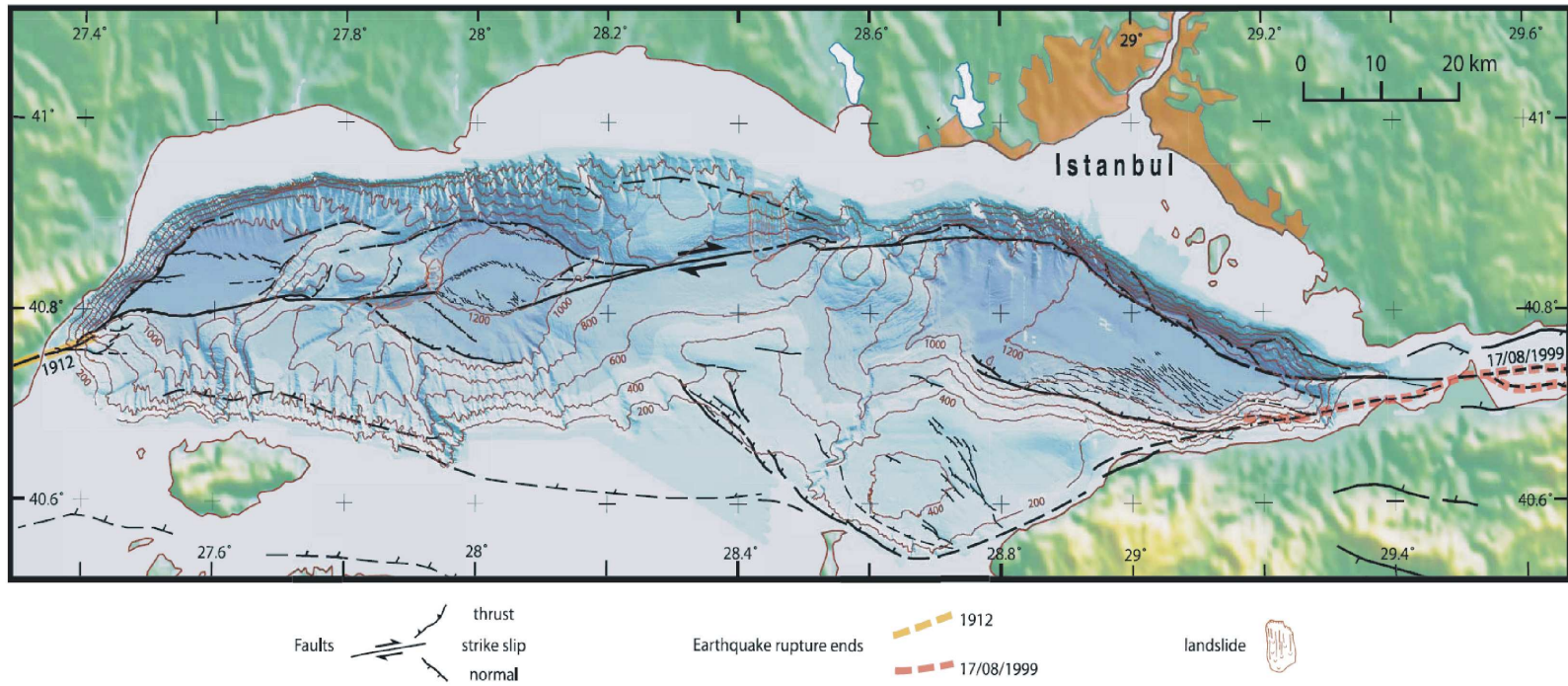


Figure 2.4: Faults in the Sea of Marmara; pull-apart basins model (Armijo et al., 2002). Abbreviations: MMF: Main Marmara Fault; ÇB:Çınarcık Basin; CB: Central Basin; TB: Tekirdağ Basin.

They described the kinematics in the Marmara pull-apart, by asymmetric slip separation in which one block boundary (NMFS) carries a greater strike-slip to normal ratio than others.

Le Pichon et al. (2001) interpreted the results of high-resolution bathymetric, sparker and deep towed seismic reflection data set collected by r/v Le Suroit of French IFREMER on the northern half of the Sea of Marmara. They prepared a detailed bathymetric and fault map (Figure 2.5) of the northern part of the Sea of Marmara and interpreted the extension of the North Anatolian fault under the Sea of Marmara as a single, through-going strike slip fault system connecting 08.17.1999 İzmit Mw=7.4 earthquake fault and 09.08.1912 Mürefte-Şarköy Ms=7.3 earthquake fault on the east (Figure 1.6). They called this fault as Main Marmara Fault and suggested that N-S to NNE-SSW active extensional structures probably indicate strain partitioning in the Sea of Marmara. According to the model, principal deformation zone (PDZ) follows northern margin on the easternmost part and southern margin in the Tekirdağ Basin.

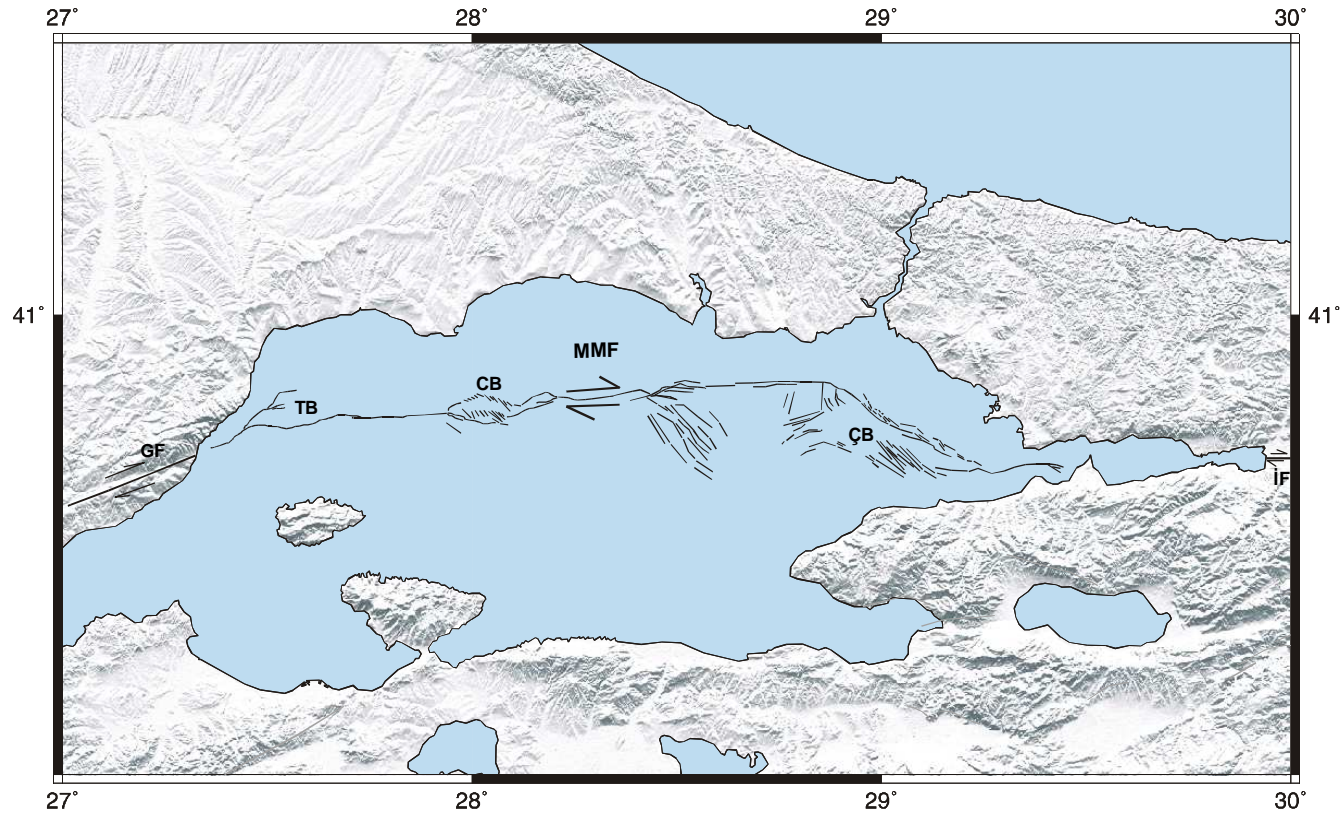


Figure 2.5: Faults in the Sea of Marmara; single master fault model (Le Pichon et al., 2001). Abbreviations: İF: İzmit Fault, MMF: Main Marmara Fault; ÇB:Çınarcık Basin, CB: Central Basin; TB: Tekirdağ Basin GF: Ganos Fault.

2.2 Deep Basins in the Sea of Marmara

The Sea of Marmara is a marine basin extending ~275 km in the E-W direction and ~80 km in the N-S direction with shallower shelf on the south and a deep trough on the north. There are three main deep basins separated with NNE-SSW trending 600 to 800 m deep highs on the northern trough. Those features are the Çınarcık Basin, the Central High, the Central Basin, the Western High and the Tekirdağ Basin from the east to the west, respectively (Figure 2.4).

The three basins had been explored after the r/v Selanik survey in 1894 (Spindler et al., 1896). But the data were not sufficient to determine the basin features in detail. Afterwards, different surveys were conducted by different groups to collect more data, such as the multi-channel seismic reflection data by Mineral Research and Exploration Institute of Turkey (MTA), the multibeam acoustic survey by the Department of Navigation, Hydrography and Oceanography of the Turkish Navy (SHOD), the National Marine Geology and Geophysics program by the Scientific and Technical Research Council of Turkey (TÜBİTAK). A complete bathymetric data of the northern Sea of Marmara was mapped by the Turkish-French collaborated cruise of r/v Le Suroit of French IFREMER and the main deep basins of the Sea of Marmara had become known in detail. In the next section, structures of those three main basins will be shortly described.

2.2.1 The Çınarcık Basin

The Çınarcık Basin is a wedge-shaped active transtensional basin (length: 50 km, width: 20 km, maximum seafloor depth: 1270 m). The surface area is 545 km². The Central Marmara Ridge in the west and steeply dipping submarine slopes in the north and south bound the Çınarcık Basin. In the east of the basin, the İzmit segment of the NAF ruptured by the İzmit earthquake with magnitude (M_w) 7.4, on 17 August 1999. It consists of nonuniformly distributed sediments having a maximum thickness of 6 km and more (Carton et al., 2007). The basin infill consists of syntransform sediments of Pliocene-Quaternary age (over 3 km) and undeformed basinal strata deposited during the post-Miocene activity of the NAF (Okay et al., 2000). Carton et al. (2007) reported that the distribution of sediments suggests an eastward migration of the main depocenter of the Çınarcık Basin. Based on the multi-channel seismic data collected in 1997 and 1999 by the Mineral Research and Exploration

Directorate (MTA), Okay et al. (2000) suggested that the Çınarcık Basin formed when the westward-propagating the NAF intersected a N-W trending pre-existing fault zone during the Pliocene forming a transform-transform-transform-type triple junction. Le Pichon et al. (2001) suggested that the Çınarcık Basin is a surface expression of active right-lateral faults based on high resolution bathymetric, sparker and deep-towed seismic reflection data set acquired by the French Ifremer r/v, Le Suroît. Based on the results of the SEISMARMARA (2001) seismic experiment, Carton et al. (2007) suggested that there is no indication in the data for a single through-going strike-slip fault, neither a cross-basin fault nor a pure strike-slip fault running along the northern margin as suggested by Le Pichon et al. (2001). They observed faster opening in the eastern part of the basin and basin-bounding faults with significant extensional component of motion along both north and south sides of the basin. They suggested that the Çınarcık Basin has developed as a transtensional basin across strike-slip segments of the northern NAF for the last few million years.

2.2.2 The Central Basin

The Central Basin is a complex structured basin of length 25 km, width 14 km and depth of 1250 m at its deeper part. Thickness of the sedimentary fill is estimated about 4725 m and its age is Miocene-Pliocene for deep-seated sediments and Quaternary to recent for shallow sediments (Demirbağ et al., 2007). There are two different tectonic models for the evolution of the depression zone in the Central Basin;

- (1) A model based on existence of a through going strike-slip fault causing a rotational depression zone (Le Pichon et al., 2001),
- (2) A model including a right stepping strike slip faulting causing a pull-apart basin (Armijo et al., 2002).

Demirbağ et al. (2007) produced a 3-D structural block diagram of the basin by means of bathymetric and seismic data. They could not observe normal faulting distributed oblique to the main strike-slip branches, which are expected to be developed in a strike slip system where two main branches of a strike slip fault have offset over a zone. Their results support the first tectonic model for the evolution of the depression zone in the Central Basin; a through going strike-slip fault causing a rotational depression zone suggested by Le Pichon et al. (2001).

2.2.3 The Tekirdağ Basin

The Tekirdağ Basin is a rhomb-shaped active strike-slip basin located between the Ganos Mountain (924 m) in the west and the Western High in the east. Its depth is around 1120 m and has an area of $\sim 85 \text{ km}^2$. Various studies have been carried on the Tekirdağ Basin using multi-channel seismic reflection, high-resolution bathymetric, sparker and deep-towed seismic reflection surveys (Okay et al., 1999; 2004; Le Pichon et al., 2001; Armijo et al., 2002; Parke et al., 2002; Seeber et al., 2004, Kanbur et al., 2007). It is bounded on one side by the NAF and on the other side by a sub parallel normal fault joining at depth along a major sub horizontal detachment fault. The basin represents a large negative flower structure. The extension of the NAFZ in the southern Thrace (45 km long) is called as the Ganos Fault. The strongly asymmetric basin consists of the syntransform strata of Pliocene and Quaternary age with thickness varying from a few tens of meters on the submarine slope to over 2.5 km adjacent to the North Anatolia (Okay et al., 1999). Most of the Pliocene-Quaternary sedimentary infill is terrigenous and most probably lacustrine. The flat floor of the depression lies at the water depth of -1150 m indicating a sudden change in facies from lacustrine sediments to deep-sea silts and clays as a result of flooding of the basin by the Aegean Sea during the late Pleistocene (Okay et al., 1999).

3. METHOD and DATA

3.1 Seismic Reflection Method

Seismic reflection and refraction surveys are commonly used by earth scientists to image the crustal structures. Seismic reflection methods are the most important tools for imaging the acoustic impedance differences. Progress in marine geophysics was rapid around early 1960's partly in response to the increasing demand for petroleum and other mineral sources necessary to sustain the rapid post-war industrial growth. Acquisition rates were slow since seismic receivers had to be kept stationary on the seabed while recording each shot. To speed up the field operations and extend exploration into deep water, much emphasis was placed on the development of methods to produce seismic profiles from a moving ship.

Marine seismic systems consist of a sound source towed behind the vessel within a few meters of the surface that produces sound pulses at a controlled frequency range at set time intervals. The sound pulse travels through the water column and penetrates the sea floor. Sound is partially reflected and refracted by each change in acoustic properties it encounters according to the Snell's Law. These waves return and are recorded by hydrophones towed further behind the vessel in a streamer or seismic cable or by recorders deployed on land or temporarily placed on the sea-floor (ocean-bottom seismographs). The vessel travels in a straight line at constant speed so the same point in the seabed can be measured repeatedly and the signals added during post-survey processing. Seismic lines are shot usually in intersecting groups so reflectors can be traced from line to line. Line spacing for reflection will depend on the purpose of the survey. In petroleum provinces, 2-D surveys tend to have closer line spacing or 3-D surveys are carried out where a relatively small area is crossed by two sets of parallel seismic lines several 10s of meters apart. The survey collects data at individual, evenly spaced shot points along the survey lines, so to give the section through the Earth's crust, the vessel moves forward at a fixed rate. The rate of movement depends on the purpose of the survey. Deep surveys require longer times for reflections to return from depth so shots occur at intervals of 9-20 or

even 30-60 seconds for refraction surveys and the vessel will move at speeds around 4-5 knots (Jones, 1999).

For the last decades, major advances in marine geophysics have been made, by providing seismic structure, first in two dimensions, then in three dimensions. Detailed seismic images of the earth within a few kilometres of the seabed have not only led to numerous petroleum discoveries but together with drilling, have brought about a much deeper understanding of how continental margins evolve. Also multi-channel seismic studies on both land and marine with recording lengths of 15 s two-way-travel time (twi) or more have provided seismic images of the entire crust beneath rifted margins and in several areas, the structure of the underlying mantle down to depths of several tens of kilometers (Figure 3.1). The upper parts of crystalline basement, down to depths of 10 km contain few reflectors. Lower crust contains many strong but discontinuous reflectors giving a laminated appearance to records.

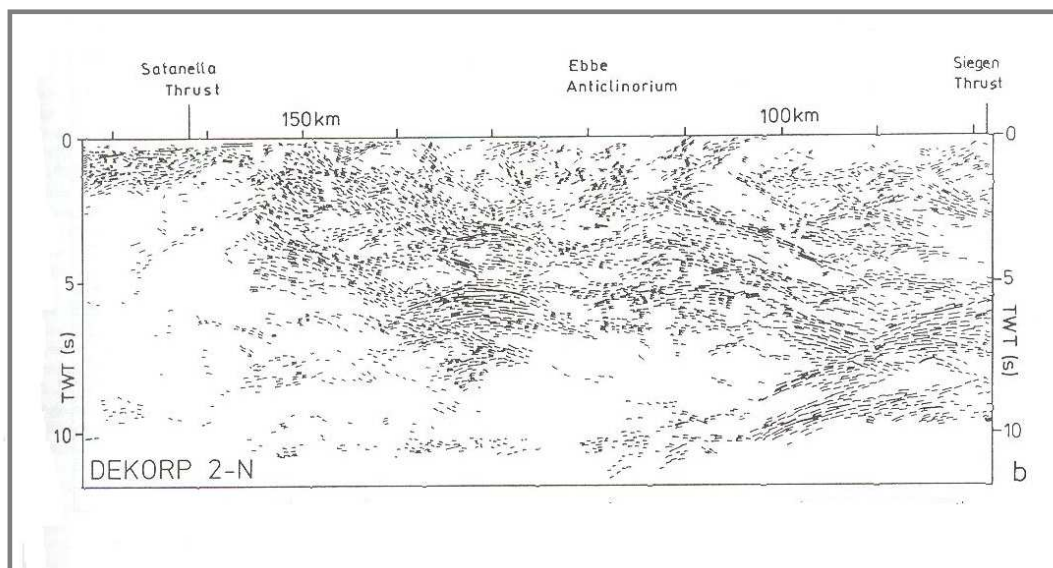


Figure 3.1: An example of deep crustal seismic reflections from DEKORP2 project from an area of thin-skinned tectonics (DEKORP Res. Group, 1985).

In the deep crustal seismic reflection studies, seismic energy source is an important parameter to define the depth and resolving power of the data. The ideal seismic source would produce a single, high-energy spike that is easily detectable in the presence of noise after travelling to the deepest parts of the Earth in limitation of the interest. Airguns are the most commonly used sources for seismic profiling at sea. They produce a wide range of pulse shapes. To provide broadband output signals, every 10-15 s, airguns of various sizes are grouped in arrays as peak energy

frequency decreases with gun size. Typically two source arrays are towed at depths of 3-10 m and are fired alternately. Gun positions are monitored by a GPS receiver and in a head buoy and by hydrophones, which receive pulses from a high-frequency (500-100 kHz) transducer to the ship. Several tens of guns with a total volume of ~1001 are used for petroleum surveys and for deep seismic profiling (Klemperer and Hobbs, 1991; Avedik et al., 1993). They deliver a peak pressure of >50 bar-m in the 12-128 Hz range which can be detected through ground waves in refraction studies (BABEL Working group, 1991). Triggering of the guns is timed so their initial high-energy pulses interfere constructively and the secondary bubble pulses suffer destructive interference. The spacing as well as the size of the guns is important in array design. If they are separated by less than one wavelength at the peak frequency the source waveform is affected by bubble interaction. Its effect on acoustic pressures can be computed and compensated for during data processing (Parkes et al., 1984).

3.2. Data Acquisition and Resolution

3.2.1 SEISMARMARA 2001 Project, deep seismic reflection data acquisition

Previous multi-channel seismic reflection surveys conducted in the Sea of Marmara were shallow targeted. Multi-channel seismic reflection data acquired by MTA Seismic-1 ship between 1997-2000 in the Sea of Marmara had high resolution for shallow depths. But due to the shallow penetration depths and small number of folds, it was not possible to recover the subsurface image beneath the first seabed multiple (İmren, 2003). Data acquisition parameters of the data are given in the Table 3.1.

In the scope of the thesis, a part of SEISMARMARA 2001 project deep seismic reflection data are processed. Turkish-French collaboration SEISMARMARA was carried on as a multi-task study in the Sea of Marmara in 2001, using combined multi-channel seismic reflection, refraction and earthquake data obtained from OBS and land stations. French Le Nadir, acquired more than 4000 km seismic reflection profiles in the Sea of Marmara using a 4 km long streamer with 360 channels. As the source, 12-air gun array with single bubble mode was used. The configuration provided a source of 8100 cu. in. or 2900 cu. in. capacity. “Single bubble” mode provides higher penetration depth with the same volume due to the low frequency content of the source bubble (Avedik et al., 1993).

Table 3.1: Acquisition parameters of multi-channel seismic reflection data acquired in the Sea of Marmara between 1997-2000 (İmren, 2003, Demirbağ al., 2007).

Data	1997a	1997b	1999	2000
Sampling (ms)	2	2	2	2
Record Length (s)	6	5, 8	5, 8	6
Number of Channels	72	72,84,96,108,120	48,60,72,84	48
Shot Interval (m)	50	50	50	50
Offset (m)	125	40, 50, 150	50	150
Fold	9	9-15	6-10	6
Station Interval (m)	12.5	12.5	12.5	12.5
CDP Interval (m)	6.25	6.25	6.25	6.25

SEISMARMARA project consisted of two legs; Leg 1 and Leg 2. In the Leg 1, data along 4 E-W directional and 30 crossing profiles were acquired (Figure 3.2). Leg 2, consisted of dense grid lines around the eastern Sea of Marmara, the Çınarcık Basin. For the thesis, parts of selected E-W and cross lines in the three deep basins, the Çınarcık, the Central and the Tekirdağ Basins are processed (Figure 3.3). Although lower source frequency of the data degraded the resolution, deeper penetration depths on the crustal scale were aimed while acquiring SEISMARMARA 2001 data. Data acquisition parameters of SEISMARMARA 2001 project, Leg 1 and Leg 2 surveys, are given in the Table 3.2.

Table 3.2: SEISMARMARA 2001 project, Leg 1 and Leg 2 data acquisition parameters.

Data	Leg 1	Leg 2
Sampling (ms)	4	4
Record Length (s)	17, 30	13
Number of Channels	360	360
Shot Interval (m)	50, 150	38
Fold	45, 15	60
Station Interval (m)	12.5	12.5
CDP Interval (m)	6.25	6.25

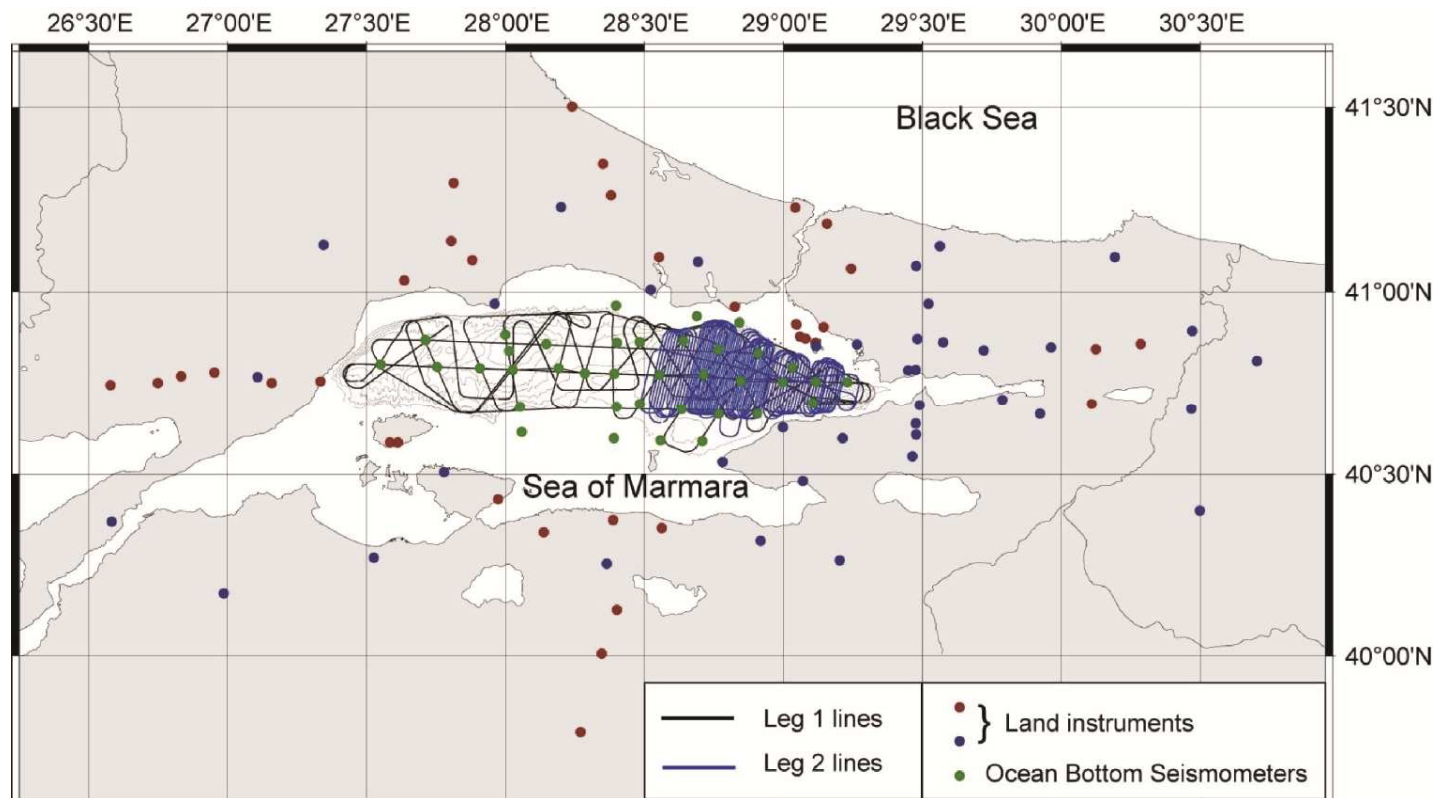


Figure 3.2: Location map for the SEISMARMARA 2001 lines (url-2).

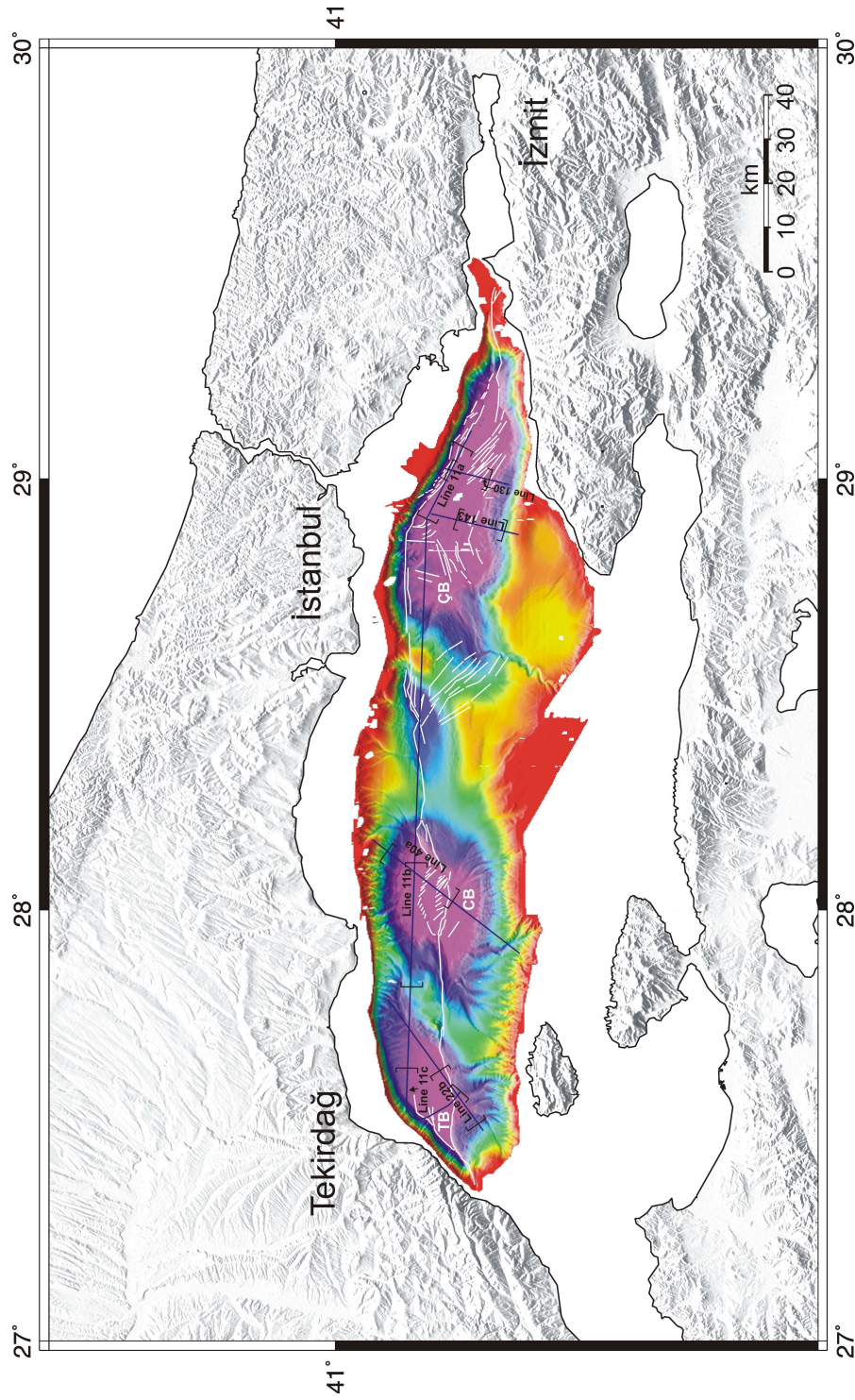


Figure 3.3: Location map for the processed SEISMARMARA 2001 lines in the Sea of Marmara including topography (NASA-SRTM) and bathymetry data (Le Pichon et al., 2001). Processed parts are shown in square brackets. Abbreviations are: TB: Tekirdağ Basin; CB: Central Basin; ÇB: Çınarcık Basin.

3.2.2 Data resolution

It is important to define limitations of the data in terms of resolution and penetration. In the next section, vertical and horizontal resolution concepts will be explained shortly. Sections related to the theory of the data process are compiled from Yılmaz (1987), McQuilin et al. (1984) and Bacon et al. (2003).

Seismic resolution is basically described as the shortest distance between two points which permits the points to be distinguished from each other. Resolution could be define in terms of vertical and lateral resolution. The measure of vertical resolution is wavelength whereas the measure of horizontal resolution is Fresnel zone.

3.2.2.1 Vertical resolution

There is a limit for shortest distance that the reflections coming from the upper and lower interface of a layer could be distinguished from each other. This limit is dependent on the thickness of the layer and related to the vertical resolution. Wavelength of a seismic wave is given by equation (3.1) as follows;

$$\lambda = \frac{V}{f} \quad (3.1)$$

In the equation, V denotes velocity, and f denotes dominant frequency. In the subsurface seismic P-wave velocities are generally between 2000 m/s and 5000 m/s and tend to increase with depth. Dominant frequency of seismic signal used in the seismic reflection experiments is generally between 20 and 50 Hz. This range differs on the purpose of the investigation. For example, this range is around 8-40 Hz for deep crustal reflection studies requiring deep penetration and it can be between 40-120 Hz for petroleum and gas industry reflection studies. Concerning the average frequency range mentioned above, typical seismic wavelengths are around 40 – 250 m and generally increase with depth. As wavelength determines the vertical resolution, to be distinguishable, deep units should be thicker than the shallow units. Plot of wavelength values for different frequencies as a function of velocity is given by Yılmaz (1987) in Figure 3.4.

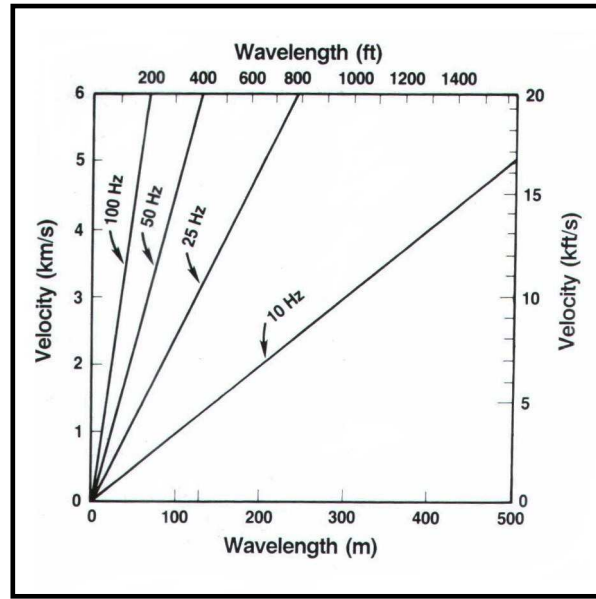


Figure 3.4: Wavelength values for different frequencies as a function of velocity (Yilmaz, 1987).

Threshold for the vertical resolution is given as the 1/4 of the wavelength. But this may vary according to the noise in the data. Threshold values of vertical resolution for different velocity and frequency values are given in Table 3.3.

Table 3.3: Threshold values for vertical resolution (Yilmaz, 1987).

V (m/s)	f (Hz)	$\lambda/4$ (m)
2000	50	10
3000	40	18
4000	30	33
5000	20	62

Vertical resolution of SEISMARMARA data for a sea-bottom at 1200 m is around 36 m.

3.2.2.2 Lateral resolution

Lateral resolution is the shortest distance that two points located side by side could be distinguished as two individual points. If we consider the wave front which hits to the A- A' horizontal reflector in Figure 3.5, this reflector could be assumed as continuous point diffractors. For a random source and receiver point (S), arrival time of energy from the subsurface (O) is $t_o = 2Z_o/V$. If we consider the wave front to move as much as $\lambda/4$, arrival time of the energy from A or A' points to the receiver is

$t_1 = 2(Z_0 + \lambda/4)/V$. Energy, from an area of radius OA' arrives to the receiver from each points of the area at a time between defined to and t_1 . Total energy arriving in the time range of $(t_1 - t_0)$ causes constructive interference. Here $A-A'$ reflection circular area is defined as the first Fresnel Zone (Sheriff, 1984). Two reflecting points meeting in this zone are not distinguishable in the observations from the surface.

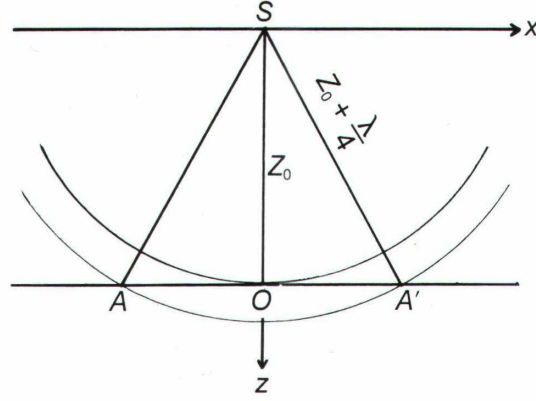


Figure 3.5: Fresnel Zone AA' in (x, z) space (Yilmaz, 1987).

Fresnel zone is also dependent on frequency due to its dependency of wavelength. If a seismic wave moving through a wave front has relatively high frequencies, then its Fresnel zones would be relatively narrow. As Fresnel zone widens, it becomes more difficult to distinguish two points from each other. Lateral resolution is also dependent on the depth of the reflective interface. Radius of the Fresnel zone is given in the equation (3.2),

$$r = \frac{V}{2} \sqrt{\frac{t}{f}} \quad (3.2)$$

Radius of the first Fresnel zone of SEISMARMARA data for a sea-bottom at 1200 m is around 300 m.

3.3 Data Processing Steps

Seismic data processing can be characterized by a sequence of steps where for each of these steps a multitude of different approaches exist. As there are various ways to acquire seismic data and also a variety of objectives for which the data can be used, processing steps are not the same for each data group. The typical data processing steps applied to the data in this thesis are shortly described in Figure 3.7.

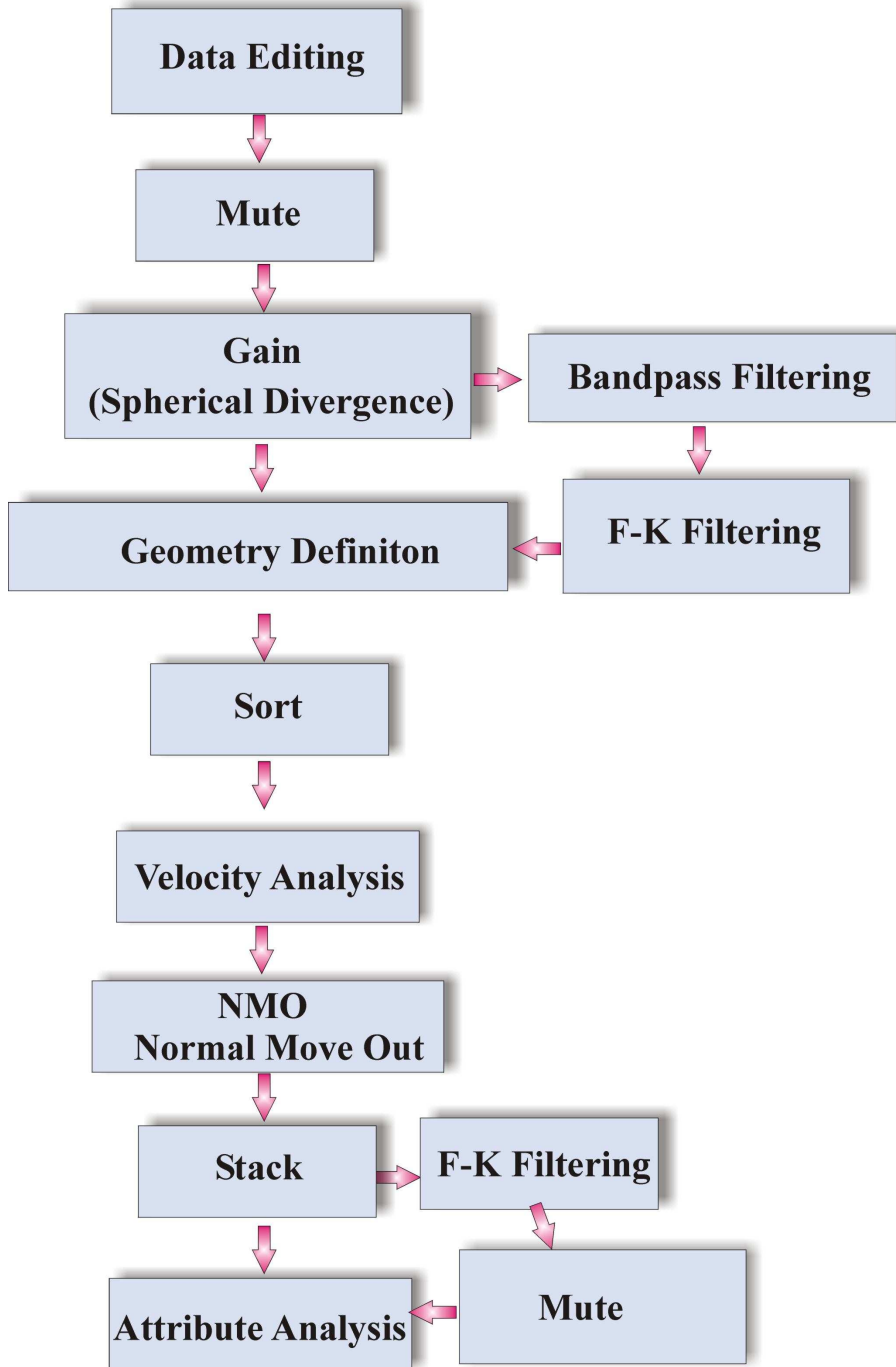


Figure 3.6: Flow diagram of data processing steps applied to the data used in the thesis.

TUBITAK-MAM provided the data used in the thesis as the Turkish team member of the Turkish-French collaboration SEISMARMARA project. The data on DVD's (Digital Versatile Disc) were transferred to Sun-Solaris platform without a format conversion, in .dsk format. They are processed in the Nezihi Canitez Data Processing Laboratory of İstanbul Technical University using Disco-Focus data processing package. Large size of the data was the main difficulty during the data processing. For example; one 15 s twt line uses the storage of five 3 s twt lines of the same

length. In other words, one deep line is equal to 3-5 shallow lines in terms of the storage, data processing work and consumed time. The long data caused to spend more time than with the normal size data, forced the limits of the system and produced storage problems. But they reveal valuable information from the deeper parts of the Earth.

3.3.1 Editing

Editing is applied to data in order to omit (drop) or kill (to zero the amplitude of the trace) or reverse the trace amplitude polarity of noisy traces caused by the inconvenient survey area conditions to prevent data to be distorted later due to the effects of bad traces. To choose the traces to be edited, traces from all shots are visually checked. An example from processed data is given in Figure 3.7. Traces with arrow are edited during data processing.

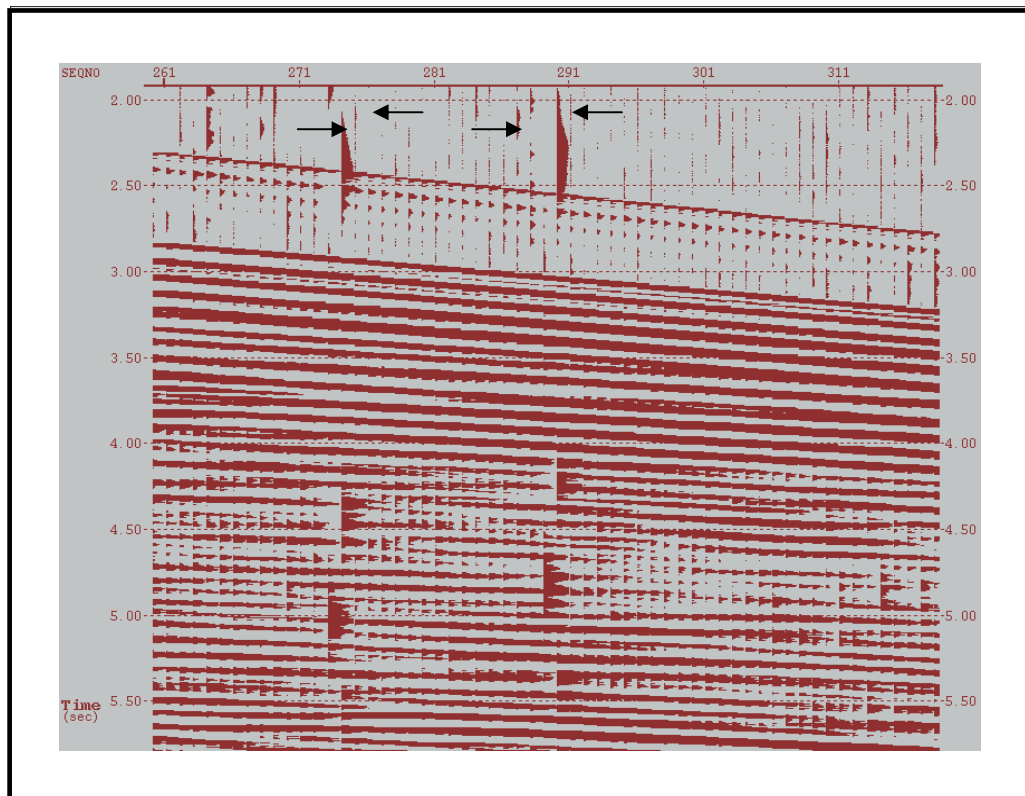


Figure 3.7: An example of edited traces in the processed data.

3.3.2 Mute

Muting is a method of reducing the amplitudes of portions of the traces to zero to eliminate undesirable components of the data. Mute can be applied at different stages of data process and also performs muting based on NMO stretch.

3.3.3 Gain

Gain is a time-variant scaling in which the scaling function is based on a desired criterion. Another gain application is for spherical spreading correction. Wave amplitudes decay as $1/r$, where r is the radius of the spherical wave front. This is true for a homogeneous medium without attenuation. For a layered earth model, amplitude decay can be described approximately by $1/[v^2(t) \cdot t]$ (Newman, 1973). Here, t is the two-way travel time, and $v(t)$ is the root mean square (rms) P-wave velocity of the primary reflections. Therefore, the gain function for geometric spreading compensation is defined by the following equation,

$$g(t) = \left[\frac{V(t)}{V(0)^2} \right] \cdot \left[\frac{t}{t(0)} \right] \quad (3.3)$$

where $v(0)$ is the velocity at specified time $t(0)$. To process the data acquired in the Sea of Marmara data, spherical divergence correction is applied. Interactive velocity analysis is used to derive the velocity function for the correction.

3.3.4 Statics correction

For the marine data, as the source and streamer are towed at the constant depth, the only statics correction needed is a constant shift of all the records to convert twts to what they would have been with shots and receivers at the sea surface. The correction is simply,

$$\frac{(ds + dr)}{V} \quad (3.4)$$

Where ds is the source depth, dr is the receiver depth and v is the velocity of sound in the seawater. For the processed data in the thesis, as the streamer and guns were at a depth of 20-25 m, statics correction of 30 ms is applied to the data.

3.3.5 Frequency filtering

Frequency filtering can be in the form of band-pass, band-reject, high-pass (low-cut), or low-pass (high cut). Band-pass filtering is the most widely used one because a seismic trace typically contains some low-frequency noise, such as ground roll and some ambient noise and some high frequency ambient noise. The usable seismic energy generally is confined to a bandwidth of approximately 10 to 70 Hz, with a dominant frequency around 30 Hz. Band-pass filtering can be performed in various stages in data processing. During processing the data, band-pass filtering between 9-10 Hz and 75-85 Hz is applied to the data. It is observed to improve the quality of the data.

3.3.6 F-K filtering

Events that dip in the (t, x) plane can be separated by their dips in the (f, k) plane. (Yilmaz, 1987). This allows us to eliminate certain types of unwanted energy from the data. By using 2-D Fourier transformation a wave field can be decomposed into its plane-wave components. Each plane wave carries a monochromatic signal which propagates at a certain angle from the vertical. Events with the same dip in the (t, x) plane are mapped onto a single line in the radial direction on the (f-k) plane. In the data, f-k filtering is applied to eliminate dipping noise. The same dipping noise existed for all the lines processed. An example to those is given in Figure 3.8. In Figure 3.9, data in (x, t) domain and and its (f-k) spectrum is given before and after f-k filtering.

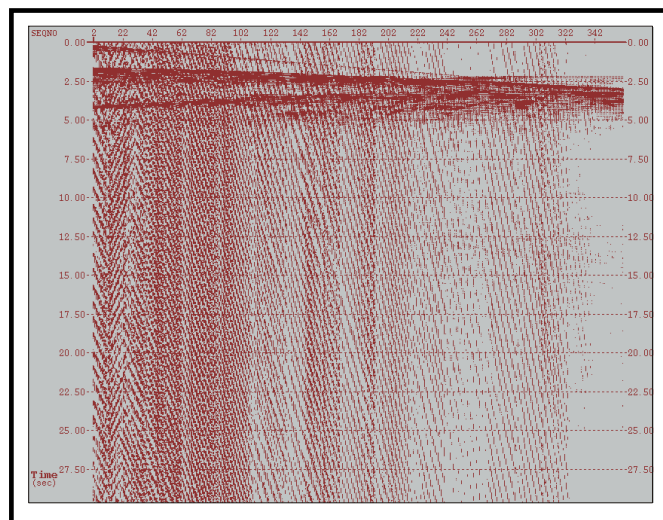


Figure 3.8: Raw data with noise (Line 22b in the Tekirdağ Basin).

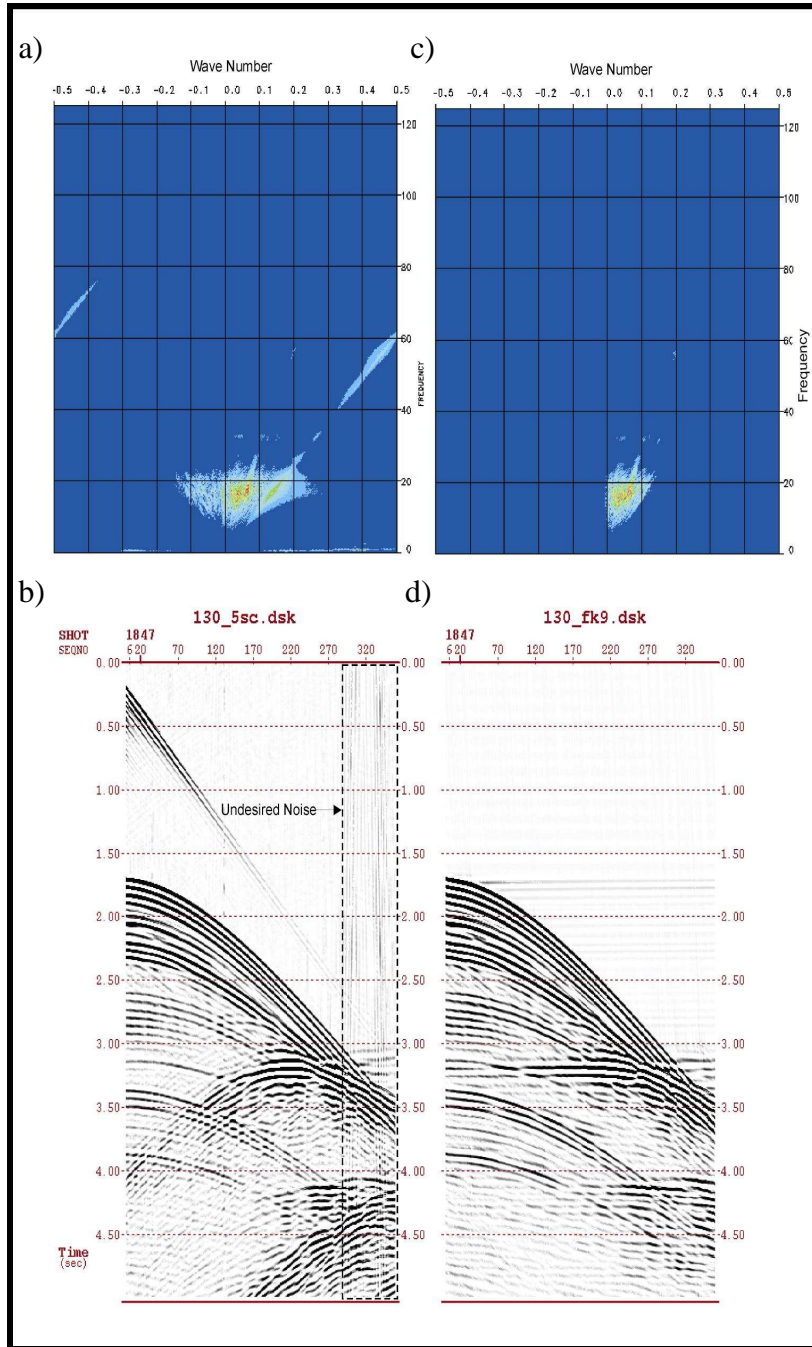


Figure 3.9: Application of f-k filter to the data: a) f-k spectrum of the data before filtering, b) data in (x-t) domain before filtering, c) f-k spectrum of the data after filtering, d) data in (x-t) domain after filtering (before filtering, mute is also performed).

Parameters to apply for the filter are chosen after f-k spectrum analysis. By selecting pass or reject zones, which are defined by corner k-f values, undesired noise (Figure 3.9.b) is highly eliminated.

3.3.7 Geometry definition

Geometry definition is independent from the digital data. By defining geometry, source, receiver locations, offset information are provided and written to the trace headers. Exact geometry information is required for the transformation of shot-receiver to midpoint-offset coordinates.

3.3.8 Sort

After initial data processing steps, the data are transformed to midpoint-offset coordinates. Seismic data acquisition with multifold coverage is done in shot-receiver coordinates whereas seismic data processing is done in midpoint-offset coordinates. This coordinate transformation is achieved by sorting data into common midpoint (CMP) gathers. Each individual trace is assigned to the midpoint between the shot and receiver locations associated with that trace. Those traces with the same midpoint location are grouped together making up a CMP gather. CMP gather is equivalent to a common depth point (CDP) gather where reflectors are horizontal and velocities do not vary horizontally.

3.3.9 Velocity analysis

Velocity analysis is performed on selected CMP gathers or groups of gathers. The output from one type of velocity analysis is a table of numbers as a function of velocity versus two-way zero offset time (velocity spectrum). Computed velocities can in turn be used to correct for normal move-out (NMO), so that the reflections are aligned in the traces of a CMP gather before stacking. There are different methods for velocity analysis such as t^2 - x^2 velocity analyses, constant velocity scans of a CMP gather (Yilmaz, 1987). It is important to obtain a reliable velocity function to get the best quality stack of signal. Velocity analysis of the data is performed using interactive velocity analysis of Disco-Focus program package by picking best fitting hyperbolas for every 100 CDP group. Obtained velocity functions are used in the NMO correction and stack.

3.3.10 NMO and stack

Once the velocity structure is known, then the gathers can be corrected for the NMO. As twt increases, NMO correction will increase. Therefore, the upper part of a trace is shifted further by the NMO correction than the lower part. This results in a

stretching of a trace causing a shift to lower frequencies. The effect can be severe on the large offset traces at small twt. This is the reason of muting these portions of the data. After the NMO correction, the traces of the CMP gather can be added together to form stacked trace. This improves the ratio of signal to random noise by \sqrt{n} , where n is the number of fold. Fold is calculated using following equation,

$$n = \frac{(Number\ of\ Channels\ .\ Station\ Interval)}{2\ .\ Shot\ Interval} \quad (3.5)$$

The stack may also be effective in suppressing multiples, because their NMO's are different from that of primaries at the same twt. Usually modern marine data have a high fold of stack, and the multiples under corrected for the NMO, will be smeared out, and at least partially attenuated (Yilmaz, 1987).

3.3.11 Attribute analysis

A seismic trace can be expressed as a complex function (Taner et al., 1979). The real part is the recorded seismic signal itself. The imaginary part is the quadrature, which is simply the 90-degree phase-shifted version of the real part. The quadrature trace is the Hilbert transform of the real part (Bracewell, 1965). After obtaining the complex seismic trace, we can easily compute so called instantaneous attributes associated with the seismic signal. The instantaneous amplitude measures the reflectivity strength $R(t)$, which is proportional to the square root of the total energy of the seismic signal at an instant of time (t) ;

$$R(t) = \sqrt{[x^2(t) + y^2(t)]} \quad (3.6)$$

Where $x(t)$ is the real part of the signal, $y(t)$ is the quadrature.

Before estimating the instantaneous parameters, the amplitude and frequency content of the signal must be preserved in each processing step. In the data used in the thesis, attribute analysis is performed to obtain enhanced sections of reflection strength where distinct reflections are observed.

3.4 Rheological Implications of Obtained Crustal Reflection Patterns and Comparison for Three Basins of the Sea of Marmara

Multi-channel reflection profiles with recording length of 15 s twt or more provide seismic images of the entire crust and in several areas, the structure of the underlying mantle down to the depths of several tens of kilometers. In the Sea of Marmara, the first deep multi-channel seismic reflection data were acquired in the SEISMARMARA 2001 project. For the thesis, three E-W, four NE-SW extended lines of the SEISMARMARA 2001 project in the Sea of Marmara are partially processed. Different high-resolution images of the three main basins of the Sea of Marmara have already been presented (Seeber et al, 2004; Demirbağ et al., 2007; Carton et al., 2007). This study focuses on the deep crustal reflections in the Sea of Marmara. Deep crustal reflection patterns and their rheological implications of the three deep basins in the Sea of Marmara are compared as relative to each other. In order to make this comparison properly, the same data processing steps are applied to all data. In this section, obtained deep crustal stack sections of three basins are presented.

3.4.1 The Tekirdağ Basin

Data acquisition parameters of Line 22b and Line 11c (Figure 3.3) are as follows:

Line 22b	Line 11c
Number of channels: 360	Number of channels: 360
Record length: 17 s	Record length: 30 s
Shot Interval: 50 m	Shot Interval: 150 m
Fold: 45	Fold: 15
Processed line length 14330 m	Processed line length 22500 m

After processing steps mentioned in the section (3.3) are applied, stack section of the Line 22b is obtained (Figure 3.10 a). In the stack section strong reflections are obtained until ~7.5 s twt. After this level, a transparent area is observable. Between 10 and 12 s twt northeast dipping reflection packages are visible. They are possible

reflections from the Moho level. Interpreted seismic stack section of the Line 22b is given in Figure 3.10 b.

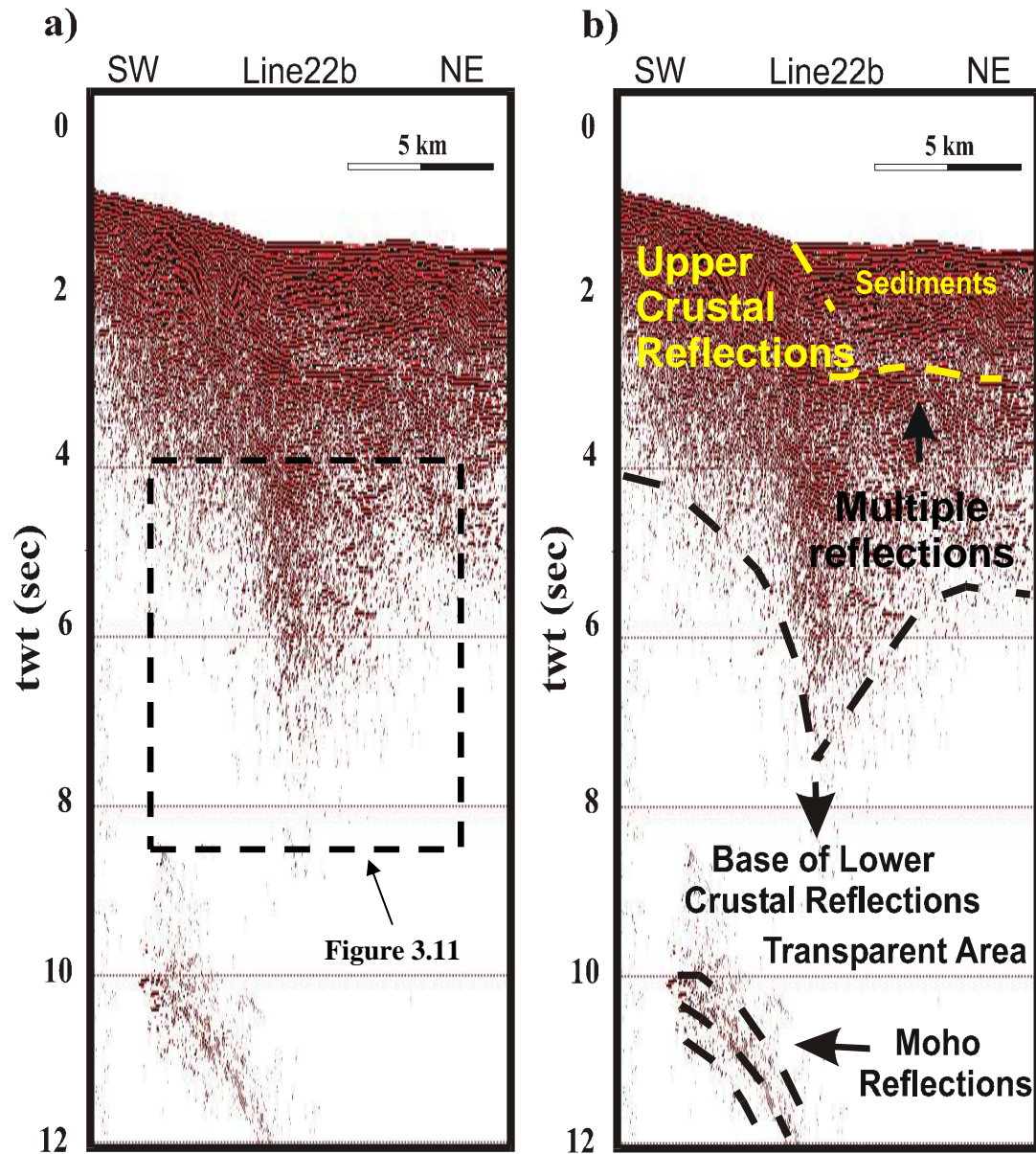


Figure 3.10: a) Stacked and b) interpreted stacked section of Line 22b in the Tekirdağ Basin.

Reflection strength image of the stacked section between ~5.3 and 8.3 s twt for a distance of 10 km is also obtained (Figure 3.11). In the reflection strength section, the boundary between the strong reflections (red and green color in Figure 3.11) and the area of transparent reflectivity (blue color in Figure 3.11) is more visible.

Line 11c starts in the E-W direction and changes direction to NW-SE after the gyration of the ship (Figure 3.3). The level of strong deep crustal reflections extend ~7.5 s twt (Figure 3.12). In the middle and eastern part of the section, reflections from the dipping units of the western slopes of the Tekirdağ Basin are visible. Below this level, there is again an area of weak seismic reflectivity. The depth to the bottom of the strong visible seismic reflections is nearly the same for two crossing lines in the Tekirdağ Basin, Line 22b and Line 11c. Interpreted stack section of Line 11c in the Tekirdağ Basin is given in Figure 3.13.

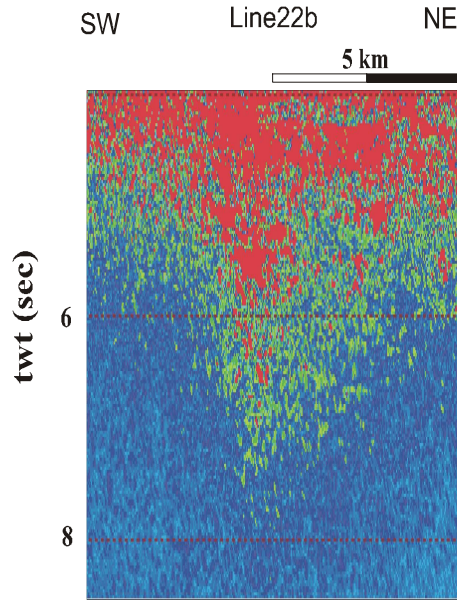


Figure 3.11: Reflection strength section of a part of Line 22b in the Tekirdağ Basin (square area in Figure 3.10 a).

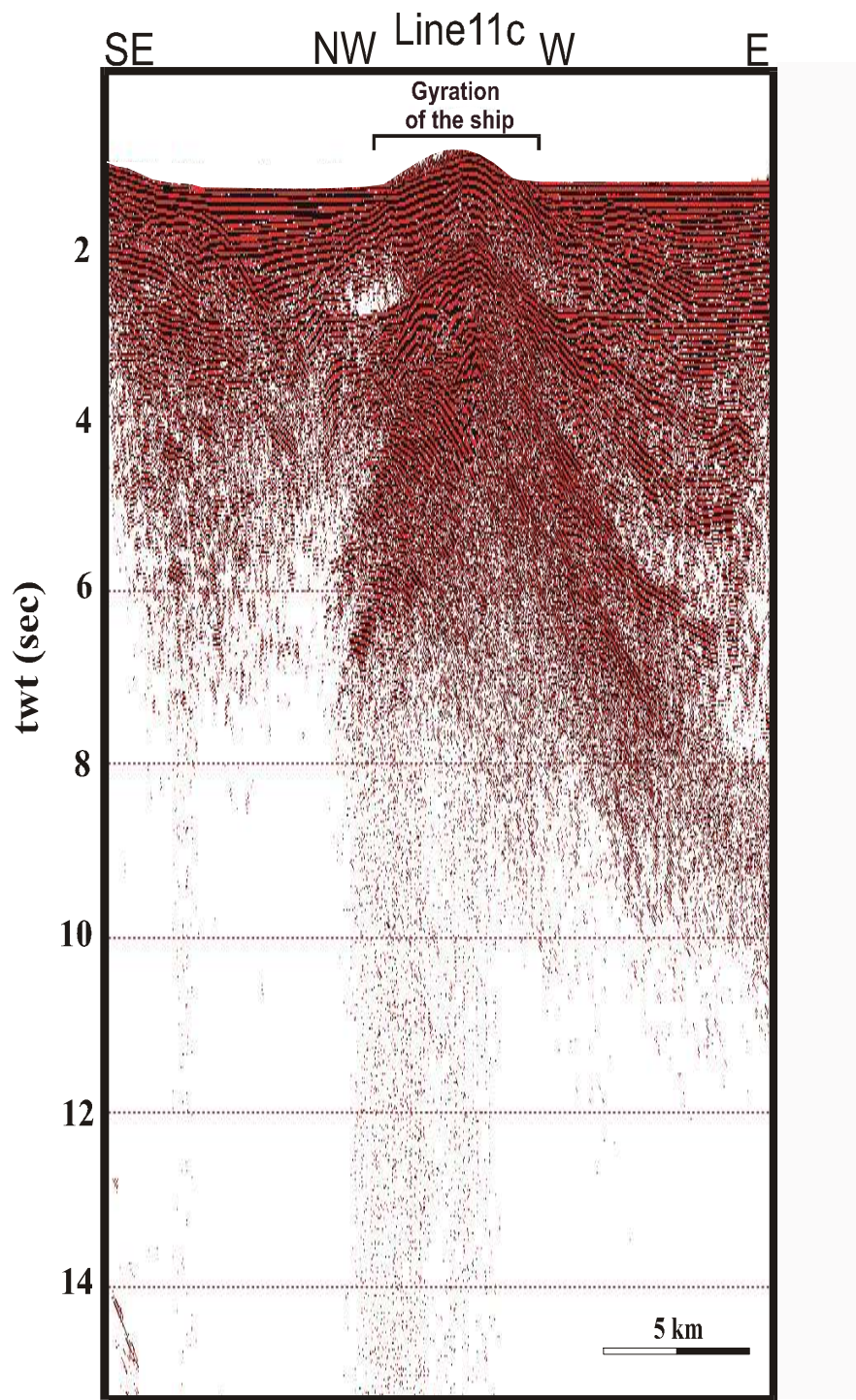


Figure 3.12: Stacked section of Line 11c in the Tekirdağ Basin.

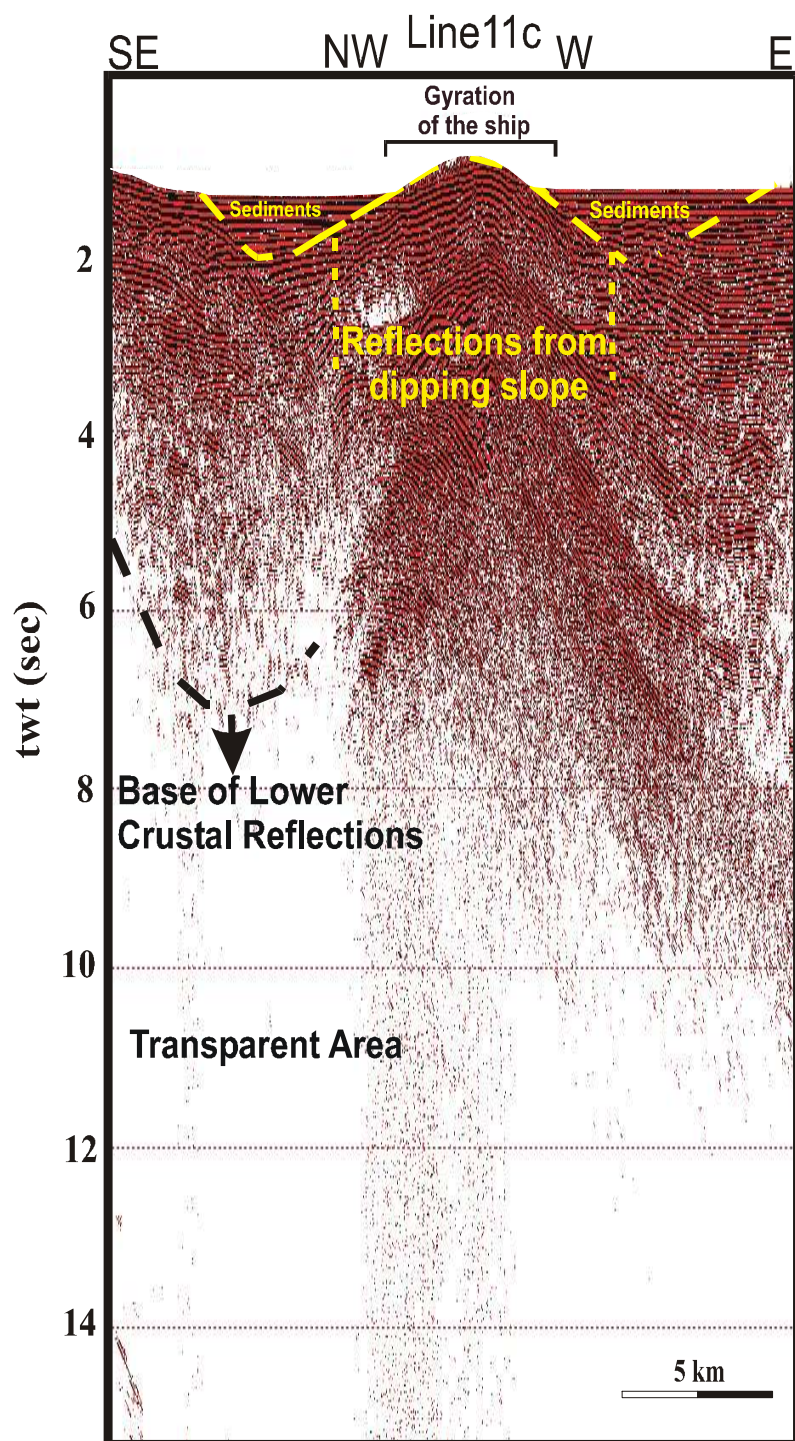


Figure 3.13: Interpreted stacked section of Line 11c in the Tekirdağ Basin.

3.4.2 The Central Basin

Data acquisition parameters of Line 40a and Line 11b (Figure 3.3) are as follows:

Line 40a	Line 11b
Number of channels: 360	Number of channels: 360
Record length: 17 s	Record length: 30 s
Shot Interval: 50 m	Shot Interval: 150 m
Fold: 45	Fold: 15
Processed line length 19437 m	Processed line length 31437 m

Complexity of the upper crustal part of the Central Basin, which corresponds to central depression, is described detail recently (Demirbağ et al., 2007). Deep seismic reflections of Line 40a on the stacked section are also quite complex (Fig 3.14 and Fig 3.15). On the southwest part of stack section of the Line 40a, strong reflections are visible at the 8 s twt. On the northeastern part of the section strong reflections between 8 and 10 s twt for a width of 5 km are visible. Beneath those reflections, diffuse reflections continue to the deeper parts of the section. A transparent zone is visible between 6-8 s twt of the southwestern side of the section. This zone continues towards northeastern part and visible to the deeper parts of the section as a transparent zone. Magnified images of the section in squares are obtained to have a closer look at the strong reflections. Magnified images of the upper and lower square areas in Figure 3.14 are given in Figure 3.16 and Figure 3.17. Reflection strength section for Figure 3.17 a is also presented in the Figure 3.17 b. As we examine the magnified images, we see the continuation of the reflections in the mentioned areas. In the reflection strength section also, high reflective area between 8-10 s twt becomes more visible. Interpreted stacked section of Line 40a is given in Figure 3.15.

In Figure 3.18, seismic reflection stack section of E-W directional Line 11b is presented. Around 6 s twt, strong reflections start to weaken and after around 8 s twt, they diminish even more. After this time limit, for the eastern part of the section no visible reflections exist. But for the western part, between 10.5 s twt and 12 s twt, there is another visible reflections area. This area is visible on the interpreted stacked

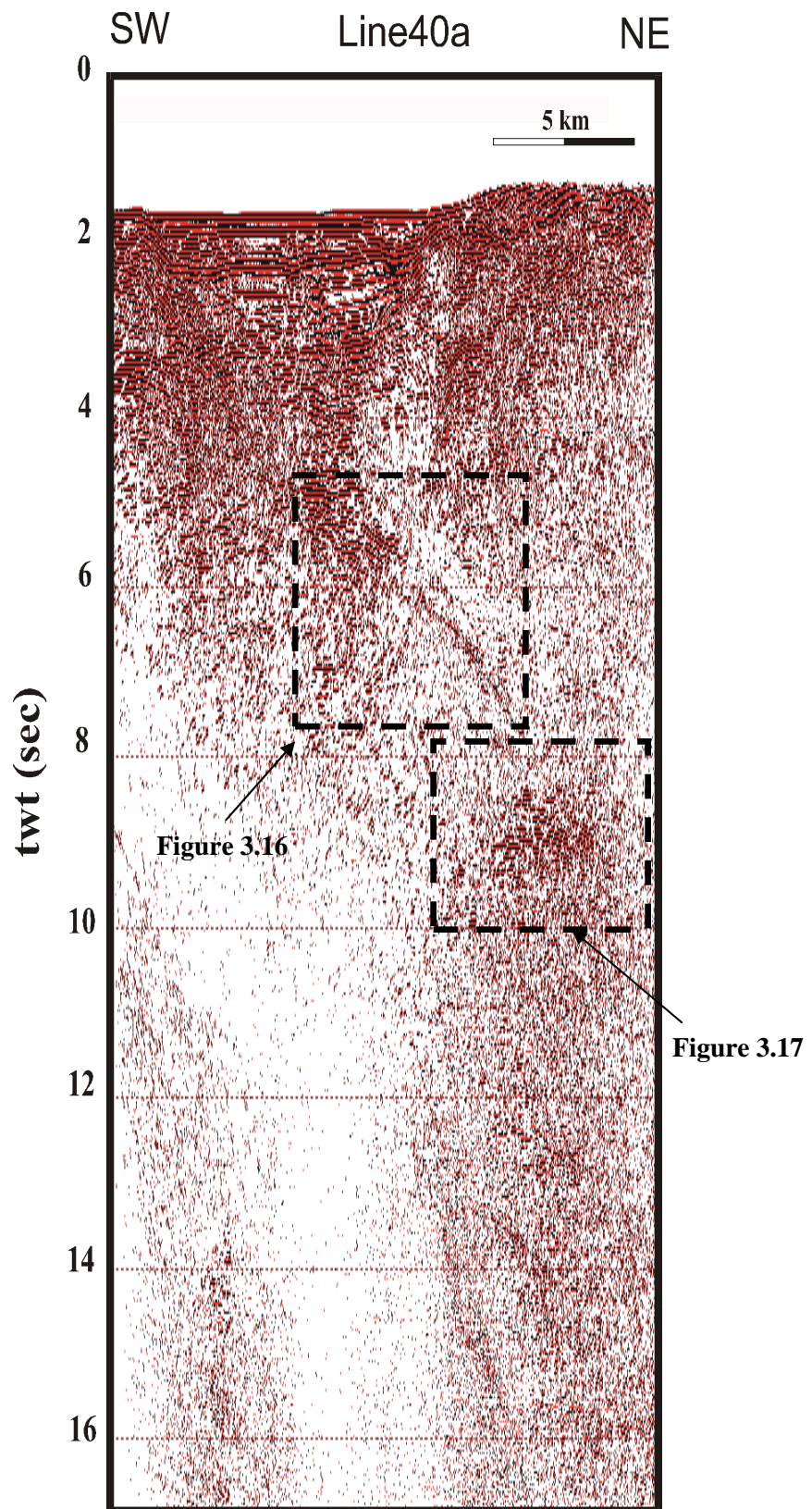


Figure 3.14: Stacked section of Line 40a in the Central Basin.

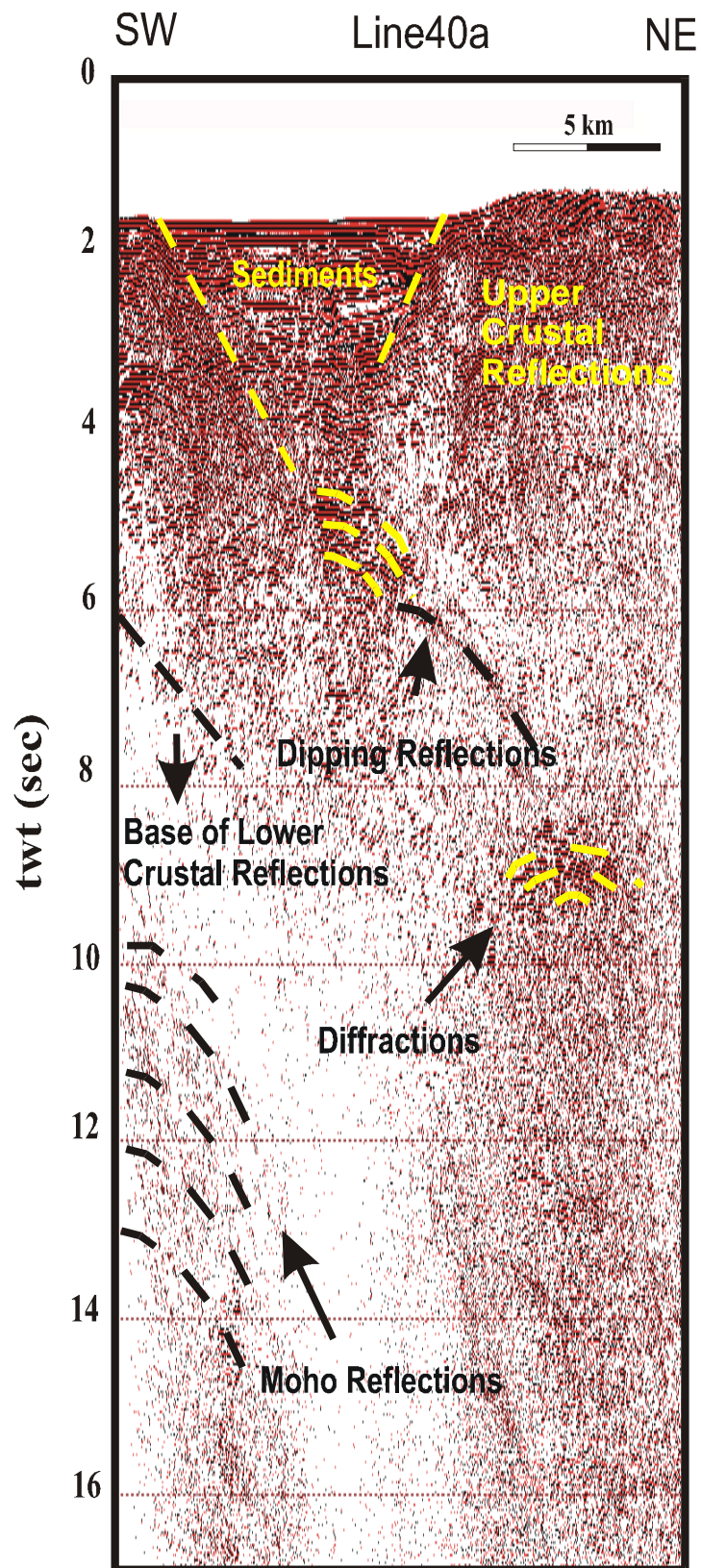


Figure 3.15: Interpreted stacked section of Line 40a in the Central Basin.

section of Line 11b (Figure 3.19) and also on the reflection strength section as seen in Figure 3.20. Depth extend of the strong reflections are consistent with those obtained from the crossed-line, Line 40a (Figure 3.15), which is around 7.5 s twt for the lower crustal reflections (Figure 3.15). Reflection packages around 10.5 s twt are visible on the both sections. On the E-W section, the zone where upper crustal reflections diminish is more clear.

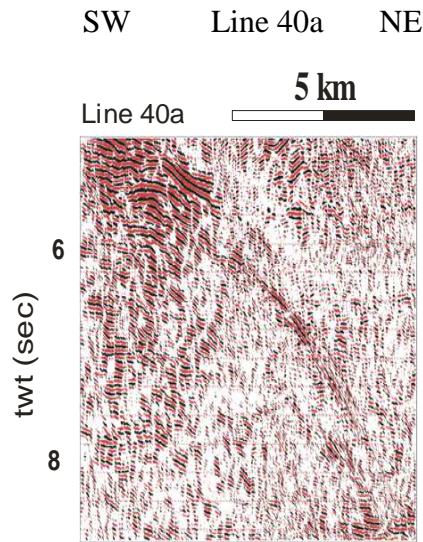


Figure 3.16: Magnified image from the stacked section of Line 40a in the Central Basin between ~4.3 and 8.3 s twt.

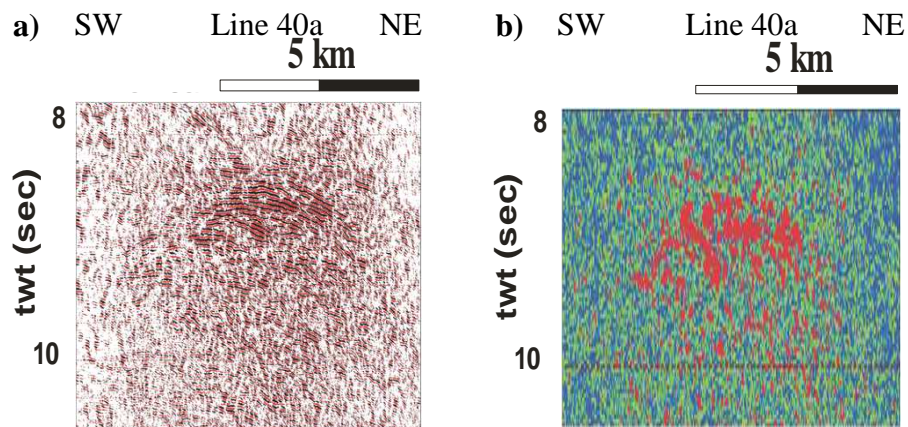


Figure 3.17: a) Magnified image from the stacked section of Line 40a in the Central Basin between ~8 and 10 s twt and b) reflection strength of the area between ~8 and 10 s twt.

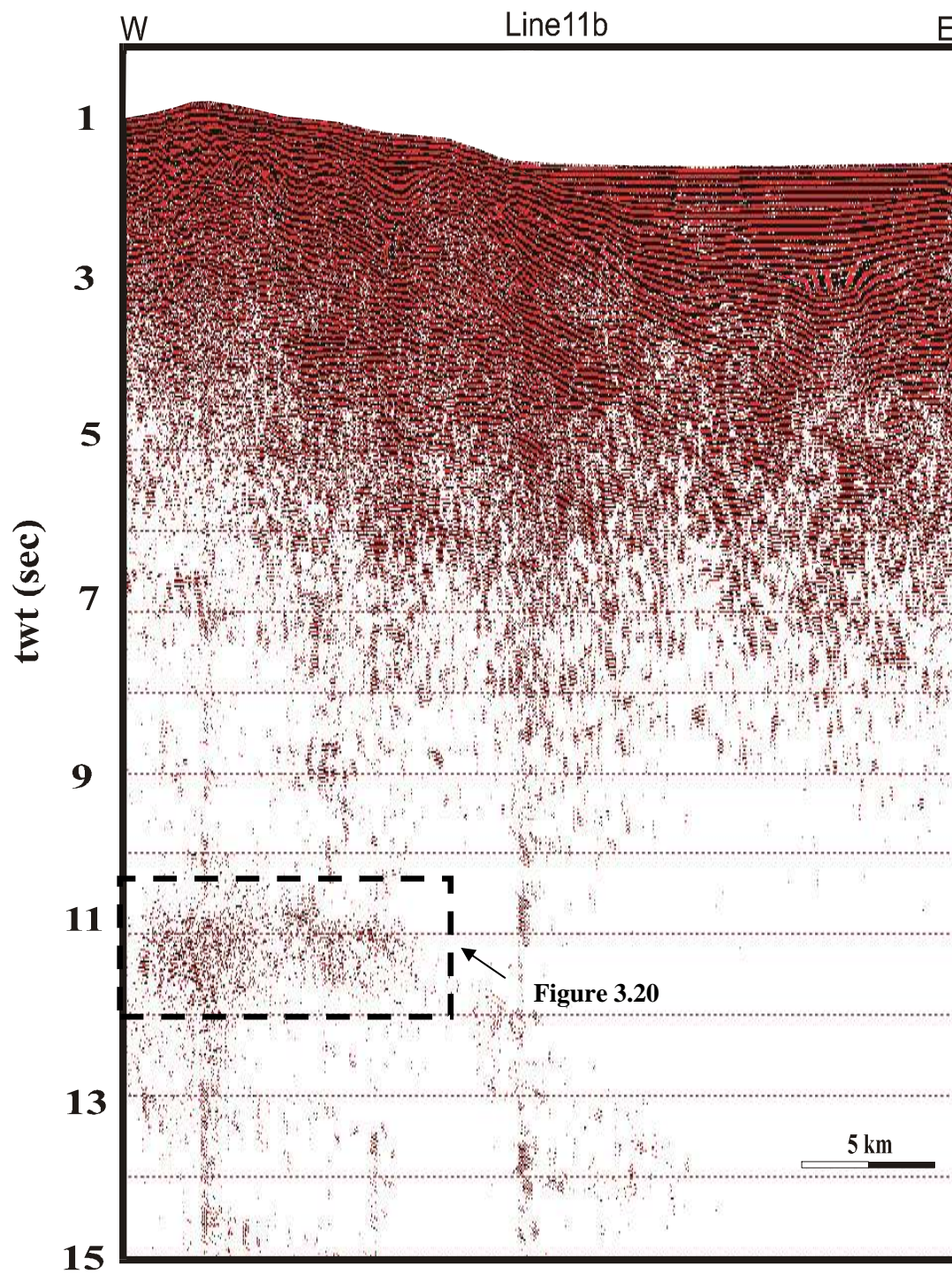


Figure 3.18: Stacked section of Line 11b in the Central Basin.

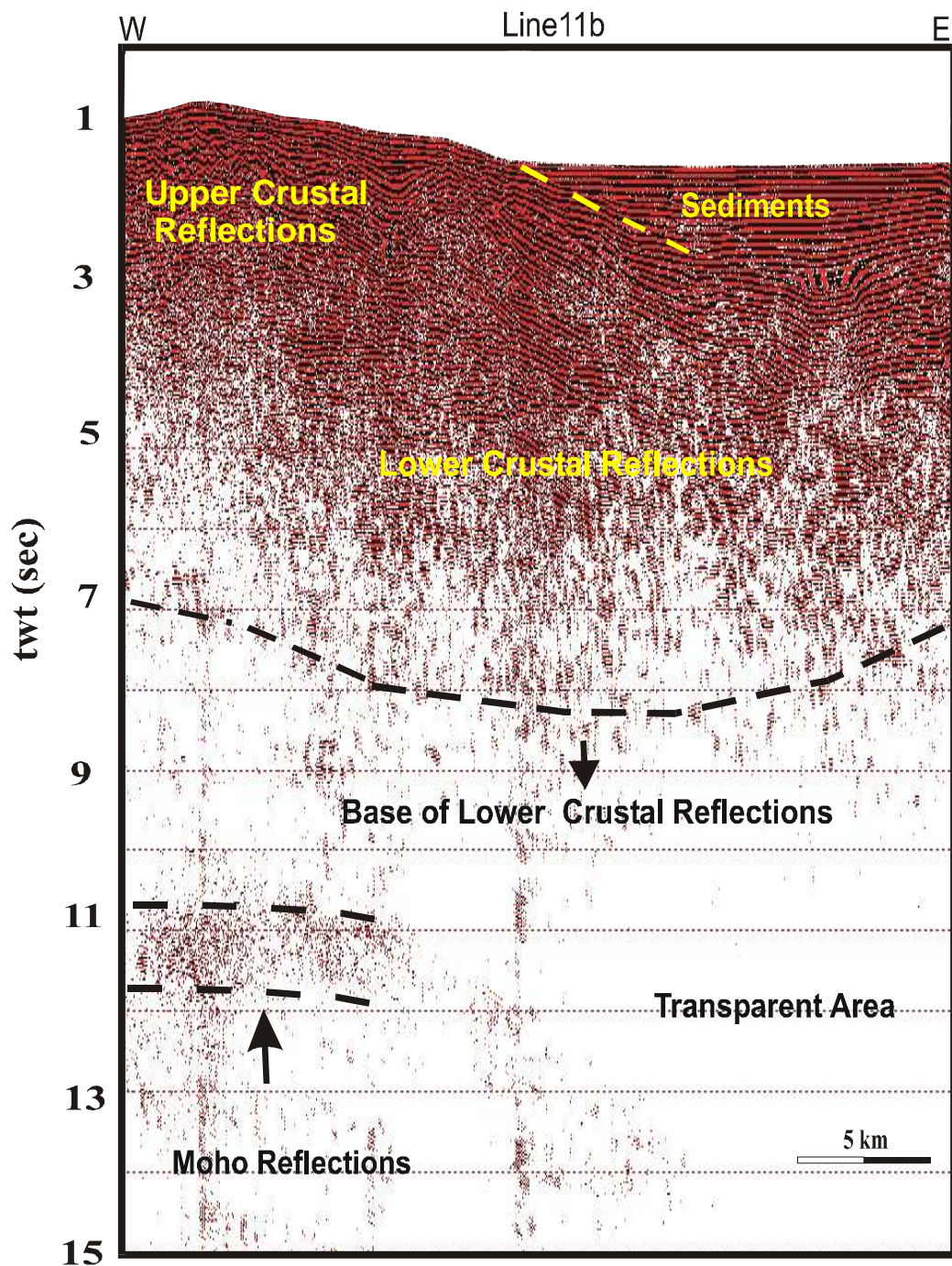


Figure 3.19: Interpreted stacked section of Line 11b in the Central Basin.

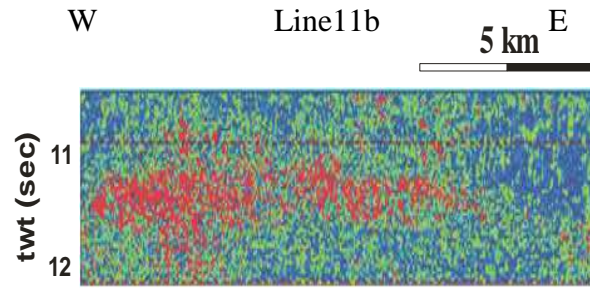


Figure3.20: Reflection strength section of a ~10 km area of stacked section (rectangle area in Figure 3.18) of Line 11 b, between ~10.5 and 12 s twt of Line 11b.

3.4.3 The Çınarcık Basin

Data acquisition parameters of Line 130, 143 and Line 11a (Figure 3.3) are as follows:

Line 130 and Line 143	Line 11a
Number of channels: 360	Number of channels: 360
Record length: 13 s	Record length: 30 s
Shot Interval: 37.5 m	Shot Interval: 150 m
Fold: 60	Fold: 15
Processed line length 9000 m, 12750 m	Processed line length 19200 m

In the Çınarcık Basin, one SE-NW directional (a part of Line 11), two NE-SW (Line 130, Line 143) directional lines are processed. In the stack section of Line 130 (Figure 3.21 b), for the upper crustal depths, faulted nature of the basin is visible, which is studied in detail by Carton et al. (2007). Crustal reflections continue to an extent of ~6.5 s twt. On the northeastern side of the section, after this depth, no visible reflections are observed. For the south-western side, reflections seems to continue to down but, as it was a very noisy part of the section, one more parallel line (Line 143) is processed to see this depth more clear. In the stack section of Line 143 (Figure 3.21 a), strong upper crustal reflections start to diminish around ~5 s twt and after ~6-6.5 s twt become invisible. Below this two-way travel time, no visible seismic reflections are observed which is consistent with Line 130 (Figure 3.21 b). Interpreted stacked sections of Line 143 and Line 130 are given in Figures 3.21 c and 3.21 d. In Figure 3.22 stacked section of Line 11a is presented. Seismic reflections continue until two-way travel time of 8 s twt. The strong reflections are visible as a double band of ~7 km width between 4.5 and 6.5 s twt. Interpreted stacked section of

Line 11a is given in Figure 3.23. Magnified image of the part of the section of Line 11a (area in square in Figure 3.22) is given in Figure 3.24. Strong reflections are very visible on the magnified image in Figure 3.24a.

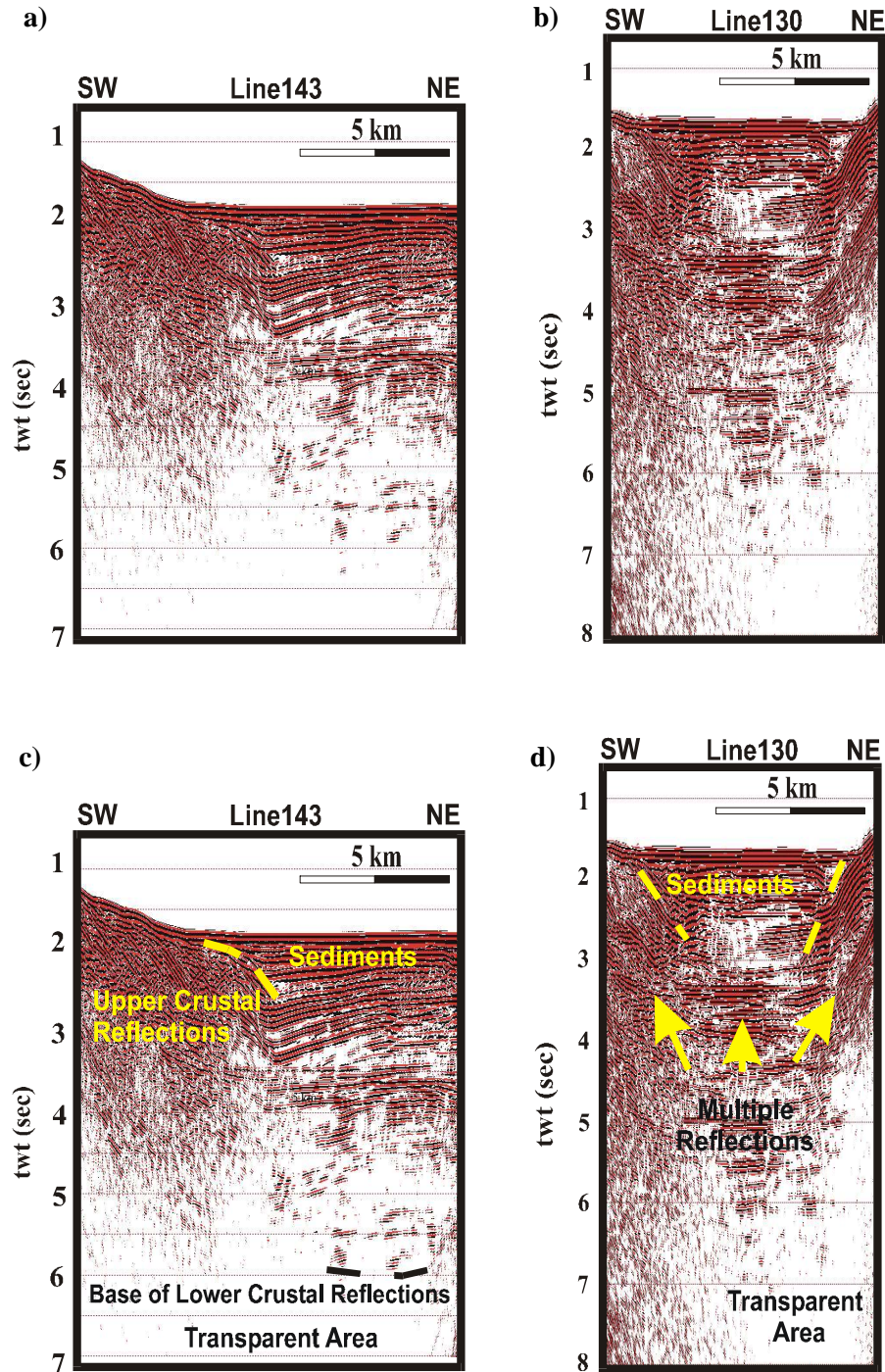


Figure 3.21: Stacked section of a) Line 130 and b) Line 143, interpreted stacked section of c) Line 130 and d) Line 143 in the Çınarcık Basin.

Reflection strength section of the area is given in Figure 3.24b. Strength and continuity of double reflection bands are clearly distinguishable on the section. In the western deep part of the section the reflections are present but their pattern is not

distinct from the upper parts. Therefore, it is quite difficult to define those reflections as Moho reflections. The boundary transition from visible reflections to non-reflective part is around ~6 s twt on the NE-SW lines and around ~8 s twt in the E-W line.

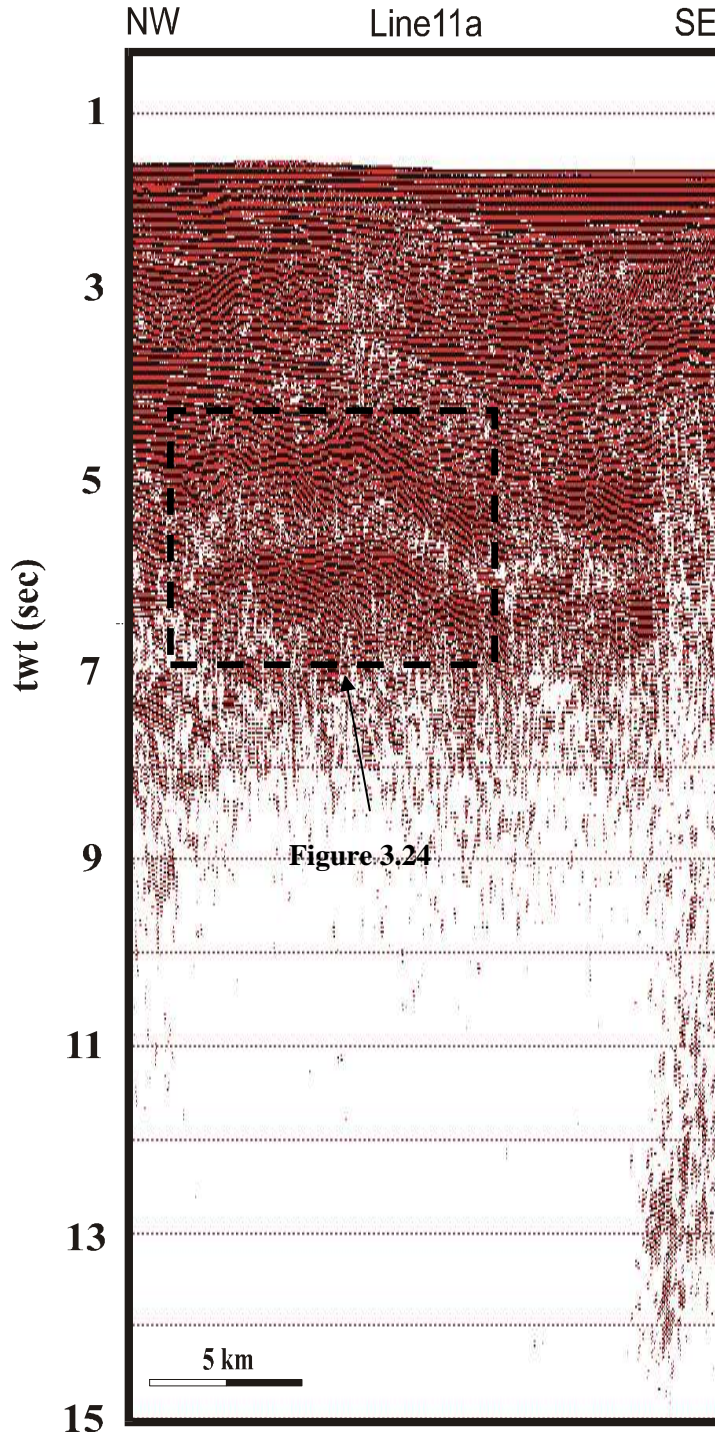


Figure 3.22: Stacked section of Line 11a in the Çınarcık Basin.

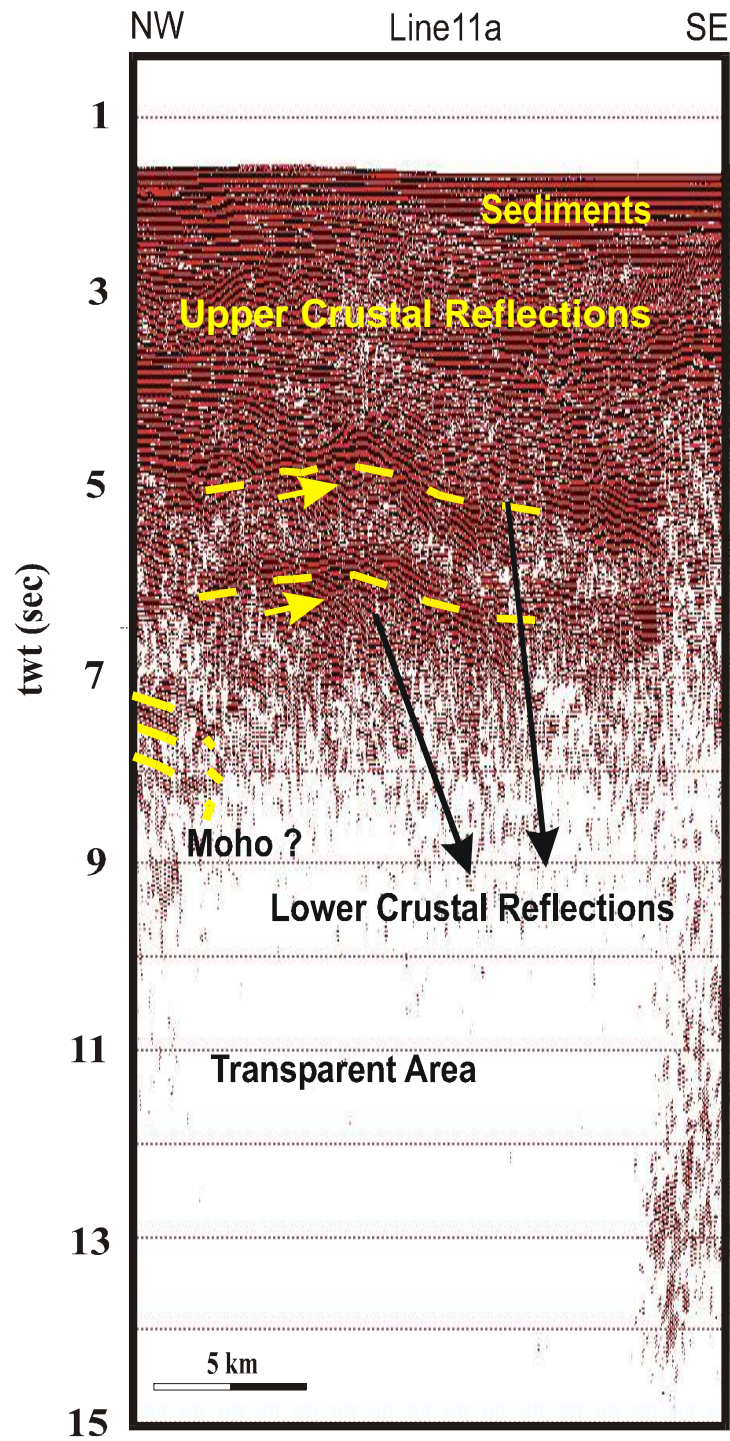


Figure 3.23: Interpreted and stacked section of Line 11a in the Çınarcık Basin.

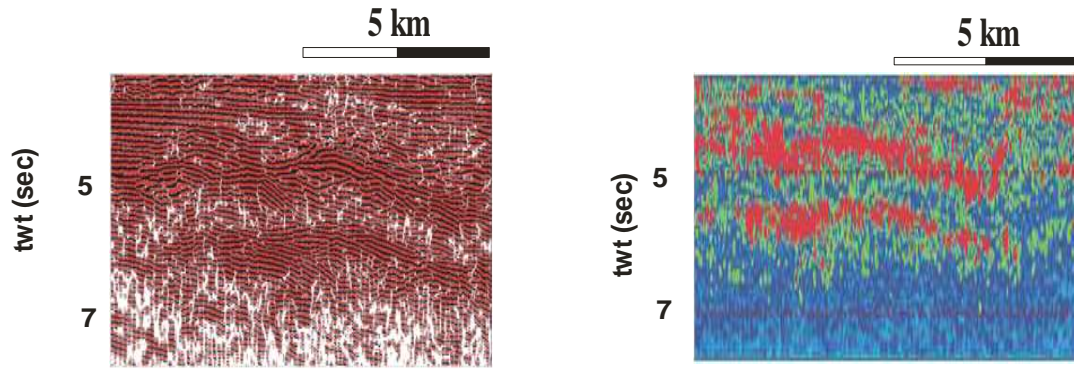


Figure 3.24: a) Magnified image from the stacked section of Figure 3.22 (area in square), b) reflection strength image from the stacked section of Figure 3.22 (area in square).

Deep seismic reflections under the deep basins of the Sea of Marmara (the Tekirdağ, the Central and the Çınarcık Basins) exhibit different seismic reflection patterns. Variation of seismic reflection patterns is important for comparison of the basins in terms of crustal rheology. Obtained seismic reflection patterns are summarized in Table 3.4 with respect to lower crustal seismic reflections and the Moho seismic reflections for the three deep basins of the Sea of Marmara.

Table 3.4 : Deep seismic reflectivity patterns of the three deep basins of the Sea of Marmara

	Tekirdağ Basin	Central Basin	Çınarcık Basin
Lower Crustal Seismic Reflections	Not dense, nearly transparent	Complex, diffractions accompanied by dipping upper crustal reflections.	Bands of reflections
Moho Seismic Reflection Patterns	Discontinuous and dipping	Discontinuous and complex	Not Clear
Depth of Moho Seismic Reflections	~10 s twt	~9 s twt	Not clear ~7 s twt

4. SKS SPLITTING ANALYSIS

4.1. Shear Wave Splitting

Seismic anisotropy is an important tool to investigate dynamics of the mantle. In the last two decades, shear wave splitting analysis has been one of the most widely used methods to map seismic anisotropy in the mantle. Vinnik et al. (1984), Kind et al. (1985), Silver and Chan (1988), Vinnik et al. (1989), Vinnik et al. (1992) are the first leading scientists improving this technique. Origin of seismic anisotropy for different depths of the Earth is given in the Table 4.1. Seismic anisotropy in the mantle is a result of strain induced lattice preferred orientation of mantle minerals such as olivine and pyroxene (Babuska and Cara, 1991). Therefore, it is possible to examine structural geology within the mantle since shear wave splitting measurements represent the orientation and depth extent of mantle strain fields. When shear waves travel in an anisotropic medium, they split into two orthogonal components which are slow and fast components (Figure 4.1, red and blue color components).

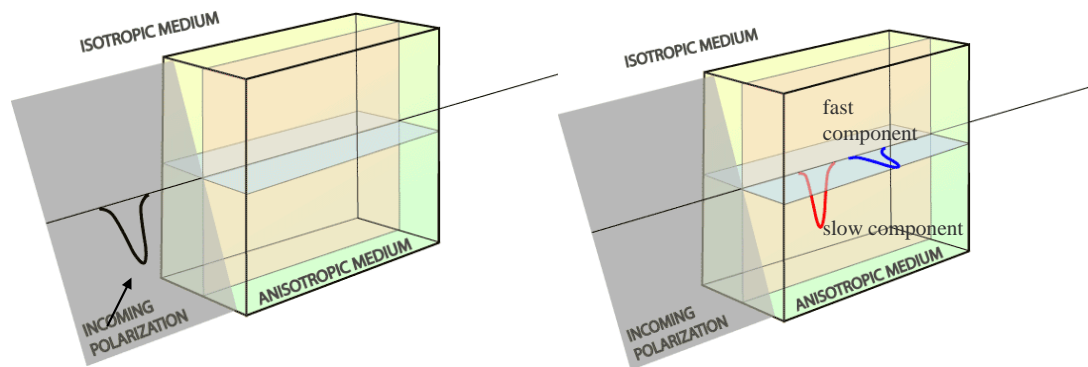


Figure 4.1 : Schematic illustration of shear wave splitting in anisotropic media. (url-3).

Table 4.1 : Origin of anisotropy and related seismic observations for the different depths of the Earth (Babuska and Cara, 1991).

	Depth range	Seismic observations	Origin of anisotropy
CRUST			
Continents			
Sedimentary Basins	~0-5 km	PH/PV velocity differences S-wave splitting S-wave splitting	Layering of sediments Vertical cracks
Upper Crystalline Crust	~0-15 km	Lg waves Reflections on faults Horizontal Reflectors	Vertical cracks and fractures Foliation of rocks Anisotropy of mylonites
Lower Crust	~15-30 km	No direct evidence	Several possible models: -laminated structures -horizontal shearing -horizontal cracks with fluids Coherent crystalline anisotropy over large volume
Oceans			
	~5-11 km	Borehole data S-wave splitting Azimuthal variations of P velocities	Layering of sediments Vertical cracks and fractures
SUBCRUSTAL LITHOSPHERE			
Continent	~30-150 km	Pn-azimuthal variations Long-range profiles P-wave residuals SKS and ScS splitting Pn-azimuthal variations	Preferred orientation of olivine and orthopyroxene, either frozen-in or reoriented within a tectonic strain fabric
Ocean	~10-100 km	Long-range profiles P-wave residuals SKS and ScS splitting Love/Rayleigh-wave incompatibility	Frozen-in preferred orientation of olivine and orthopyroxene
ASTENOSPHERE			
Continent	~150-400 km	Love/Rayleigh-wave incompatibility	Orientation of olivine in the present day flow?
Ocean	~50-300 km	Love/Rayleigh-wave incompatibility Azimuthal variation of Rayleigh-wave velocity	Orientation of olivine in the present day flow?
UPPER MANTLE TRANSITION REGION	~300-700 km	No clear evidence	Anisotropy in subducted slabs due to mineral orientation?
LOWER MANTLE	~700-2600 km	No evidence	
D'' REGION	~2600-2900 km	Splitting or diffracted S waves?	Not known
INNER CORE	~5154-6371 km	Splitting or core modes?	Preferred orientation of high pressure iron phase

Splitting of shear waves arriving at nearly vertical incidence at the station are observed on SKS waves at teleseismic distances. SKS wave travels as a P-wave within the liquid core of the Earth and results from P to S conversion at the core-

mantle boundary (Figure 4.2). As the SKS ray is nearly vertical beneath the station, it is observed as radially polarized phase in the horizontal plane. In anisotropic medium, energy in the transverse component of SKS waves, perpendicular to the vertical plane containing the ray path, are observed (Vinnik et al., 1984; Silver and Chan, 1988).

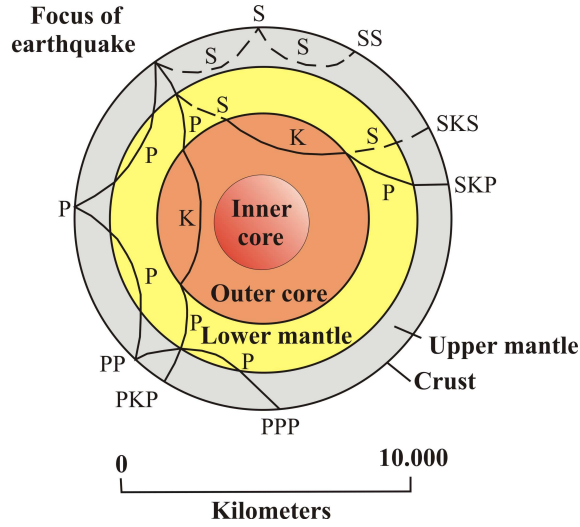


Figure 4.2: SKS wave results from P to S conversion at the core-mantle boundary (redrawn from url-4).

Radial R and transverse T components of the split SKS wave can be expressed as (Vinnik et al., 1992);

$$R(t) = \cos^2 \phi \sin \omega t + \sin^2 \phi \sin \omega(t - \delta t) \quad (4.1)$$

$$T(t) = 0.5 \sin 2\phi [\sin \omega t - \sin \omega(t - \delta t)] \quad (4.2)$$

Where t is the time, ω is the circular frequency, ϕ is the angle shown in Figure 4.3, and δt is the delay time between split waves. As seen in the equation (4.2) if there is no delay time, there will be no energy on the transverse component. In the existence of anisotropy, particle motion is observed to be elliptical. Shear wave splitting analyses are performed measuring the polarization of the fast component (ϕ) and the time delay time (δt) between the fast and slow components. Those parameters provide information on the orientation of the anisotropy and the thickness of the anisotropic layer. Information obtained from the parameters evaluated together with absolute plate motion, geological setting, geodynamic history of the area, enlighten the current and past lithospheric deformation. Evaluation of shear-wave splitting in the ray-coordinate LQT system (L: longitudinal; Q: radial, normal to the (L–T) plane) is given in Figure 4.3.

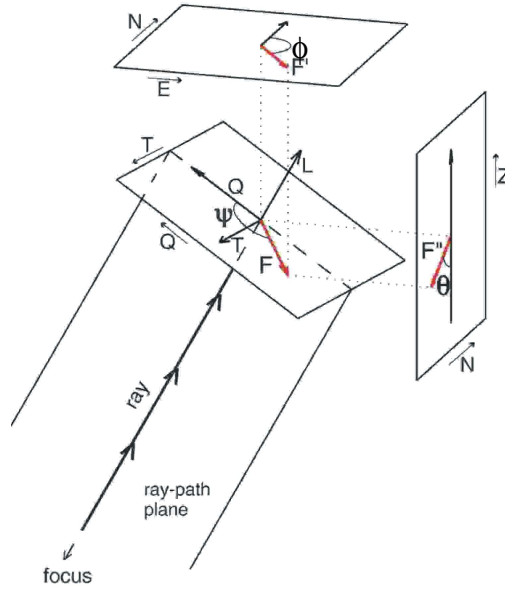


Figure 4.3: Evaluation of shear-wave splitting in the ray-coordinate LQT (L: longitudinal; Q: radial, normal to the (L–T) plane) system (Vecsey et al., 2008). The fast polarization direction F lies in the plane (Q–T) perpendicular to the ray path and its orientation in the plane is given by angle ϕ measured from axis Q . The fast polarization direction F can be also defined by two Euler angles: azimuth ϕ angle (measured from the N axis in the horizontal plane) and inclination θ angle (measured from the Z axis oriented downward in the vertical plane).

4.2 Method and Data

Preliminary SKS splitting parameters (ϕ , δt) are obtained by using SKSspl.f shear wave splitting code (Ivan, 2001). For the better accuracy of the obtained results, the data are re-analysed by using automated shear wave splitting code Ass.f (Teanby et al., 2004). Both codes were based on the splitting correction method of Silver and Chan (1991). In Silver and Chan's method (1991), a shear-wave analysis window is manually selected. The best correcting splitting parameter pair is calculated within the manually selected window by using a grid search algorithm. After the splitting correction, it is expected that the particle motion is linear and corrected waveforms in the analysis window match. In the Teanby's code (2004), shear wave analysis window is not manually chosen, instead, splitting parameters are calculated over a wide range of different analysis windows. Thus, robust parameters are obtained since the shear-wave analysis windows are chosen automatically and objectively in this code.

In this study broad-band teleseismic earthquake data from three different broad-band stations, Istanbul (ISK), Ankara (ANTO) and Isparta (ISP), are used to examine fossil and current deformation of the upper mantle beneath the north-western, central and southwestern Turkey (Figure 4.4). Variation or coherency of the splitting parameters between stations provides wider aspects to see the extent of the deformation model in the area around the stations. For ANTO (IRIS-GSN) and ISP (IRIS-GE) stations, data are provided from IRIS-WilberII online earthquake database. For ISK station data are provided by the KOERI-NEMC. To use in SKS splitting analyse, earthquakes with a magnitude greater than 5.0, focal depth greater than 100 km are chosen from the epicentral distance between 85° and 110° . From the earthquakes which fit mentioned criteria above, the ones with good signal to noise ratio are selected after visual inspection. For three stations, over 450 earthquakes are found to meet the criteria. After examining data and waveforms, only ones with clear SKS phases are selected. The selected earthquakes for ISK (41.0656°N , 29.0592°E), ANTO (39.867°N , 32.794°E) and ISP (37.823°N , 30.522°E) stations are given in Table 4.2, 4.3 and 4.4 respectively. List of the earthquakes studied in the thesis are given in Appendix B.

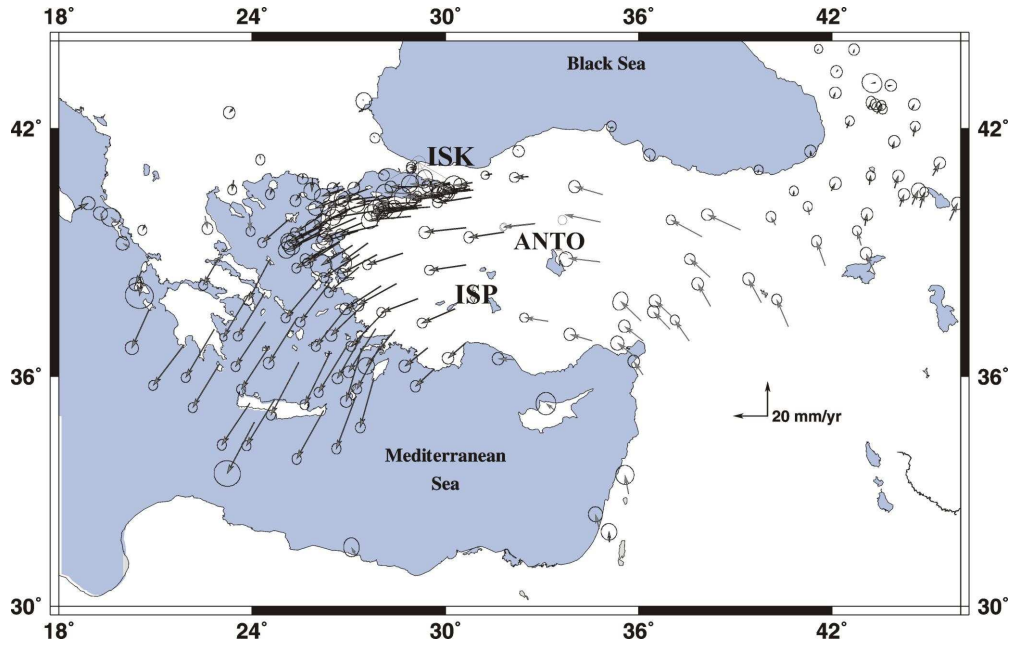


Figure 4.4 : ISK, ANTO, ISP broad -band stations used in the thesis and GPS displacement vectors of Turkey (Mc Clusky et al., 2000).

Table 4.2: Selected earthquakes for İstanbul broad-band station (ISK). (-) latitudes represent south direction, (-) longitudes represent west direction.

DATE (year/month/day)	Lat (°)	Lon (°)	Depth (km)	Mag (Mw)	Region
2004/07/25	-2.40	104.02	577.5	7.3	Indonesia
2003/05/26	6.8	123.75	559.7	6.8	Philippines
2002/10/12	-8.26	-71.53	535.9	6.8	Western Brazil
2002/10/03	-7.42	115.77	315.2	6.2	Bali Sea
2000/08/07	-7.02	123.36	648.5	6.5	Banda Sea
2000/08/06	28.86	139.56	394.8	7.3	Bonin Island
2000/06/16	-33.88	-70.09	120.02	6.4	Argentina
2000/05/12	-23.55	-66.45	225	7.2	Argentina
2000/04/23	-28.31	-62.99	608.5	7	Argentina
2000/03/28	22.34	143.73	126.5	7.6	Volcano Islands
1999/05/10	-5.16	150.88	138	7.1	New Britain
1999/05/04	-5.59	149.57	150	7.4	New Britain
1998/08/20	28.93	139.93	441	7.0	Bonin Island
1998/03/04	-8.15	-74.24	165	6.6	Peru-Brazil
1997/12/22	7.2	147.87	179.3	7.2	Eastern New Guinea

Table 4.3: Selected earthquakes for Ankara broad-band station (ANTO).

DATE (year/month/day)	Lat (°)	Lon (°)	Depth (km)	Mag (Mw)	Region
1998/04/03	-8.15	-74.24	165.0	6.6	Peru-Brazil
1997/11/28	-13.74	-68.79	586.0	6.7	Peru-Bolivia
2002/09/08	-3.23	142.87	33	7.5	New-Guinea
1997/07/06	21.97	142.83	241	6.2	Mariana
1996/06/09	17.44	145.46	149	6.5	Mariana
1997/10/06	9.79	125.78	106	6.4	Philippines
2003/07/27	-19.84	-64.94	347.6	6.0	Bolivia
2003/06/20	-7.5	-71.62	553.0	6.7	Western Brazil
2003/05/26	6.8	123.75	559.7	6.8	Philippines

Table 4.4 : Selected earthquakes for Isparta broad-band station (ISP).

DATE (year/month/day)	Lat (°)	Lon (°)	Depth (km)	Mag (Mw)	Region
1996/11/02	-7.56	117.30	302.0	5.8	Bali Sea
1997/01/23	-22.0	-65.72	276.2	7.1	Southern Bolivia
1997/02/19	4.56	-76.49	100.7	5.8	Colombia
1997/12/22	-5.50	147.87	179.30	7.2	New Guine
1999/04/05	-5.59	149.57	150.0	7.4	New Britain
2000/02/26	9.41	-78.53	65	6.1	Panama
2000/03/03	-7.32	128.49	141.9	6.3	Banda Sea
2000/04/23	-28.38	-62.94	609.8	6.1	Argentina
2000/05/12	-23.55	-66.45	225	7.2	Jujuy Province
2000/06/16	-33.88	-70.09	120.2	6.4	Chile -Argentina
2000/06/21	14.11	144.96	112.2	5.9	Mariana Island
2000/10/04	11.12	-62.56	110.30	6.1	Winward Island
2001/03/14	0.45	121.89	109.40	5.9	Sulawesi
2001/06/29	-19.52	-66.25	273.9	6.1	Southern Bolivia
2002/10/12	-8.26	-71.53	535.9	6.8	Western Brazil
2003/04/27	-8.14	-71.51	545.7	5.9	Western Brazil

Basic steps to prepare the data for SKS splitting analysis are given below:

- 1) SAC2000, Seismic Analyses Code, (Goldstein et al., 1999) is used for reviewing and cutting the data. Therefore, to process data in SAC, format conversion (Seed-SAC) is applied to vertical and horizontal components of the data using RdSeed code in Linux.
- 2) Arrival times of SKS phases of the earthquakes are calculated using IASPEI automatical calculation code. Inputs parameters for the code are; focal depth, magnitude and epicentral distance of the earthquake. According to the origin time of the earthquake, arrival time of the SKS phase to the station is calculated.
- 3) Three components of the data are cut properly to include the SKS phase.
- 4) For noisy data, band-pass filter is applied to data with in the range of 0.02-0.3 Hz (Ivan, 2001).
- 5) SKS phase initial times of the data components are written to data header in SAC.

After the basic steps, data are recorded to be processed in the splitting code ASS.f. Parameters such as start times of the analysis window, end time of the analysis

window, increment for the start and end of the window, distance between shear wave onset and start of the window are provided to code by user to obtain the best polarization direction (ϕ), delay time (δt) couple using a grid search algorithm, repeating the analysis through different analysis windows. To decrease the influence of noise and prevent cycle skipping, the selected time window on the records should be representative of the shear wave and long enough to include several periods of the dominant frequency. To stabilize the results and reduce cycle-skipping effects, start of the window should be chosen slightly before the onset of the shear wave. It is also important that over a wide range of different analysis windows, splitting parameters are stable to provide robust measurements (Teanby, 2004). The code transforms data into radial, transverse components and provides plotted output of corrected components after the processing data (Figure 4.5).

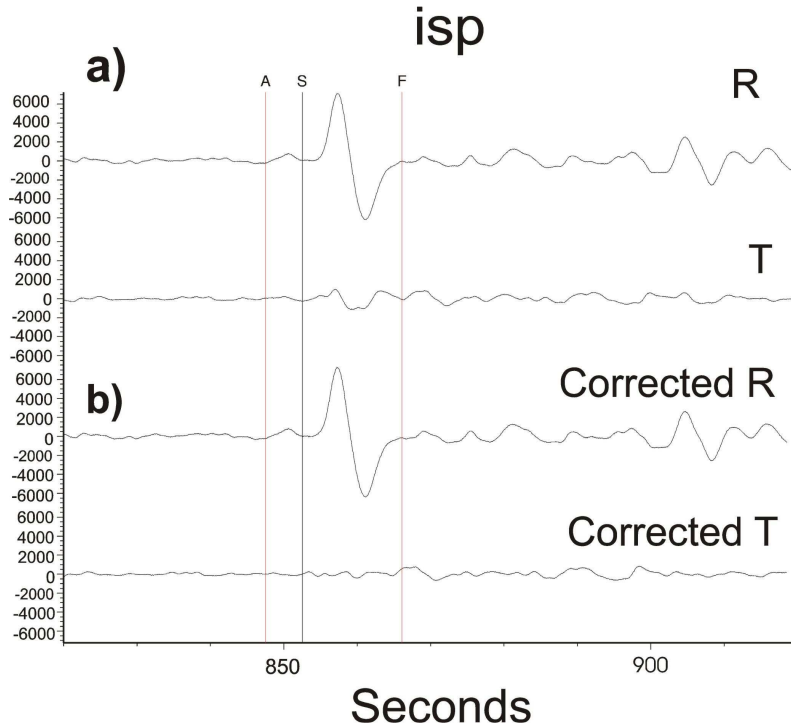


Figure 4.5: An example of the processed data using ASS.f. a) Radial (R) and transverse (T) components. b) Corrected radial and transverse components. S: start of the SKS phase; F: end of the SKS phase; A: start of the analysis window.

After the correction has been applied, energy on the transverse component should disappear on the corrected transverse component. In the analysis window, fast and slow components with δt delay time should also match after the correction and elliptical particle motion should be linear. An example for the fast and slow

components before and after correction is given in Figure 4.6 a. Particle motion diagrams before and after the correction are also given in Figure 4.6 b.

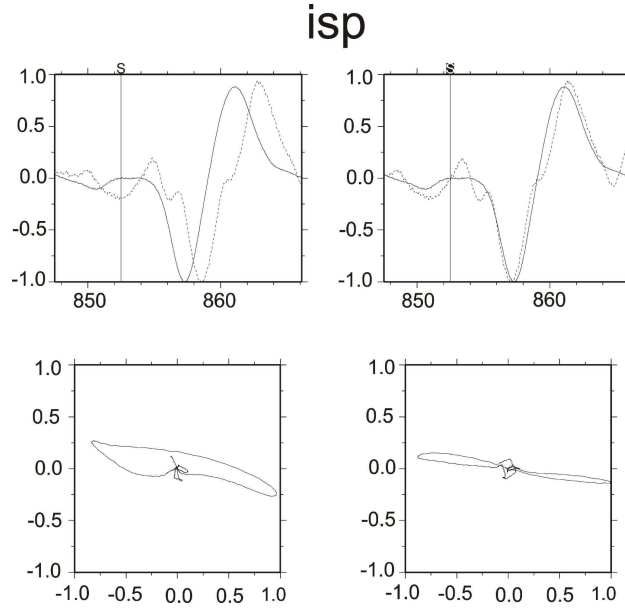


Figure 4.6: Fast (dashed line) and slow (bold line) waveforms a) before and b) after the correction (upper diagrams). Particle motion diagram, a) before and b) after the correction (lower diagrams).

An example for the grid search step of the process is given in Figure 4.7. The best pair of splitting parameters (ϕ , δt) marked by a cross (+) sign in Figure 4.7 minimizes the energy on the transvers component, provides linear particle motion and clears off delay time between the fast and slow components. The thick contour line around the cross (+) sign in Figure 4.7 represents 95% confidence interval for the calculated splitting parameters. For each single earthquake, a ϕ - δt pair is estimated. Calculated parameters for each station are given in rose diagrams on the map of Turkey in Figure 4.8.

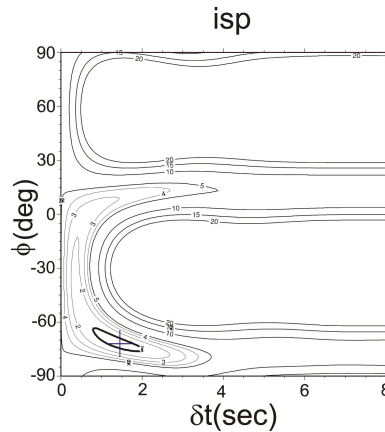


Figure 4.7: Contour diagram with the best pair of splitting parameters ϕ - δt (“+” symbol) after a grid search is performed.

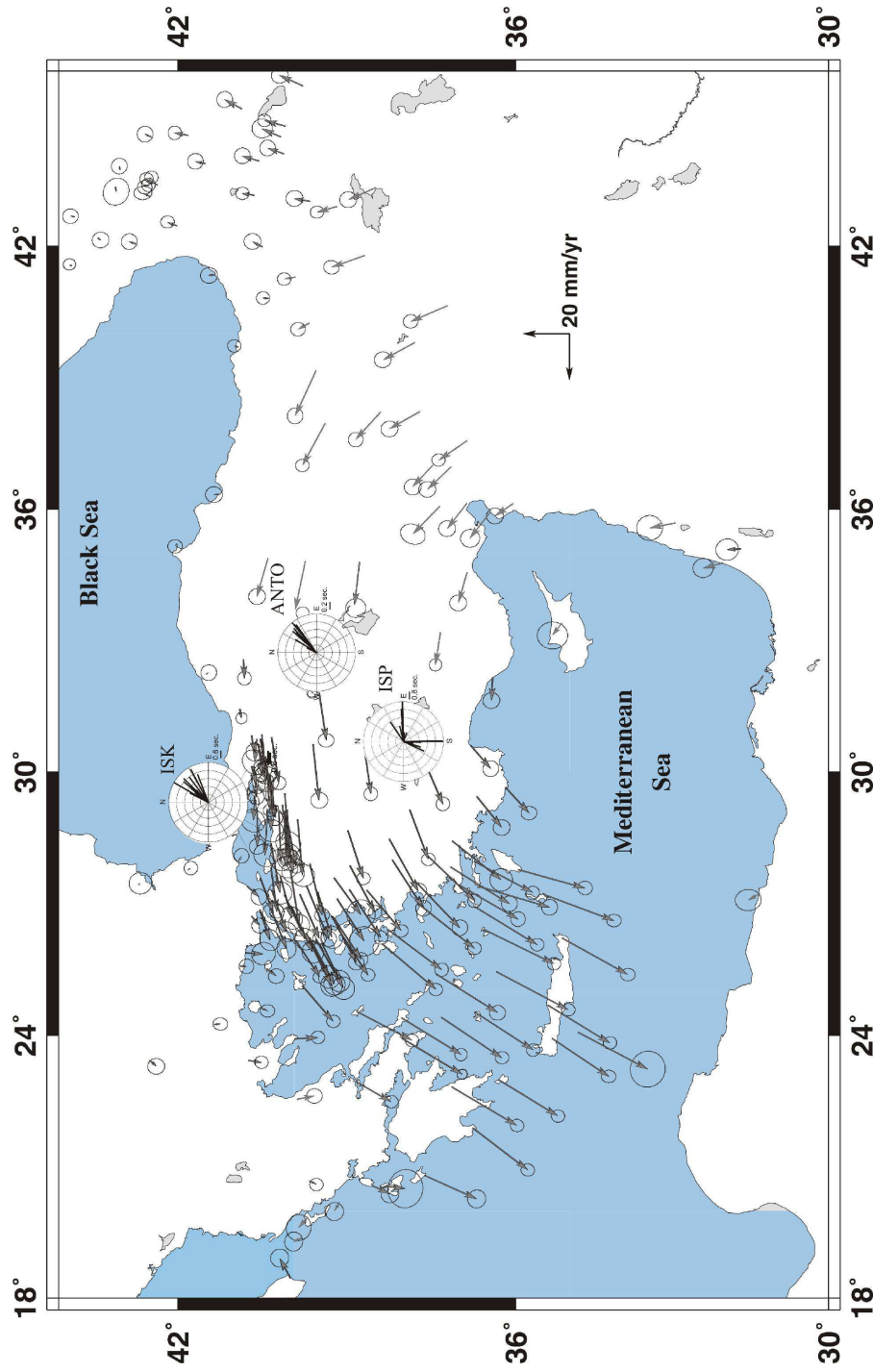


Figure 4.8: Rose diagrams of SKS splitting parameters for three broad-band stations ISK, ANTO and ISP calculated in this study. In the rose diagrams, black lines point to the fast polarization direction (ϕ) and length of the lines indicates the duration of the delay time (δt) in second. GPS vectors are from McClusky et al.(2000).

Since only 17 good quality seismic events out of nearly 250 earthquakes are chosen, the data to be processed are limited. Also back-azimuthal coverage of the data for all three stations is poor (Figure 4.9). Testing of all possible solutions causes large amount of models which are difficult to handle. Due to this difficulty, models are constrained using geological data and priority information from ANTO and ISK broad-band stations which are 230 and 379 km away from ISP broad-band station. Average SKS splitting parameters are $\phi=43.7^\circ$, $\delta t=1.96$ s for ISK station and $\phi=43^\circ$, $\delta t=0.74$ s for ANTO station. Fast polarization directions are consistent with each other. Obtained delay times indicate that anisotropy is related to the upper mantle anisotropy (Silver and Chan, 1988). Sandvol et al. (2003) investigated shear wave splitting parameters for the Eastern Turkey. According to their results, the fast polarization directions are mainly NE-SW oriented in the Eastern Turkey with delay times from 0.7 s to 2.0 s. ISK and ANTO stations also show similar polarization directions and do not show azimuthal variations (Figure 4.10) suggesting one layer anisotropy model with a horizontal symmetry axis (Şapaş and Boztepe-Güney, 2005). However, splitting parameters of ISP station scatter between $\phi=56^\circ$ - 205° and $\delta t=0.3 - 0.4$ s showing back-azimuthal variations. Observed back-azimuthal splitting parameter variations may result from complicated anisotropic structures such as dipping axis of symmetry, laterally varying anisotropy or multilayer anisotropy beneath the ISP station. One of the models is two-layer anisotropy model with a horizontal symmetry axis (Silver and Savage, 1994). In order to explain the azimuthal dependency of the splitting parameters for ISP station with the backazimuth, a two-layer modeling is performed.

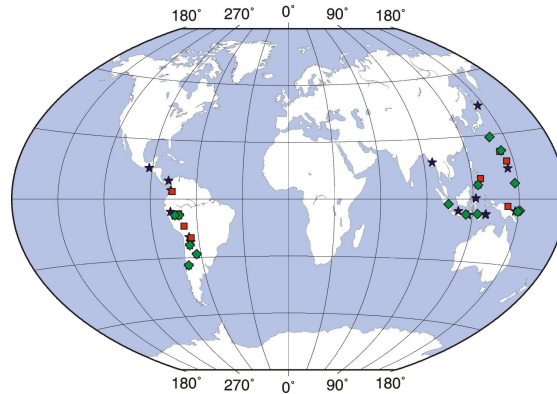


Figure 4.9: Azimuthal distribution of the earthquakes used in the analysis. Green squares, red squares, blue stars indicate earthquakes recorded at ISK, ANTO, ISP broad-band stations, respectively.

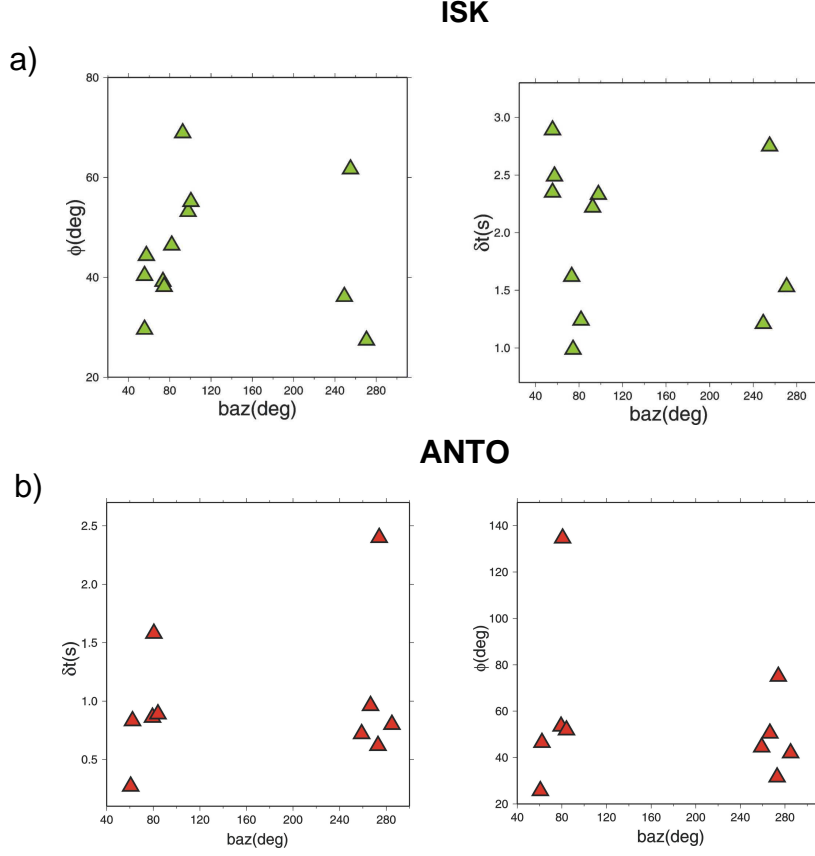


Figure 4.10: Backazimuthal distribution of SKS splitting parameters ϕ and δt for a) ISK and b) ANTO stations.

Two-layer anisotropy models with a horizontal symmetry axis are tested using the average splitting parameters calculated at ANTO and ISK stations ($\phi \approx 43^\circ$, $\delta t \approx 1$ s) as the constrain parameters for the upper layer of our proposed model. The best fitting two-layer anisotropy model ($\phi = 40^\circ$, $\delta t = 1$ s (upper layer), $\phi = 150^\circ$, $\delta t = 2$ s (lower layer) has been derived from the analytical equations (equation 4.3, 4.4, 4.5) given by Silver and Savage (1994) given in equations and presented in Figure 4.11 a and b (curved lines). In the presence of two anisotropic layers, measured apparent splitting parameters show azimuthal variations. Following the derivations, if $\alpha_{1,2} = 2\phi_{1,2}$, where $\phi_{1,2}$ is the angle between ϕ_p (backazimuth) and the fast polarization direction of the layer (1,2), let $\theta_{1,2} = \omega \delta t_{1,2} / 2$, and define a_p , $a_{p\perp}$, C_c , C_s by:

$$\begin{aligned}
 a_p &= \cos \theta_1 \cos \theta_2 - \sin \theta_1 \sin \theta_2 \cos(\alpha_1 - \alpha_2) \\
 a_{p\perp} &= -\sin \theta_1 \sin \theta_2 \sin(\alpha_2 - \alpha_1) \\
 C_c &= \cos \theta_1 \sin \theta_2 \cos \alpha_2 + \cos \theta_2 \sin \theta_1 \cos \alpha_1 \\
 C_s &= \cos \theta_1 \sin \theta_2 \sin \alpha_2 + \cos \theta_2 \sin \theta_1 \sin \alpha_1
 \end{aligned} \tag{4.3}$$

Then, the apparent splitting parameters α_a and θ_a can be expressed as,

$$\tan \alpha_a = \frac{a_{p\perp}^2 + C_s^2}{a_{p\perp} a_p + C_s C_c} \quad (4.4)$$

$$\tan \theta_a = \frac{a_{p\perp}}{C_s \cos \alpha_a - C_c \sin \alpha_a} = \frac{C_s}{a_p \sin \alpha_a - a_{p\perp} \cos \alpha_a} \quad (4.5)$$

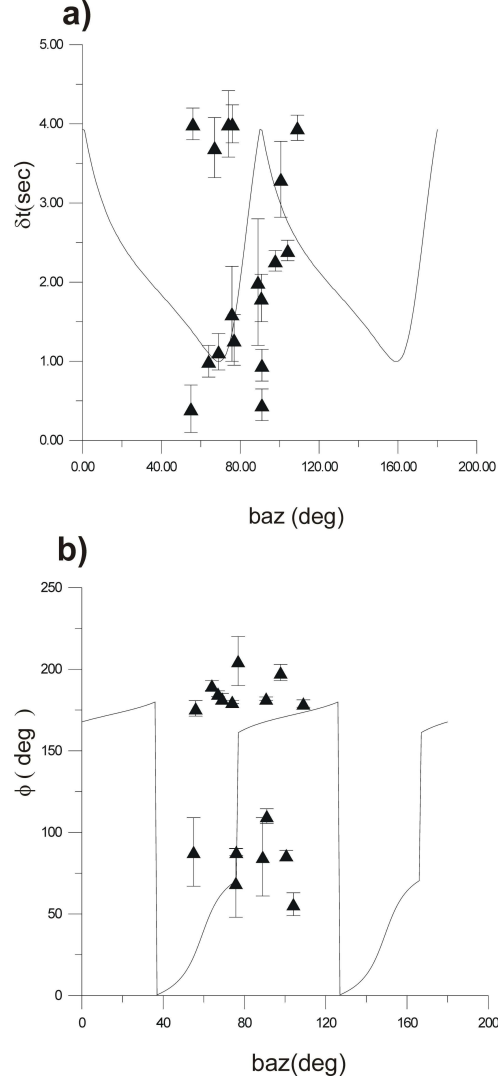


Figure 4.11: a) Delay times (δt), and b) fast polarization directions (ϕ) versus back-azimuths for the ISP broad-band station. Calculated delay times (a) and polarization directions (b) are marked by filled triangles together with their error bars. Delay times δt (a) and polarization directions ϕ (b) obtained from the model study ($\phi=40^\circ$, $\delta t=1$ s for upper layer, $\phi=150^\circ$, $\delta t=2$ s for lower layer) for two-layer anisotropy models are plotted with the curved lines.

Pn anisotropy observations sustain information related to the uppermost mantle whereas SKS anisotropy estimations preserve information from the upper mantle.

Therefore comparative evaluation of Pn anisotropy and SKS anisotropy provide better interpretations in terms of anisotropic structure of the upper mantle. Pn anisotropy of Turkey is studied by Al-Lazki et al. (2004) and given in Figure 4.12. It is suggested that anisotropy orientations are NW-SE in the east of the Sea of Marmara and change direction around the central part and turn to NE-SW in the west of the Sea of Marmara.

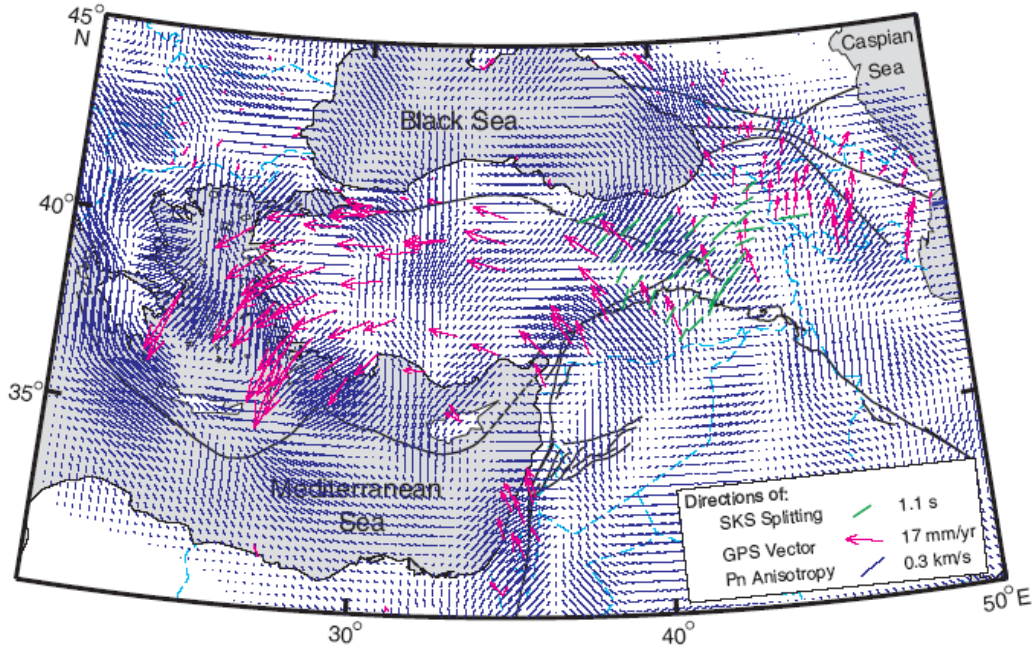


Figure 4.12: Pn anisotropy map of Turkey comparing GPS vectors and SKS splitting measurements in the Eastern Turkey (Al-Lazki et al., 2004).

Calculated SKS splitting parameters indicate two layer anisotropy for ISP broad-band station (upper layer; $\phi=40^\circ$, $\delta t=1$ s, lower layer; $\phi=150^\circ$, $\delta t=2$ s) and one layer anisotropy for ISK ($\phi=43.7^\circ$, $\delta t=1.96$ s) and ANTO ($\phi=43^\circ$, $\delta t=0.74$ s) broad-band stations.

5. DISCUSSION and CONCLUSIONS

The deep geodynamic processes effect tectonics and evolution of the Earth's crust and mantle significantly. The features on the Earth's surface and ongoing deep geodynamic processes are not mutually exclusive. Continents should be evaluated together with their deep roots since their evolution is determined by the rheological properties and the density of materials in their deep roots. This thesis aims to deduce rheological implications of seismic reflection patterns and also correlate seismic anisotropy and existing results of prior studies in the Sea of Marmara. To achieve this, multi-channel deep seismic reflection data and earthquake data are processed. Seismic reflection patterns are obtained by processing multi-channel seismic reflection data, acquired for the SEISMARMARA 2001 multidisciplinary project, in the Sea of Marmara deep basins. The data is the first deep seismic reflection data acquired in the Sea of Marmara and the results are important since they provide the first insights to understand the nature of the deeper parts of the basins, the shallow parts of which are already densely investigated (Okay et al., 1999; 2004; Le Pichon et al., 2001; Seeber et al., 2004; Demirbağ et al., 2007; Carton et al., 2007;) Teleseismic earthquake data of KOERI-NEMC ISK (Istanbul) broad-band station are used to determine seismic anisotropy in the mantle, which is an efficient tool to correlate tectonics with mantle dynamics. For interpretation purposes, data of two broad-band stations ISP (Isparta) and ANTO (Ankara) are processed and the results are correlated with those obtained from ISK broad-band station. Results of prior Pn anisotropy studies are also used as complementary data in the interpretation. Deep seismic reflectivity, SKS and Pn anisotropy are used to understand deformation characteristics of different levels of crust and mantle.

Deep seismic reflectivity patterns beneath the deep basins of the Sea of Marmara are compared in terms of their depth (twt) and visibility (i.e existence of lower crustal and Moho reflections). Obtained seismic reflection patterns display remarkable changes for the three deep basins of the Sea of Marmara (Tekirdağ, Central and Çınarcık Basin). Seismic stack sections of processed seismic lines (Appendix A),

exhibit different deep crustal seismic reflections (Table 3.4). Comparison of W-E extending seismic stack sections (Line 11c, 11b and 11a) reveals a quite complicated scenery. From west to east, dense upper crustal reflections are observed on the seismic sections of three deep basins. Lower crustal seismic reflections are distinguishable on Line 11b (the Central Basin) and Line 11a (the Çınarcık Basin). Beneath the Tekirdağ Basin (Line 11c), reflections from the slopes of the Tekirdağ Basin obscure most of the crustal reflections preventing nature of the lower crustal reflections from being visible, but on the western part of the section, the base of the lower crustal reflections are around 7 s twt. On the stack section of Line 11b (Central Basin), diffuse lower crustal reflections are visible with the base of lower crustal reflections around 7-8 s twt. Nature of lower crustal reflections change beneath the Çınarcık Basin (Line 11a). They are multiple bands of lower crustal reflections disappearing after 8 s twt.

Moho reflections are not clear beneath the Tekirdağ and the Çınarcık Basins on the W-E extending stack sections. Only clear Moho reflections identified from W-E sections are beneath the Central Basin. They are visible around 11 s twt as dense reflections confined to a band after a quite transparent area from the base of reflections.

Seismic stack sections of NE-SW extending lines are also complicated . Unlike E-W extending lines, depths of NE-SW extending lines are different from each other (12, 17, 7 and 8 s twt for the lines 22b, 40a, 143 and 130, respectively) which makes comparison more difficult for shorter twts.

Dense and complex upper crustal reflections, the most complex of which are identified on the Line 40a (Central Basin), are present for all of the NE-SW extending lines. Lower crustal reflections are not visible for the Line 22b (the Tekirdağ Basin), which exhibit a transparent area after the crustal reflections. The lower crustal levels are quite complex for the Line 40a (the Central Basin) since diffractions accompanied by dipping upper crustal reflections are visible on the seismic stack section. Deep crustal reflections for the Line 40a seem to reflect the same complexity as the upper crustal reflections on the section. Line 130 and Line 143 are two parallel NW-SE extending lines acquired in the Çınarcık Basin. Both of the seismic stack sections of those lines exhibit similar views indicating no

prominent reflections after 6-7 s twt. On the seismic stack section of Line 130, multiple reflections obscure lower crustal reflections.

Moho reflections exist on the seismic stack section of the Line 22b (the Tekirdağ Basin), which are visible between 10-12 s twt as dipping reflections. Beneath the Central Basin (Line 40a) similar dipping and discontinuous Moho reflections are distinguishable after 9 s twt. No clear Moho reflections are visible on the seismic stack sections of Line 143 and Line 130 (the Çınarcık Basin).

The general lack of mantle reflectivity has been attributed to the comparatively high viscosity and/or rather mono-mineralic mantle composition (Meissner, 1989). Synthetic seismograms were produced for three different Moho models by Braile and Chiang (1986) to investigate the information content of the reflection data. The seismograms were calculated for three laterally homogeneous Moho models at frequencies of 5, 10 and 20 Hz to illustrate the amplitude and waveform responses of these possible Moho models (Figure 5.1). According to the study, the velocity gradient model for Moho may represent an explanation for the apparent absence of Moho reflections on reflection profiles.

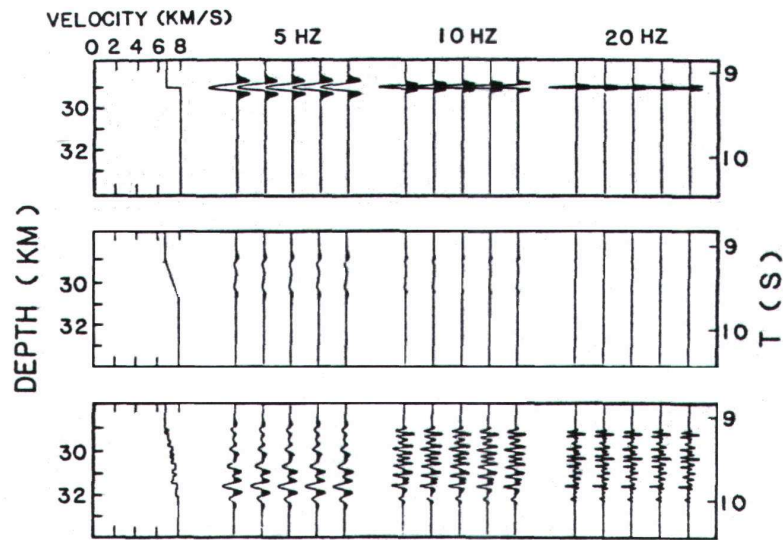


Figure 5.1: Seismic reflections of three laterally different Moho velocity models at three different frequencies (Braile and Chiang, 1986).

Different crustal seismic reflectivity patterns exhibit differences with changing tectonic regimes being independent of acquisition and processing parameters (Allmendinger et al., 1987; Trappe et al., 1988). This conclusion is deduced after the compilation of many deep seismic reflection profiles acquired by different scientific

groups such as COCORP in USA, LITHOPROBE in Canada, DEKORP in Germany, ECORS in France and BIRPS in Great Britain. A comparative study of the products of different deep seismic reflection profiles of the continental crust permitted a classification of seismic reflectivity patterns that is also used in the interpretation of the processed SEISMARMARA lines used in this study. Classification of seismic reflectivity patterns (Sadowiak et al., 1991) is given in Figure 5.2.

Bands of reflections (Figure 5.2 b) and diffractions accompanied with upper crustal reflections (Figure 5.2 d) are characteristic of deep seismic reflectivity patterns, which are identified, in the processed SEISMARMARA lines of the Çınarcık Basin (Line 11a) and the Central Basin (Line 40a), respectively.

Bands of reflections and lamellae are observed often in Western and Central Europe (BIRPS and ECORS, 1986; Lüschen et al., 1987; Klemperer et al., 1986) and in the Basin and Range Province of the Western United States. Lamellae and bands of reflections in the lower crust are widespread in young extensional areas. It is suggested that the younger the extension, the denser the reflective layering: Paleozoic extensional areas exhibit only Moho band reflectivity, while Cenozoic extensional areas show pronounced lamellae or multiple bands of enhanced reflectivity over much of the lower crust (Sadowiak et al., 1991).

In the SEISMARMARA multi-channel seismic lines, bands of reflections (Line 11a, between ~3-5 s twt) observed in the Çınarcık Basin point out an extensional area which is consistent with the reported complex focal mechanisms related to the normal faulting in the central part (Sato et al., 2004). Chapter 1 and prior SEISMARMARA results (Carton et al., 2007) indicate basin bounding faults with significant extensional component of motion. Diffractions with inclined upper crustal reflections are mostly observed in the middle or lower crust. This pattern was first recognized on DEKORP line 2-S (DEKORP Res. Group, 1985) in the area of the suture zone between Variscan Moldanubian and Saxothuringian units in southern Germany (Sadowiak et al., 1989). Similar examples are observed in KTB profiles in Germany, BIRPS lines around Britain, USGS and COCORP profiles in USA (Sadowiak and Wever, 1990) and in Australian profiles (Goleby et al., 1988). The strong similarity of seismic patterns of those suture-crossing seismic profiles leads to the conclusion that the typical patterns could be a diagnostic tool for identifying

continent-continent collisions in areas where out crops are hidden by e.g., post collision sediments (Wever and Sadowiak, 1991).

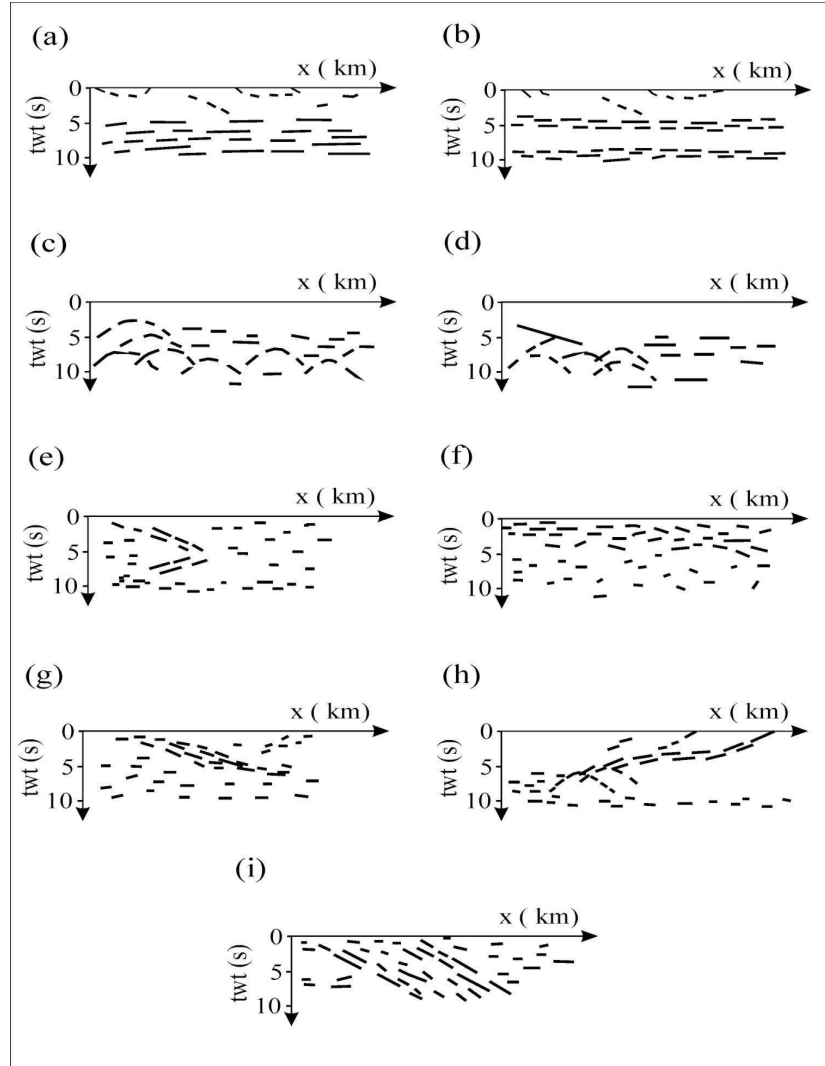


Figure 5.2: Classification of crustal seismic reflectivity patterns: a) lamellae, b) bands of reflections, c) diffractions, d) diffractions accompanied with upper crustal reflections, e) seismic crocodiles, f) decreasing reflectivity with depth, g) deep-reaching, steeply dipping reflection zones, h) ramp and flat structure, i) seismic duplex (Sadowiak et al., 1991).

As stated in the previous paragraphs, diffractions with inclined upper crustal reflections are identified on the seismic sections of the Central Basin (Line 40a). The Sea of Marmara is situated in a critical location where continental collision had taken place and also it is reported that Intra-Pontid suture zone (Figure 2.2) is disguised under the Sea of Marmara (Okay and Tüysüz 1999). The tectonic interpretation of the obtained seismic reflectivity pattern exhibits a consistent sight. Apart from the uppermost crustal reflections, complex lower crustal reflections

display the traces of complex tectonic history of the area. Similar traces are not followed to the east, beneath the Çınarcık Basin. But on the seismic stack of the Line 22b (Tekirdağ Basin) a keel-like structure is distinguishable. Similar examples are observed in the regions of subduction-related tectonics; such as Iapetus convergence zone (Freeman et al., 1988) and Ringkobing-Fyn High, where a keel structure marks the complex structure resulting from closure of the Tornquist Sea (Thybo, 1997). An example of keel-like structure from Iapetus suture (Freeman et al., 1988) is given in Figure 5.3 for comparison with seismic stack section of Line 22b in the Tekirdağ Basin.

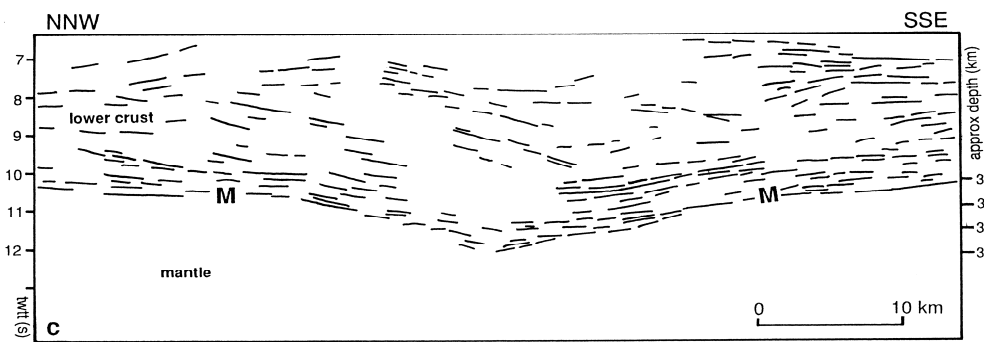


Figure 5.3: Keel-like structure from Iapetus suture (Freeman et al., 1988).

Deep seismic reflection patterns of two lines Line 22b and Line 40a probably exhibit the traces of the Intra-Pontid suture zone but it is difficult to attain a definite conclusion without different detailed supporting data such as gravity and magnetic. If a prominent gravity signature provided, that the “keel” has a different density compared to the adjacent mantle, this indicates that the “keel” is likely to be composed of pure basaltic eclogite to explain mantle reflectivity within relict subduction zone complexes (Warner et al., 1996).

Evaluation of rheological implications of the crustal reflectivity patterns also requires the consideration of the parameters which affect rheology such as temperature, pressure, fluids and lithology. Rheology and deformation mechanisms may vary over short spatial (shear zone) and temporal (earthquake cycle) scales (Bürgmann and Dresen, 2008). The pressure-dependent increase of the frictional strength of rocks with depth is bounded by thermally activated creep processes reducing viscous strength with increasing temperature and depth (Brace and Kohlstedt, 1980; Goetze and Evans, 1979). An example of strength-depth models for different heat flow regions is given in Figure 5.4 to show the effect of temperature on the rock strength.

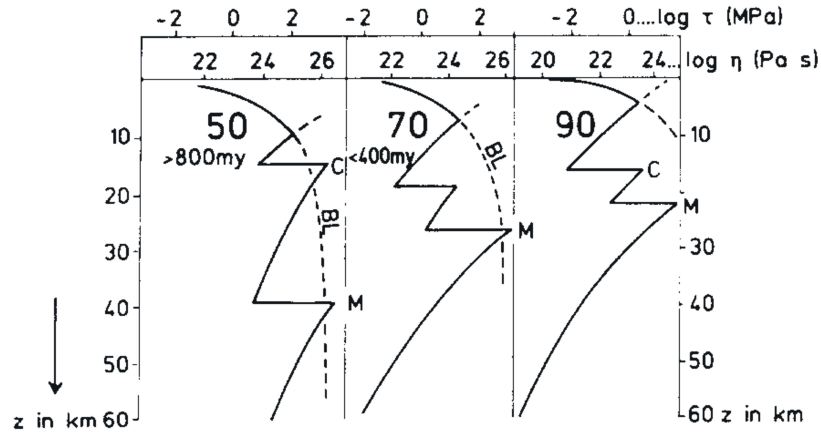


Figure 5.4: Strength-depth models for different heat flow regions (Meissner, 1996).

In the Sea of Marmara, recent microearthquake activity shows that the focal depth distributions are shallower than 20 km along the western part of the Main Marmara Fault and shallower than 15 km along the eastern part of the fault (Sato et al., 2004). CPD distribution in the region (Figure 1.4) also exhibits coherent depth estimations for the brittle-ductile transition. Depth of the Moho reflections obtained from the seismic sections also indicates that Moho is shallower in the east than in the west (Table 5.1) suggesting a crustal thinning from west to east in the Sea of Marmara.

Pn velocities, Pn and SKS anisotropy provide significant contributions to the interpretations of the mantle anisotropy. Pn phase is a high-frequency compressional wave propagating within a high velocity mantle lid (Menke and Richards, 1980; Beghoul et al, 1993). Pn wave velocity, which changes with the physical parameters of the uppermost mantle rocks such as temperature, composition, presence of water and volatiles, is often used to infer uppermost mantle rheology. Pn-wave velocity and anisotropy for the region are given by Al-Lazki et al. (2004) and presented in Figure 4.12. Higher Pn velocities ($>8\text{ km/s}$) imply a tectonically stable mantle lid and very low Pn velocities (<7.8) are usually an indication of partial melt (Hearn 1999; Calvert et al., 2000).

Al Lazki et al. (2004) have reported Pn velocities $>8\text{ km/s}$ for the west and $<8\text{ km/s}$ for the east of the Sea of Marmara. According to the data, east of the Sea of Marmara has potential for extension and partial melt whereas west of the Sea of Marmara indicates a tectonically stable mantle lid. Pn anisotropy directions for the eastern part of the Sea of Marmara including the Çınarcık Basin region mark an orientation of NW-SE, rotate to the west and exhibit NE-SW orientation for the western part of the

Sea of Marmara including the Tekirdağ Basin. The results also consistent with the prior Pn anisotropy observations in the region (Hearn, 1999).

SKS anisotropy direction, which is analyzed for the east of the Sea of Marmara (Figure 4.8), is not consistent with the Pn anisotropy data (Figure 4.12). Comparison of those two different data is important as they convey information from the different depth levels of the earth. Present-day Eurasia fixed vector directions are also not consistent for Pn anisotropy direction the east of the Sea of the Marmara. If the plate motion is decoupled from the flow beneath it, the fast polarization directions would coincide with the direction of the flow but might differ from the direction of plate motion (Tanimoto and Anderson, 1984). For the west of the Sea of Marmara, SKS (Hatzfeld et al., 2001), Pn anisotropy (Hearn, 1999; Al Lazki et al., 2004), GPS directions (McClusky et al., 2000) and strain directions (Allmendinger et al., 2007) are observed to be quite consistent. On the basis of the Pn anisotropy and SKS anisotropy, GPS vectors, it is suggested that, for the eastern Sea of Marmara uppermost mantle and upper mantle are decoupled from the crust. The decoupling process of continental lower crust and upper mantle from the overlying crust is defined as delamination. It causes highly reflective lower crust (as in the Çınarcık Basin) and heating follows delamination (Meissner and Mooney, 1998). A weak lower crust is necessary for decoupling and escape tectonics to take place (Kay and Mahlburg Kay, 1993). Decoupling of the crust and the mantle and partial melt (low Pn velocities) suggest weak lower crust and upper mantle for the eastern part of the Sea of Marmara. High Pn velocities, consistent GPS, Pn and SKS anisotropy directions suggest a strong mantle for the western Sea of the Marmara. Summary of the evaluations of this study and parameters obtained from prior studies are given in Table 5.1.

Different models are used to describe varying views of the distribution of rheological properties and strength in the Earth (Bürgmann and Dresen, 2008). The pressure-dependent increase of the frictional strength of rocks with depth is ultimately bound by thermally activated creep processes reducing viscous strength with increasing temperature and depth. Schematic view of first-order models of strength through continental lithosphere are given in Figure 5.5. Jelly Sandwich and Cream Brulee Models (Figure 5.5 a and b) are assumed for a strike-slip tectonic regime. A strong mantle characterizes a jelly sandwich model. In the model, weak middle and lower

Table 5.1: Variation of different physical parameters in the three deep basins of the Sea of Marmara.

	Tekirdağ Basin	Central Basin	Çınarcık Basin
Seismic Reflectivity (Lower Crust)	Not dense, nearly transparent	Complex, diffractions accompanied by dipping upper crustal reflections.	Bands of reflections
Seismic Reflectivity (Moho)	Dipping, discontinuous	Discontinuous, complex	Not clear
Pn Velocities	High (> 8km/s)	Moderate (~8 km/s)	Low (<8km/s)
Pn Anisotropy	NE-SW (Al-Lazki et al., 2004)	NW-SE + N-S (Al-Lazki et al., 2004)	NW-SE (Al-Lazki et al., 2004)
SKS Anisotropy	NE-SW (Hatzfeld et al., 2001)	Not available	NE-SW (Şapaş and Güney, 2009)
GPS Vectors	NE-SW (McClusky et al., 2000)	Transition (NE-SW / E-W) (McClusky et al., 2000)	E-W (McClusky et al., 2000)
Active Deformation	NE-SW Extension (Allmendinger et al., 2007)	NE-SW Extension (Allmendinger et al., 2007)	NE-SW Extension (Allmendinger et al., 2007)
Depth of Seismicity	Shallower than 20 km (Sato et al, 2004)	~20km (Sato et al, 2004)	Shallower than 15 km (Sato et al, 2004)
Magnetic Anomalies	Lower (-110 –30 nT) (Ateş et al., 2008)	Low (-10-100 nT) (Ateş et al., 2008)	High (310 – 380 nT) (Ateş et al., 2008)
Crust	Strong	Strong	Strong
Upper Mantle	Strong	Strong and Weak	Weak

crust sandwiched by strong upper mantle and strong upper crust (Hirth and Kohlstedt, 2003). In the cream brulee model, crust is strong and upper mantle is weak due to high temperatures and water content (Jackson, 2002). According to the banana split model, relative weakness of fault zones may exist everywhere and strength of the lithosphere decreases along the plate boundaries in spite of the thermal fluids and strain effects (Brudy et al., 1997).

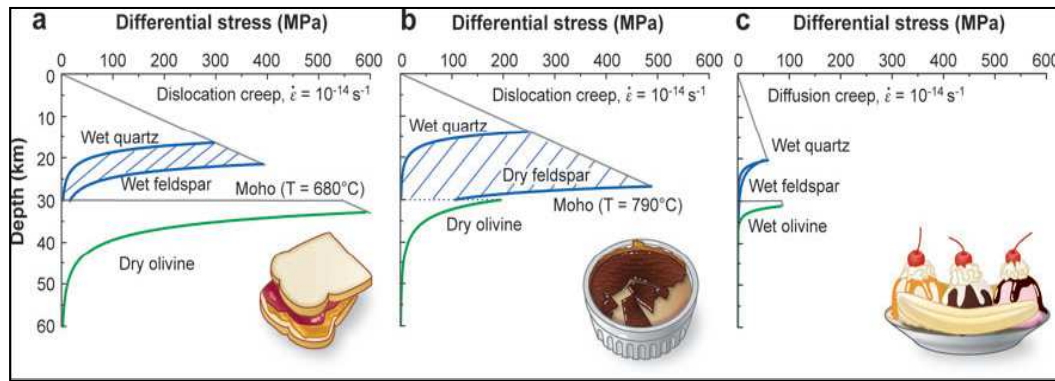


Figure 5.5: Different models of varying views of the rheological properties distribution and strength in the Earth. a) Jelly Sandwich Model, b) Cream Brulee Model, c) Banana Split Model (Bürgmann and Dresen, 2008).

Deep crustal reflections exhibit varying and complicated patterns under the basins. Reflectivity points out a highly reflective lower crust and probably hot region under extension beneath the Çınarcık Basin. In contrast, nearly transparent reflectivity and possible traces of Intra Pontid suture zone are observed beneath the Tekirdağ Basin. Observations are also supported with Pn velocity and Pn / SKS anisotropy variations, focal mechanism solutions, aeromagnetic measurements. The Central Basin seems to be the key location for the changing rheological properties since investigated parameters display moderate values between those of the Tekirdağ Basin and Çınarcık Basin (Table 5.1). Correlated data indicates weak mantle for the east of the Sea of Marmara (The Çınarcık Basin) due to different GPS, SKS and Pn anisotropy orientations (decoupling), low Pn velocities (partial melt), thinner crust (probable shallower Moho reflections). For the west of the Sea of Marmara (the Tekirdağ Basin), high Pn velocities, probable subduction traces (comparatively cold region) indicate a strong mantle. Differing strength of the mantle requires two different rheological models to explain the mechanical behaviour of the region. In the light of the classified parameters, investigated region is expressed in terms of two different rheological models (Figure 5.5), jelly sandwich for the west and cream brulee for the east of the Sea of Marmara considering the fact that rheology and deformation mechanisms may vary over short spatial (shear zone) scales (Bürgmann and Dresen, 2008). Such a rheological distinction is provided for the first time in the scope of the thesis, but detailed heat flow, gravity-magnetic and magnetotelluric future studies beneath the basins would provide significant contributions to the model presented.

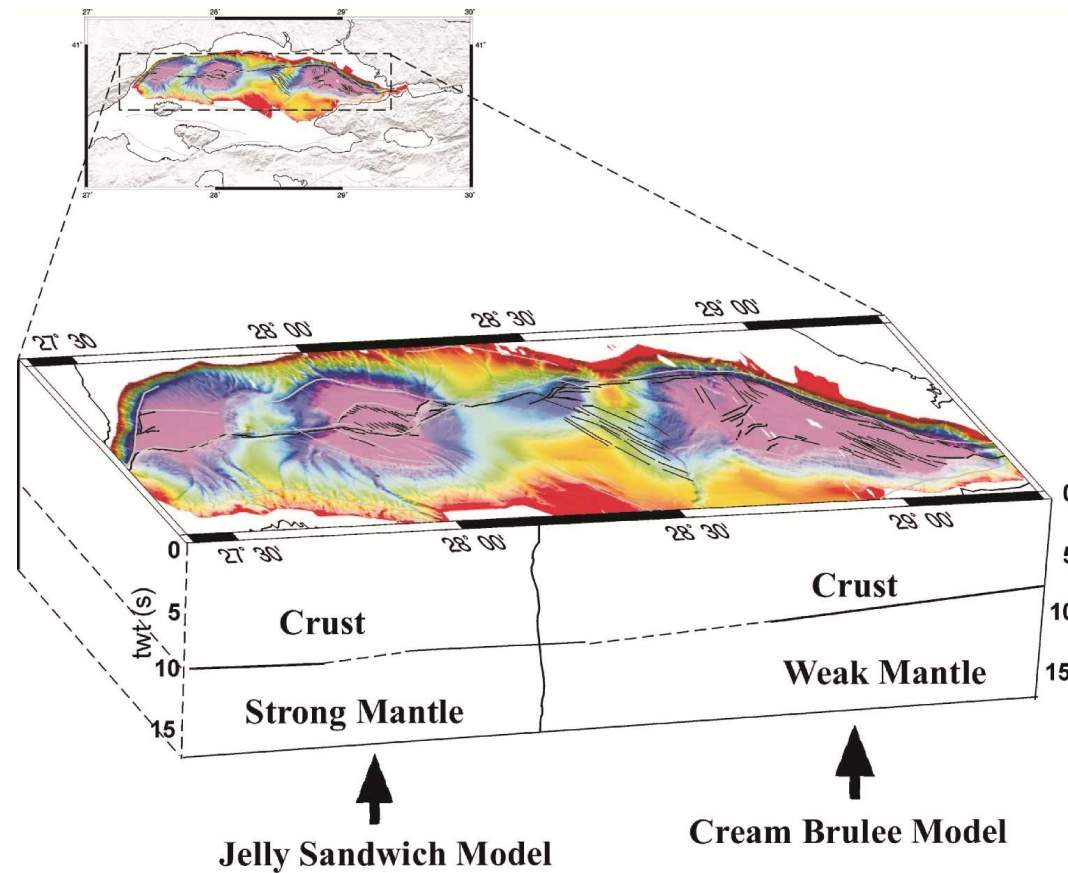


Figure 5.6: Schematic model for proposed rheological models for the Sea of Marmara including faults and bathymetry data (Le Pichon et al., 2001). Solid lines represent the results obtained from processed SEISMARMARA 2001 lines, dashed lines represent interpolation between obtained results.

REFERENCES

- Aksu, A. E., Calon, T. J., Hiscott, R.N., and Yaşar, D., 2000. Anatomy of the North Anatolian fault zone in the Marmara Sea, western Turkey: Extensional basins above a continental transform, *GSA Today*, **10**(6), 3-7.
- Al-Lazki, A., Sandvol, E., Seber, D., Barazangi, M., Turkelli, N., and Mohamad, R., 2004. Pn tomographic imaging of mantle lid velocity and anisotropy at the junction of the Arabian, Eurasian, and African plates, *Geophys. J. Int.*, **158**, 1024-1040.
- Alpar, B. and Yaltırak, C., 2002. Characteristic features of the North Anatolian Fault in the Eastern Marmara region and its tectonic evolution, *Mar. Geol.* **190**, 1/2. 329-350.
- Allmendinger, R., W., Nelson, K., D., Potter, C., J., Barazangi, M., Brown, L., D. and Oliver, J., E., 1987. Deep seismic reflection characteristics of the continental crust, *Geology*, **15**, 304-31.
- Allmendinger, R. W., Reilinger, R., and Loveless, J. P., 2007. Strain and rotation rate from GPS in Tibet, Anatolia, and the Altiplano, *Tectonics*, **26**, TC3013, doi:10.1029/2006TC002030.
- Ambraseys, N.N., 1970. Some characteristics features of the North Anatolian Fault Zone, *Tectonophysics*, **9**, 143-165.
- Ambraseys, N.N., 2002. The seismic activity of the Marmara Sea Region over the last 2000 Years, *Bull. Seism. Soc. Am.*, **92**, (1), 1 - 18.
- Ambraseys, N. N. and Jackson J. A., 2000. Seismicity of the Sea of Marmara (Turkey) since 1500, *Geophys. J. Int.*, **141**(3), F1-F6.
- Armijo, R., Meyer, B., Navarro, S., King, G. and Barka, A., 2002. Asymmetric slip partitioning in the Sea of Marmara pull-apart: a clue to propagation, *Geophys. J. Int.*, **171**(3), 1185-1197.
- Armijo, R. Pondard, N. Meyer, B. Mercier de Lepinay, B. Uçarkus, G., Malavieille, J. Dominguez, S., Gustcher, M-A. Beck, Çağatay, N. Çakir, Z., İmren, C., Kadir, E. and Natalin, and MARMARASCARPS cruise party *et al.*, 2005. Submarine fault scarps in the Sea of Marmara pull-apart (North Anatolian Fault): implications for seismic hazard in Istanbul, *Geochem. Geophys. Geosyst.*, **6**, 1-29.
- Ateş, A., Buyuksaraç, A., Bilim, F., Bektas, O., Şendur, Ç., and Komanovalı, G., 2008. Spatial correlation of the aeromagnetic anomalies and seismogenic faults in the Marmara region, NW Turkey, *Tectonophysics*, doi 10.1016/j.tecto.2008.09.025

- Ateş, A., Kayıran, T. and Sincer, I.,** 2003. Structural interpretation of the Marmara region from aeromagnetic, seismic and gravity data, *Tectonophysics*, **367**, 41-99.
- Avedik, F., Renard, V., Allenou, J. P. and Morvan, B.,** 1993. Single-bubble airgun for deep exploration, *Geophysics*, **58**, 366-382.
- Aydın, I., Karat, H., İ., and Koçak, A.,** 2005. Curie-point depth map of Turkey, *Geophys. J. Int.*, **162**(2), 633-640.
- BABEL Working Group,** 1991. Deep seismic survey images crustal structure of Tornquist Zone beneath Southern Baltic Sea, *Geophys. Res. Lett.*, **18**(6), 1091–1094.
- Babuska, V. and Cara, M.,** 1991. *Seismic anisotropy in the earth*, Kluwer Academic Publishers, Dordrecht, The Netherlands, 232 p.
- Bacon M., Simm R. and Redshaw T.,** 2003. *3-D seismic interpretation*, Cambridge University Press, New York, 212 pages.
- Baris, S., J. Nakajima, A. Hasegawa, Y. Honkura, A. Ito and S. B. Ucer,** 2005. Three-dimensional structure of Vp, Vs and Vp/Vs in the upper crust of the Marmara region, NW Turkey, *Earth Planets Space*, **57**, 1-21.
- Barka, A. A,** 1992. The North Anatolian fault zone, *Annales Tectonicae*, **6**, 164-195.
- Barka, A.,** 1997. Neotectonics of the Marmara Region, In *Active Tectonics of NW Anatolia-The Marmara Poly-project*, Schindler and Pfister (eds.), VDF, ETH Zurich, 55-87.
- Barka, A. and Gülen, L.,** 1989. Complex evolution of the Erzincan Basin (eastern Turkey), *J. Struct. Geol.*, **11**, 275–83.
- Barka, A. and Kadinski-Cade, K.,** 1988. Strike-slip fault geometry in Turkey and its influence on earthquake activity, *Tectonophysics*, **7**, 663– 684.
- Barka, A., et al.,** 2000. The August 17, 1999 Izmit earthquake, M = 7.4, eastern Marmara region, Turkey: Study of surface rupture and slip distribution, in *the 1999 İzmit and Düzce Earthquakes: Preliminary Results*, edited by A. A. Barka et al., pp. 15– 30, Istanbul Tech. Univ., Istanbul.
- Bayrak, M., Gürer, A., and Gürer, Ö. F.,** 2004. Electromagnetic imaging of the Thrace Basin and Intra-Pontide Subduction Zone, northwestern Turkey, *International Geology Review*, **46**, 64–74.
- Beghoul, N., Barazangi, M., and Isacks, B. L.,** 1993. Lithospheric structure of Tibet and western North America: Mechanisms of uplift and a comparative study, *J. Geophys. Res.*, **98**, 1997-2016.
- Bécel, A., et al.,** 2009. Moho, crustal architecture and deep deformation under the North Marmara Trough, from the SEISMARMARA Leg 1 offshore–onshore reflection–refraction survey, *Tectonophysics*, doi:10.1016/j.tecto.2008.10.022
- Bhattacharyya, B. K., and Leu, L. K.,** 1977. Spectral analysis of gravity and magnetic anomalies due to two-dimensional structures, *Geophysics*, **42**, 41-50.

- BIRPS and ECORS**, 1986. Deep seismic reflection profiling between. England, Ireland and France, *J. Geol. Soc. London*, **143**, 45-52.
- Bozkurt, E. And Koçyiğit, A.**, 1996. The Kazova basin: an active negative flower structure on the Almus Fault Zone, a splay fault system of the North Anatolian Fault Zone, Turkey, *Tectonophysics*, **265**, 239–54.
- Braile, L., W. and Chiang, C., S.**, 1986. The continental Mohorovicic discontinuity: results from near-vertical and wide-angle seismic reflection studies, *Geodynamics Series*, **13**, 257-271.
- Brace, W. F., and Kohlstedt, D., L.**, 1980. Limits on lithospheric stress imposed by laboratory experiments, *J. Geophys. Res.*, **B85**, 6248-6252.
- Bracewell, R.**, 1965. *The Fourier transform and its application*, Mc-Graw-Hill Book Co.
- Brudy, M., Zoback M.D., Fuchs, K., Rummel, F. and Baumgärtner, J.**, 1997. Estimation of the complete stress tensor to 8 km depth in the KTB scientific drill holes: implications for crustal strength. *J. Geophys. Res.*, **102**, 18453–18475.
- Bürgmann, R., and Dresen, G.** 2008. Rheology of the lower crust and upper mantle: Evidence from rock mechanics, geodesy and field observations, *Ann. Rev. Earth Plan. Sci.*, 36, doi:10.1146/annurev.earth.36.031207.124326, 531-567.
- Calvert, A., Sandvol, E., Seber, D., Barazangi, M., Vidal, F., Alguacil, G. and Jabour, N.**, 2000. Propagation of regional seismic phases (Lg and Sn) and Pn velocity structure along the Africa-Iberia plate boundary zone: tectonic implications, *Geophys. J. Int.*, **142**, 384-408.
- Carton, H., Singh, C., Hirn, A., Bazin, S., de Voogd, B., Vigner, A., Ricolleau, A., Çetin, S., Oçakoğlu, N., Karakoç, F. and Sevilgen, V.**, 2007. Seismic imaging of the three-dimensional architecture of the Çınarcık Basin along the North Anatolian Fault, *J. Geophys. Res.*, **112**, B06101, doi:10.1029/2006JB004548.
- Connard, G., Couch, R. and Gemperle, M.**, 1983. Analysis of aeromagnetic measurements from the Cascade Range in central Oregon, *Geophysics*, **48**, 376–390.
- Crampin, S., and Ucer, S. B.**, 1975. The seismicity of the Marmara Sea region of Turkey, *Royal. Astro. Soc. Geophys. Jour.*, **40**, 269-288.
- DEKORP Research Group**, 1985. First results and preliminary interpretation of deep-reflection seismic recordings along profile DEKORP 2-South, *J. Geophys.*, **57**, 137-163.
- Demirbağ, E., Rangin, C., Le Pichon, X., and Şengör, A.M.C.**, 2003. Investigation of the tectonics of the Main Marmara Fault by means of deep-towed seismic data, *Tectonophysics*, **361**, 1-19.
- Demirbağ, E., Kurt, H., Düşünür, D., Sarıkavak, K., and Çetin, S.**, 2007. Constructing a 3D structural block diagram of the Central Basin in Marmara Sea by means of bathymetric and seismic data, *Marine Geophys. Res.*, **28**, 343–353.

- Dewey, J. F. and Şengör, A. M. C.,** 1979. Aegean and Surrounding Regions; Complex Multiplate and Continuum Tectonics in a Convergent Zone, *Geol. Soc. Am. Bull.*, part 1, **90**, 84-92.
- Egeran, N.,** 1947. Tectonique de la Turquie et Relation Entre Les Unites Tectoniques et Les Gites Metalliferes de la Turquie, 1, 8, 197p, These, Nancy.
- Erden, F., and Oray, E.,** 1977. Türkiye Gravite Haritası. 1/500,000 İstanbul Bouguer Anomali Haritası, Maden Tetkik ve Arama Enstitüsü, Ankara.
- Ergün, M., and Özel, E.,** 1995. Structural relationship between the sea of Marmara Basin and the North Anatolian Fault Zone, *Terra Nova*, **7**, 278-288.
- Eyidoğan, H.,** 1988. Rates of crustal deformation in western Turkey as deduced from major earthquakes, *Tectonophysics*, **148**, 83-92.
- Flerit, F., Armijo, R., King, G. C. P., Meyer, B., and Barka, A.,** 2003. Slip partitioning in the Sea of marmara pull-apart determined from GPS velocity vectors, *Geophys. J. Int.*, **154**, 1-7.
- Freeman B., Klemperer S. L., and Hobbs R. W.,** 1988. The deep structure of northern England and the Iapetus Suture zone from BIRPS deep seismic reflection profiles, *J. Geol. Soc.*, **145**, 727 - 740.
- Goldstein, P., D. Dodge and M. Firpo,** 1999. SAC2000: Signal processing and analysis tools for seismologists and engineers, UCRL-JC-135963, Invited contribution to the IASPEI, *International Handbook of Earthquake and Engineering Seismology*.
- Goleby, B., R., Wright, C., Collins, C., D., N. and Kennett B., L. .N.,** 1988. Seismic reflection and refraction profiling across the Arunta Block and the Ngalia and Amadeus Basins. Australia, *J. Earth Sci.*, **35**, 275–294.
- Goetze, Ch., and Evans, B.,** 1979. Stress and temperature in the bending lithosphere as constrained by experimental rock mechanics, *Geophys. J.R. astr. Soc.*, **59**, 463-478.
- Gürbüz, C., Aktar, M., Eyidoğan, H., Cisternas, A., Haessler, H., Barka, A., Ergin, M., Türkelli, N., Polat, O., Üçer, S. B., Kuleli, Baris, Ş., Kaypak, B., Bekler, T., Zor, E., Biçmen, F., and Yörük, A.,** 2000. The seismotectonics of the Marmara region (Turkey): results from a microseismic experiment, *Tectonophysics*, **316**, 1-17.
- Gürbüz, C., Üçer, S. B. and Özdemir, H.,** 1980. Preliminary results of a seismic experiment in the Adapazarı region, Turkey, *Bull. Earthquake. Res. Ins.* **31**, 73-88 (in Turkish).
- Gürer, A.,** 1996. Deep conductivity structure of the North Anatolian Fault Zone and the İstanbul Sakarya zones along the Gölpaazarı–Akçayaova profile, Northwest Anatolia, *International Geology Review*, **38**, 727–737.

- Hatzfeld, D., Karagianni, E., Kassaras, I., Kiratzi, A., Louvari, E., Lyon-Caen, H., Makropoulos, K., Papadimitriou, P., Bock, G. and Priestley, K., 2001.** Shear wave anisotropy in the upper mantle beneath the Aegean related to internal deformation, *J. Geophys. Res.*, **106** (12), 30737–30753.
- Hearn, T.M., 1999.** Uppermost mantle velocities and anisotropy beneath Europe, *J. Geophys. Res.*, **104**, 15 123–15 139.
- Hearn, E. H., Bürgmann, R. and Reilinger, R., 2002.** Dynamics of İzmit earthquake postseismic deformation and loading of the Düzce earthquake hypocenter, *Bull. Seism. Soc. Am.*, **92**, 172-193.
- Hirth, G., and Kohlstedt, D.L., 2003.** Rheology of the upper mantle and the mantle wedge: A view from the experimentalists, in Eiler, J., (ed.), *Inside the Subduction Factory*, **138**, *Geophysical Monograph*, American Geophysical Union, 83-105.
- Honkura, Y., Işıkara, A., M., Kolçak, D., Orbay, N., Sipahioğlu, S., Oshiman, N., and Tanaka, H., 1985.** Magnetic Anomalies and Low Ground Resistivity as possible indicators of Active Fault Location: Preliminary results of Electric and Magnetic Observations from the western part of the North Anatolian Fault Zone, *J. Geomag. Geoelectr.*, **37**, 169-187.
- Horasan, G. and Boztepe-Güney, A., 2004.** S-wave attenuation in the Sea of Marmara, *Phys. Earth Plan. Int.*, **142**, 215-224.
- Horasan, G., Gülen, L., Pinar, A., Kalafat, D., Özel, N., Kuleli, H., S., and Işıkara, A., M., 2002.** Lithospheric Structure of the Marmara and Aegean Regions, Western Turkey, *Bull. Seism. Soc. Am.*, **92**, 322 – 329.
- Hubert-Ferrari, A., Armijo, R., King, G. C. P, Meyer, B. and Barka, A., 2002.** Morphology, displacement, and slip rates along the North Anatolian Fault, Turkey, *J. Geophys. Res.*, **107**, no.10.1029.
- İlkışık, O.M., 1995.** Regional heat flow in western Anatolia using silica temperature estimates from thermal springs, *Tectonophysics*, **244**, 175-184.
- İlkışık, O.M., Alptekin, Ö., Ezen, Ü. and Üçer, S.B., 1990.** Heat flow, seismicity and crustal structure of western Anatolia, Proceedings, 2, in *IESCA (Intern. Earth Sci. Cong. on Aegean Region)*, Savaşçın, M.Y. Eronat, A.H.,(editors), 1-112, İzmir, Turkey.
- İlkışık, O.M., Öztürk, S., Şener and Çokgöz, T., 1995.** Geothermic investigations in Turkey, *Jeofizik*, **9** (1-2), 117–122 (in Turkish).
- İmren, C., Le Pichon, X., Rangin, C., Demirbağ, E., Ecevitoglu, B. and Görür, N., 2001.** The North Anatolian Fault within the Sea of Marmara : a new evaluation based on multichannel seismic and multibeam data, *Earth. Planet. Sci. Lett.*, **186**, 143-158.
- İmren, C., 2003.** Marmara Denizi faal tektonizmasının sismik yansıma ve derinlik verileri ile incelenmesi, *Ph.D. Thesis*, Istanbul Technical University Institute of Science and Technology, 201 pages.

- Ivan, M.**, 2001. SKS splitting observed at GEOFON station MLR in Vrancea area - Romania, *Rev. Roum. GEOPHYSIQUE*, **44**, 79-86.
- Jackson, J.**, 2002. Faulting, flow, and the strength of the continental lithosphere, *Int. Geol. Rev.* **44**, 39–61.
- Jones E.J.W.**, 1999. *Marine Geophysics* - University College, London, UK, Wiley, Chichester, West Sussex PO19IUD, England, 466 pp.
- Kahle, H.G., Cocard, M., Peter, Y., Geiger, A., Reilinger, R., Barka, A. and Veis, G.**, 2000. GPS-derived strain rate field within the boundary zones of the Eurasian, African, and Arabian Plates, *J. Geophys. Res.*, **105**, 23 353–23 370.
- Kanbur, Z. Alptekin, O. Utkucu, M. and Kanbur, S.**, 2007. Imaging the basin and fault geometry from the multi-channel seismic reflection data in the Tekirdağ Basin, Marmara Sea, Turkey, *Geophys. J. Int.* **169**(2), 659-666.
- Karabulut, H., Bouin, M.P., Bouchon, M., Dietrich, M., Cornou, C. and Aktar, M.**, 2002. The seismicity of Eastern Marmara Sea after the 17 August 1999 İzmit earthquake, *Bull. Seism. Soc. Am.*, **92**, 387–393.
- Karabulut, H., Özalaybey, S., Taymaz, T., Aktar, M., Selvi, O. and Kocaoğlu, A.**, 2003. A tomographic image of the shallow crustal structure in the Eastern Marmara, *Geophys. Res. Lett.*, **30** (24), 10.1-10.4.
- Karabulut, H. and Özalaybey, S.**, 2006. Crustal structure in the Marmara Region and the seismicity along the North Anatolian Fault Zone. *International Workshop in Comparative Studies of the NAF and the San Andreas Fault*, İTÜ Maslak Campus, 14 August 2006, İstanbul.
- Kay, R., W., and Mahlburg, Kay, S.**, 1993. Delamination and delamination magmatism, *Tectonophysics*, **219**, 177-189.
- Ketin, İ.**, 1948. Über die tektonisch–mechanischen Folgerungen aus den grossen anatolischen Erdbeben des letzten Dezenniums, *Geol. Rundsch.*, **36**, 77–83.
- Ketin, İ.**, 1969. Kuzey Anadolu Fayı hakkında, *MTA Dergisi*, **72**, 1-27.
- Kind, R., Kosarev, G. L., Makeyeva, L. I. and Vinnik, L. P.**, 1985. Observations of laterally inhomogeneous anisotropy in the continental lithosphere, *Nature*, **318**, 358–361.
- Klemperer, S.L., Hauge, T.A., Hauser, E.C., Oliver, J.E. and Potter, C.J.**, 1986. The Moho in the northern Basin and Range province, Nevada, along the COCORP 400N seismic reflection transect, *Geol. Soc. Am. Bull.*, **97**, 603–618.
- Koçyiğit, A.**, 1988. Tectonic setting of the Geyve Basin: Age and total displacement of the Geyve Fault Zone, *METU J. Pure Appl. Sci.*, **21**, 81–104.
- Koçyiğit A.**, 1989. Su, şehri basin: an active fault wedge basin on the North Anatolian Fault Zone, Turkey, *Tectonophysics*, **167**, 13–29.

- Koçyiğit, A.**, 1991. An example of an accretionary forearc basin from northern central Anatolia and its implications for the history of subduction of Neo-Tethys in Turkey, *Geol. Soc. Am. Bull.*, **103**, 22–36.
- Laigle, M., Becel, A., Voogd, B., Hirn, A., Taymaz, T. and Özalaybey S.**, 2008. Members of SEISMARMARA Leg1 Team, A first deep seismic survey in the Sea of Marmara: Deep basins and whole crust architecture and evolution, *Earth. Planet. Sci. Lett.*, **270**, 168–179.
- Le Pichon, X., Şengör, A.M.C., Demirbağ, E., Rangin, C., İmren C., Armijo, R., Görür, N., Çağatay, N., de Lepinay, B.M., Meyer, B., Saatçılar, R., and Tok, B.**, 2001. The active main Marmara fault, *Earth. Planet. Sci. Lett.*, **192**, 595-616.
- Lüschen, E., Wenzel, F., Sandmeier, K., J., Menges, D., Rühl, T., Stiller, M., Janoth, W., Keller, F., Söllner, W., Thomas, R., Krohe, A., Stenger, R., Fuchs, K., Wilhelm, H. and Eisbacher, G.**, 1987. Near-vertical and wide-angle seismic surveys in the Black Forest, SW-Germany, *J. Geophys.*, **62**, 1–30.
- Meade, B.J., Hager, B.H., McClusky, S.C., Reilinger, R.E., Ergintav, S., Lenk, O., Barka, A., and Özener, H.**, 2002. Estimates of seismic potential in the Sea of Marmara region from block models of secular deformation constrained by Global Positioning System Measurements, *Bull. Seism. Soc. Am.*, **92**, 208-215.
- McClusky, S., S. Bassalanian, A. Barka, C. Demir, S. Ergintav, I. Georgiev, O. Gurkan, M. Hamburger, K. Hurst, H.-G. Hans-Gert, K. Karstens, G. Kekelidze, R. King, V. Kotzev, O. Lenk, S. Mahmoud, A. Mishin, M. Nadariya, A. Ouzounis, D. Paradissis, Y. Peter, M. Prilepin, R. Relinger, I. Sanli, H. Seeger, A. Tealeb, M.N. Toksaz, and G. Veis**, 2000. Global Positioning system constraints on plate kinematics and dynamics in the eastern Mediterranean and Caucasus, *J. Geophys. Res.*, **105** (B3), 5695-5719.
- McClusky, S., Reilinger, R., Mahmoud, S., Ben Sari, D. and Tealeb, A.**, 2003. GPS constraints on Africa (Nubia) and Arabia plate motion, *Geophys. J. Int.*, **155**, 126-138.
- McKenzie, D.**, 1972. Active Tectonics of Mediterranean Region, *Geophys. J. R. Astro. Soc.*, **30**, 109-185.
- McQuillin, M. Bacon and W. Barclay**, 1984. An introduction to seismic interpretation, *Reflection Seismics in Petroleum Exploration*, 287 pp.
- Meade, B.J., Hager, B. H. and Reilinger, R. E.**, 2002. Estimates of seismic potential in the Marmara region from block models of secular deformation constrained by GPS measurements, *Bull. Seism. Soc. Am.*, **92**, 208-215.
- Meissner, R.**, 1989. Rupture, creep, lamellae and crocodiles: happenings in the continental crust, *Terra Nova*, **1**, 17-28.
- Meissner, R.**, 1996. Faults and folds, facts and fiction, *Tectonophysics*, **264**, 279–293.

- Meissner, R. and Mooney, W.D.**, 1998. Weakness of the lower continental crust: a condition for delamination, uplift, and escape, *Tectonophysics*, **296**, pp. 47–60
- Menke, W. and Richards P. G.**, 1980. Crust-mantle whispering gallery phases: A deterministic model of teleseismic Pn wave propagation, *J. Geophys. Res.*, **85**, 5416-5422.
- Nakamura, A., Hasegawa, A., Ito, A. Üçer, B., Barış, Ş., Honkura, Y., Kono, T., Hori, S., Pektaş, R., Komut, T., Çelik, C. and Işıkara, A. M.**, 2002. P-wave structure of the crust and its relationship to the occurrence of the 1999 İzmit, Turkey earthquake and aftershocks, *Bull. Seism. Soc. Am.*, **92**, 330-338.
- Newman, P.**, 1973. Divergence effects in a layered earth, *Geophysics*, **38**, 481–488.
- Okay, A.I.**, 1989. Tectonic units and sutures in the Pontides, northern Turkey: ed. A.M.C. Şengör, Tectonic Evolution of the Tethyan Region, *Kluwer Academic Publ.*, 109-116.
- Okay, A. I. and Tüysüz, O.**, 1999. Tethyan sutures of Northern Turkey. In the “Mediterranean Basins: Tertiary extension within the Alpine Orogen “ (eds. B.Durand, L. Jolivet, F. Horváth and M Séranne), *J. Geol. Soc. London, Special Publication*, **156**, 475-515.
- Okay, A., Şengör A.M.C., Görür, N.**, 1994. Kinematic history of the Black Sea and its effect on the surrounding regions, *Geology*, **22**, 267–270.
- Okay, A., Şatır, M., Maluski, H., Siyako, M., Monie, P, Metzger, R and Akyüz, S.**, 1996. Palaeo and Neotethyan events in northwest Turkey: geological and geochronological constraints in: *Tectonics of Asia*, Yin, A. and Harrison, M.(eds), Cambridge University Press, 420-441.
- Okay, A.I., Demirbağ, E., Kurt, H., Okay, N., Kuşçu, İ.**, 1999. An active, deep marine strike-slip basin along the North Anatolian Fault in Turkey, *Tectonics*, **18**,129–47.
- Okay, A.I., Kaşlılar-Özcan, A., İmren, C., Boztepe-Güney, A., E. Demirbağ, and Kuşçu, İ.**, 2000. Active faults and evolving strike-slip basins in the Marmara Sea, northwest Turkey: a multichannel seismic reflection study, *Tectonophysics*, **321**, 189-218.
- Okay, A.I., Tüysüz, O. and Kaya, S.**, 2004. From transpression to transtension: changes in morphology and structure around a bend on the North Anatolian Fault in the Marmara region, *Tectonophysics*, **391**, 259-282.
- Özalaybey, S., Karabulut, H., Ergin, M., Tapırdamaz, C., Yörük, A., Biçmen, F. and Aktar, M.**, 2002. SEISMARMARA 2001: A Marine Seismic Survey and Offshore-Onshore Artificial Source and Natural Earthquakes in the Seismogenic Regions of the Sea of Marmara, *1st International Symposium of ITU the Faculty of Mines on Eartrh Sciences and Engineering*, May 16-18, Istanbul.
- Parkes, G. E., Ziolkowski, A. M., Hatton, L. and Haugland, T.**, 1984. The Signature of an Air Gun Array: Computation From Near-Field Measurements Including Interactions-Practical Considerations, *Geophysics* , **49**, 105-111.

- Parke, J. R., Minshull, T. A., Anderson, G., White, R. S., McKenzie, D., Kuşcu, İ., Bull, J. M., Görür, N. and Şengör, C.,** 1999. Active faults in the Sea of Marmara, western Turkey, imaged by seismic reflection profiles, *Terra Nova*, **11** (5), 223-227.
- Parke, J. R., White, R.S., McKenzie, D., Minshull, T. A., Bull, J. M., Kuşcu, İ. Görür, N. and Şengör, C.,** 2002. Interaction between faulting and sedimentation in the Sea of Marmara, western Turkey, *J. Geophys. Res.-Solid Earth*, **107**, art. no.2286.
- Parsons, T., Toda, S., Stein, R., A. Barka, and J. Fieterich,** 2000. Heightened odds of large earthquakes near Istanbul: an interaction-based probability calculation, *Science*, **288**, 661-665.
- Pfannenstiel, M. ,** 1944. Diluviale Geologie des Mittelmeergebietes: die diluvialen Entwicklungstadien und die Urgeschichte von Dardanellen, Marmara Meer und Bosphorus, *Geol. Rund.*, **34**, 342-334.
- Pınar, N. ,** 1943. Marmara denizi havzasının sismik jeolojisi ve meteorolojisi, *Fen Fak. Monografileri*, A7, 64 pages.
- Pollack, H. N., Hurter, S. J. and Johnson, J. R.,** 1993. Heat flow from the Earth's interior: analysis of the global data set, *Rev. Geophys.*, **31**, 267–280.
- Rangin, C., Demirbağ, E. and İmren C,** 2001. *Marine Seismic Atlas of the Sea of Marmara*. 7 A0 and one booklet. Special publication. Brest, France: Ifremer Technology Center.
- Reilinger, R., McClusky, S., Vernant, P., and 20 others,** 2006. GPS constraints on continental deformation in the Africa-Arabia-Eurasia continental collision zone and implications for the dynamics of plate interactions, *J. Geophys. Res.*, **111**, B05411, doi:10.1029/2005JB004051.
- Reilinger, R. and Barka, A., A.,** 1997. GPS constraints on slip rates in the Arabia-Africa-Eurasia plate collision zone: Implications for the earthquake recurrence times, *NATO ASI Series*, **28**, 91-108.
- Rudnick, R.L.,** 1996. Making continental crust: *Nature*, **378**, 571-578.
- Sadowiak, P., Voss, J. and Meissner, R.,** 1989. 3 D modelling of diffractions observed on deep reflection line DEKORP 2-S. *Geophys. Prospect.* **37**, 623–637.
- Sadowiak, P. and Wever, Th.,** 1990. Reflection-diffraction seismic patterns at crustal suture zones, *Tectonics*, **9**, 495–1513.
- Sadowiak P., Wever, Th. and Meissner, R.,** 1991. Deep seismic reflectivity patterns in specific tectonic units of western and central Europe, *Geophys. J. Int.*, **105**, 45-54.
- Sakıncı, M., Yalırak C. and Oktay, F. Y.,** 1999. Palaeogeographical evolution of the Thrace Neogene Basin and the Tethian–Paratethian relations at northwest Turkey (Thrace), *Palaeogeogr. Palaeoclimatol. Palaeoecol.*, **15**, 17–40.

- Sandvol, E., Türkelli, N., Zor, E., Gök, R., Bekler, T., Gurbuz, C., Seber, D., and Barazangi, M.,** 2003. Shear wave splitting in a young continent continent collision: An example from Eastern Turkey, *Geophys. Res. Lett.*, **30**(24), 8041.
- Sato, T., Kasahara, J., Taymaz, T., Ito, M., Kamimura, A., Hayakawa, T. and Tan, O.,** 2004. A study of microearthquake seismicity and focal mechanisms within the Sea of Marmara (NW Turkey) using ocean bottom seismometers (OBSs), *Tectonophysics*, **391**, 1-4, 303-314.
- Seyitoğlu, G. and Scott, B.,** 1991. Late Cenozoic crustal extension in west Anatolia, Turkey, *Tethyan Workshop*, Edinburgh University, Scotland, UK.
- Seyitoğlu, G., Scott, B.C. and Rundle, C.C.,** 1992. Timing of Cenozoic extensional tectonics in west Turkey, *J. Geol. Soc. London*, **149**, 533-538.
- Seeber, L., Emre, O., Cormier, M. H., Sorlien, C.C., McHugh, C.M.G., Polonia, A., Özer, N., Çağatay, N. and The team of the 2000 R/V Urania Cruise in the Marmara Sea,** 2004. Uplift and subsidence from oblique slip: the Ganos–Marmara bend of the North Anatolian Transform, western Turkey, *Tectonophysics*, **391**, 239-258.
- Sheriff, R. E.,** 1984. *Encyclopedic dictionary of exploration geophysics*, Society of Exploration Geophysics, 323 p.
- Shuey, R. T., Schellinger, D. K., Tripp A. C. and Alley, L. B.,** 1977. Curie depth determination from aeromagnetic spectra, *Geophys. J. R. Astr. Soc.*, **50**, 75–101.
- Silver, P., G. and Chan, W.,** 1988. Implications for continental structure and evolution from seismic anisotropy, *Nature*, **335** , 34–39.
- Silver, P. G. and Chan, W.** 1991. Shear wave splitting and subcontinental mantle deformation, *J. Geophys. Res.*, **96**, 16429–16454.
- Silver, P. G. and M. K. Savage,** 1994. The interpretation of shear-wave splitting parameters in the presence of two anisotropic layers, *Geophys. J. Int.*, **119**, 949-963.
- Siyako, M., Taniş, T. and Şaroğlu, F.,** 2000. Active fault geometry of the Marmara, Sea, *Science and Technology*, **388**, 66–71.
- Smith, W. H. F. and Sandwell, D. T.,** 1997. Global seafloor topography from satellite altimetry and ship depth soundings, *Science*, **277**, 195-196.
- Spindler , I.,** 1896. Materiali po gidrologii Mramornago Morya. In: I.B. Spindler, Editor, *Mramornoe More Ekspeditsia Imperatorskago Russkago Geograficheskago Obshestva v 1894 godu Zapiski Imperatorskago Russkago Geograficheskago Obshestva*, po Obshei Geografii, Sanktpeterburg, **33** (2), 1–123.
- Spindler I, Andrusov, N. and Ostroumov, A.,** 1896. Marmornoe More. Ekspeditsia Imperatorskago Russkago Geograficheskago Obshestva v 1894 godu, *Zapiski Ekspeditsia Imperatorskago Russkago Geogr. Obshestva Obshei Geogr.*, **33**, 2, VII+180 pp.+V foldout plates.

- Straub, C., H.G. Kahle, and C. Schindler**, 1997. GPS and geologic estimates of the tectonic activity in the Marmara sea region, NW Anatolia, *J. Geophys. Res.*, **102**, 27 587-27 601.
- Şapaş, A. and Boztepe-Güney, A.**, 2005, The analysis of SKS splitting in Western Turkey, *International Earth Sciences Colloquium on the Aegean Regions*, Abstracts Book, p.262., Dokuz Eylül University, 4-7 October 2005, İzmir, Turkey.
- Şapaş, A. and Boztepe-Güney, A.**, 2009. SKS splitting in the Isparta Angle, the Southwestern Turkey: Anisotropic Complexity in Mantle, *Journal of Earth System Science*, **118**, 71-80.
- Şaroğlu F.**, 1988. Age and offset of the North Anatolian Fault. *METU J. Pure Appl. Sci.* **21**, 65–79.
- Şaroğlu, F., Emre, Ö. and Kuşçu, İ.**, 1992. *Türkiye Diri Fay Haritası*, Maden Tetkik Arama, Genel Müdürlüğü, Ankara.
- Şengör, A. M. C.**, 1979. The North Anatolian transform fault: its age, offset and tectonic significance, *J. Geol. Soc. London*, **136**, 269-282.
- Şengör, A. M. C.**, 1984. The Cimmeride Orogenic System and Tectonics of the Mediterranean Cimmerides, evolution of the western termination of Paleotethys. In: Dixon, J. E. and Robertson, A.H.F.(eds.) *the Geological evolution of the Eastern Mediterranean. Spec. Publ.*, **14**, Geol. Soc., 77-112.
- Şengör, A. M. C. and Yılmaz, Y.**, 1981. Tethyan evolution of Turkey: a plate tectonic approach, *Tectonophysics*, **75**, 181-241.
- Şengör, A. M. C., Görür, N. and Şaroğlu, F.**, 1985. Strike-slip faulting and related basin formation in zones of tectonic escape: Turkey as a case study, Strike-slip Deformation, Basin Formation, and Sedimentation, *Soc. Econ. Paleont. Min. Spec. Pub.*, **37**, (in honor of J.C. Crowell), 227-264.
- Şengör, A.M.C., Tüysüz, O., İmren, C., Sakınc, M., Eyidoğan, H., Görür, N., Le Pichon, X. and Claude Rangin, C.**, 2005. The North Anatolian Fault. A new look, *Ann. Rev. Earth Planet. Sci.*, **33**, 37-112.
- Tanaka, A., Okubo, Y. and Matsubayashi, O.**, 1999. Curie point depth based on spectrum analysis of the magnetic anomaly data in East and Southeast Asia, *Tectonophysics*, **306**, 461–470.
- Taner, M. T., Koehler, F., and Sheriff, R. E.**, 1979. Complex seismic trace analysis, *Geophysics*, **44**, 1041-1063.
- Tanimoto, T., and Anderson, D., L.**, 1984. Mapping convection in the mantle, *Geophys. Res. Lett.* **11**, 287-290.
- Tank, S., B., Honkura, Y., Ogawa, Y., Oshiman, N., Tunçer, M., K., Matsushima, M., Çelik, C. Tolak, E. and Işıkara, A. M.**, 2003. Resistivity structure in the western part of the fault rupture zone associated with the 1999 İzmit earthquake and its seismogenic implication, *Earth Planets Space*, **55**, 437–442.

- Tank, S., B., Honkura, Y., Ogawa, Y., Matsushima, M., Oshiman, N., Tuncer, M., K., Celik, C., Tolak, E. and Isikara, A., M., 2005,** Magnetotelluric imaging of the fault rupture area of the 1999 Izmit (Turkey) earthquake, *Physics of the Earth and Planetary Interiors*, **150**, 213-225.
- Taner, M. T., Koehler, E., and Sheriff, R. E., 1979.** Complex Seismic Trace Analysis, *Geophysics*, **44**, 1041-1063.
- Taymaz, T., 1999.** Seismotectonics of the Marmara Region: Source characteristics of 1999 Gölcük-Sapanca-Düzce earthquakes, *Proceedings of ITU-IAHS*, International Conference On The Kocaeli Earthquake 17 August 1999, Istanbul-Turkey, 2 - 5 December 1999, 55-78.
- Teanby, N. A., Kendall, J., M. and Van der Baan, M., 2004.** Automation of shear-wave splitting measurements using cluster analysis, *Bull. Seism. Soc. of Am.*, **94** (2), 453-463.
- Tezcan, A. K., 1979.** Geothermal Studies, Their Present Status and Contribution to Heat Flow Contouring in Turkey, in *Terrestrial Heat Flow in Europe*. Ceimak, V., Rybach, L. (Editors), Springer-Verlag; Berlin, p.,283-292.
- Tezcan, A.K., 1995.** Geothermal explorations and heat flow in Turkey, in *Terrestrial Heat Flow and Geothermal Energy in Asia*, Gupta, M.L., Yamano, M., (editors), Oxford and IBH publishing Co. Pvt. Ltd., pp. 23-42 New Delhi .
- Thybo, H., 1997.** Geophysical characteristics of the Tornquist fan area Northwest Trans-European suture zone; indication of Late Carboniferous to Early Permian dextral transtension, *Geol. Mag.*, 597-606.
- Tunçer, M. K., Honkura, Y., Oshiman, N., Ikeda, Y., and Işıkara, A. M., 1991.** Magnetic Anomalies Related to Active Folds in the North Anatolian Fault Zone, *J. Geomag. Geoelectr.*, **43**, 813-823.
- Toprak, V., 1988.** Neotectonic characteristics of the North Anatolian Fault Zone between Koyulhisar and Su,sehri (NE Turkey), *METU J. Pure Appl. Sci.*, **21**,155-66.
- Trappe, H., Wever, Th., and Meissner, R., 1988.** Crustal reflectivity pattern and its relation to geological provinces. *Geophys. Prosp.*, **36**, 265-281.
- Tüysüz, O., Barka, A., and Yiğitbaş, E. 1998.** Geology of the Saros graben and its implications for the evolution of the North Anatolian fault in the Ganos-Saros region, northwestern Turkey, *Tectonophysics*, **293**, 105-126.
- Url-1** <<http://atlas.cc.itu.edu.tr/~okay/>>, accessed at 12.09.2008
- Url-2** <<http://www.ipgp.fr>>, accessed at 18.05.2007.
- Url-3** <<http://garnero.asu.edu>>, accessed at 16.09.2008.
- Url-4** <<http://pubs.usgs.gov/gip>>, accessed at 15.07.2009.
- Üçer, B., Eyidoğan, H., Barka, A., Gürbüz, C. and Barış, Ş., 1997.** Seismic investigations of the Marmara Region, In *Active Tectonics of*

Northwestern Anatolia-The Marmara Poly-Project, (Eds. C. Shindler and M. Pfister), Hochschulverlag AG an der ETH Zurich, 89-99.

- Vacquier, V. and Affleck J.**, 1941. A computation of the average depth to the bottom of the earth's magnetic crust on a statistical study of local magnetic anomalies, *Trans. Amer. Geophys. Union*, **22**, 446-450.
- Vecsey, L., Plomerová, J. and Babuška, V.**, 2008. Shear-wave splitting measurements-problems and solutions, *Tectonophysics*, **462**, 178-196.
- Vinnik, L. P., Kosarev, G. L. & Makeyeva, L. I.** 1984. Anisotropy of the lithosphere from observations of SKS and SKKS, *Dokl. Akad. Nauk USSR* (in Russian), **278**, 1335-1339.
- Vinnik, L., P., Kind, R., Kosarev, G., L. and Makeyeva L., I.**, 1989. Azimuthal anisotropy in the lithosphere from observations of long-period S-waves, *Geophys. J. Int.*, **99**, 549-559.
- Vinnik, L., P., Makeyeva, L., Milev, A., and Usenko, A.Y.**, 1992. Global patterns of azimuthal anisotropy and deformations in the continental mantle, *Geophys. J. Int.* **111**, 433-447.
- Warner M., Morgan J., Barton P., Morgan P., Price C. and Jones K.**, 1996. Seismic reflections from the mantle represent relict subduction zones within continental lithosphere, *Geology*, **24**, 39-42.
- Wever, Th. and Sadowiak, P.**, 1991. Crustal structure zones: seismic signature and structural interpretation. In: R. Meissner *et al.*, *Continental Lithosphere: Deep Seismic Reflections Geodyn. Ser.*, **22**, 371-375 Washington, DC .
- Westaway, R.**, 1994. Present-day kinematics of the Middle East and Eastern Mediterranean, *J. Geophys. Res.*, **99**, 12071-12090.
- Westaway, R.**, 2004. Kinematic consistency between the Dead Sea Fault Zone and the Neogene and Quaternary left-lateral faulting in SE Turkey, *Tectonophysics*, **391**, 203-237.
- Wong, H. K., Ludmann, T., Uluğ, A. and Görür, N.**, 1995. The Sea of Marmara: A plate boundary sea in an escape tectonic regime, *Tectonophysics*, **244**, 231-250.
- Yaltrak, C.**, 1996. Ganos Fay Sisteminin tektonik tarihi, *Türk Petrol Jeol. Dern. Bül.*, **8**, 137-156.
- Yaltrak, C.**, 2002. Tectonic evolution of the Marmara Sea and its surroundings, *Mar. Geol.* **190**, 1/2, 493-530.
- Yaltrak, C., Alpar, B., and Yüce, H.**, 1998. Tectonic elements controlling the evolution of the Gulf of Saros (Northeastern Aegean Sea, Turkey), *Tectonophysics*, **300**, 227-248.
- Yaltrak, C., Sakıncı, M. and Oktay, F.Y.**, 2000. Westward propagation of North Anatolian Fault into the northern Aegean: Timing and kinematics. Comment, *Geology*, **28**, 187-89.
- Yılmaz, O.**, 1987. *Seismic Data Processing*, Society of Exploration Geophysicists.

- Yılmaz, Y., Genç S. C., Yigitbaş, E., Bozcu, M., and Yılmaz, K.,** 1995. Geological evolution of the late Mesozoic continental margin of Northwestern Anatolia, *Tectonophysics*, **243**, 155–171.
- Zhao, X., Zhao, W., Zheng, X., Rafailovich, M., H., and Sokolov, J.,** 1992. Configuration of grafted polystyrene chains in the melt: Temperature and concentration dependence, *Phys. Rev. Lett.*, **69**, 776 – 779.
- Zor, E., Özalaybey, S. and Gürbüz, C.,** 2006. The crustal structure of the Eastern Marmara Region (Turkey) by teleseismic receiver functions, *Geophys. J. Int.* **167**, 213–222.

APPENDICES

APPENDIX A : Location Map, Stack Sections and Interpreted Stack Sections For the Processed SEISMARMARA2001 Lines; Line 11c, Line 22b (the Tekirdağ Basin), Line 11b, Line 40a (the Central Basin), Line 11a, Line 43, and Line (the Çınarcık Basin).

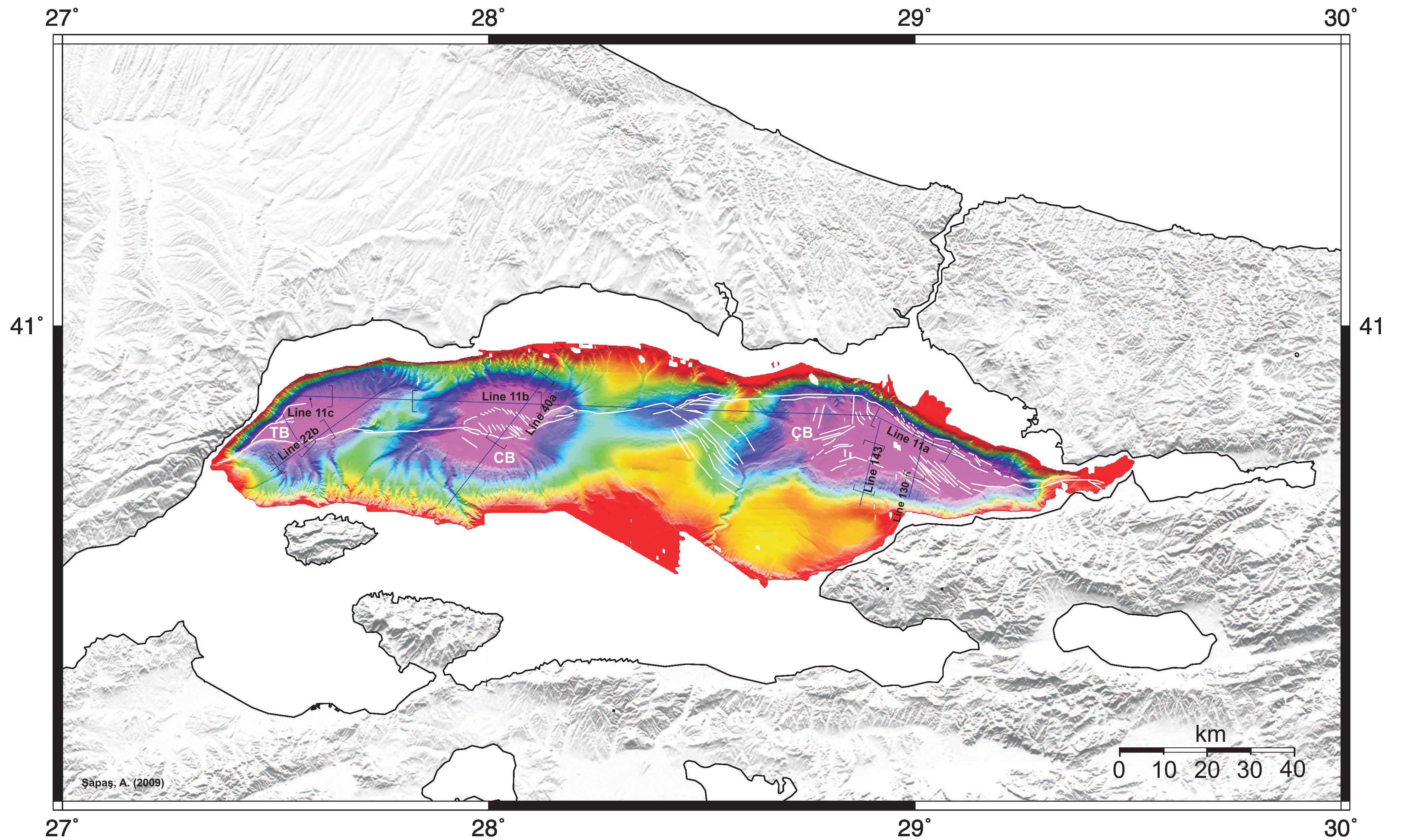


Figure A.1 :Location map for the processed SEISMARMARA 2001 lines.

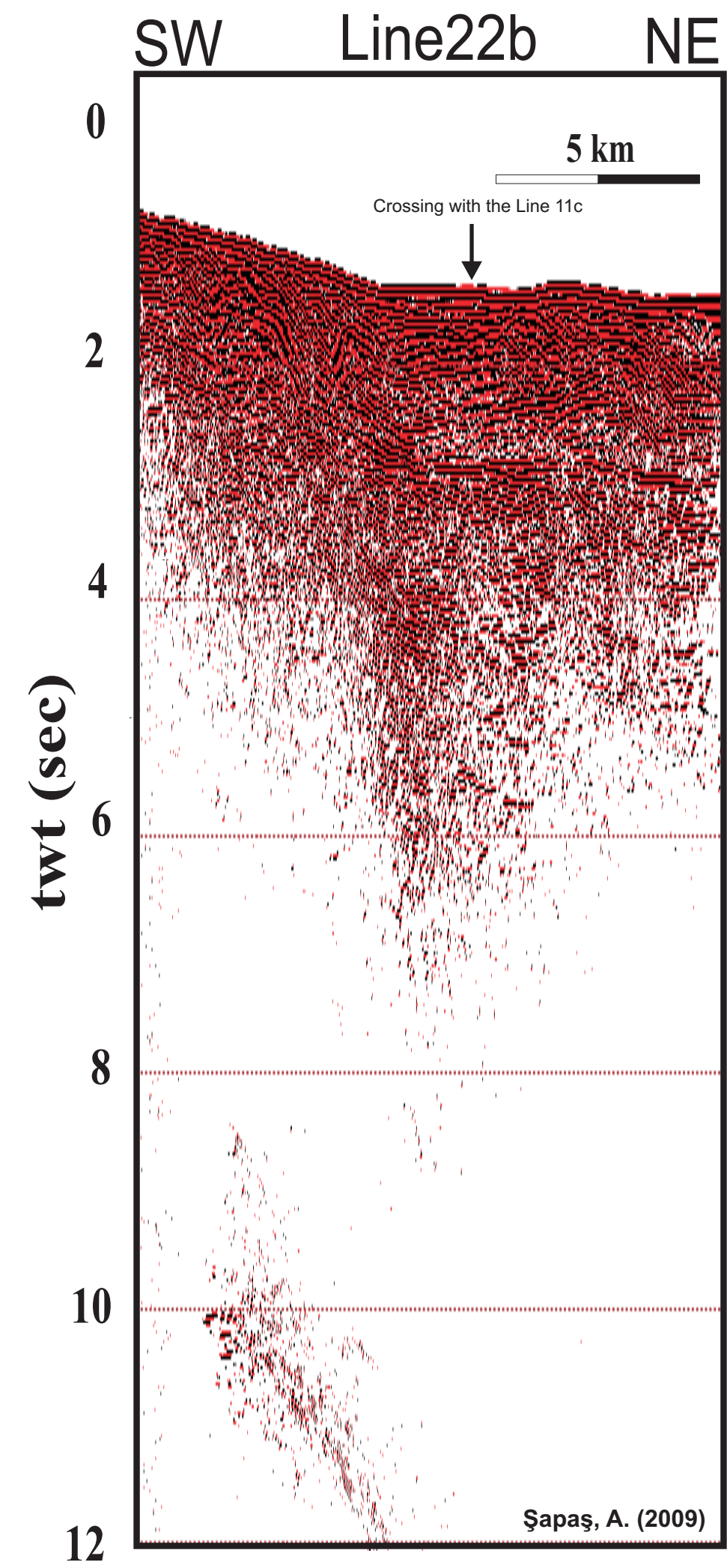
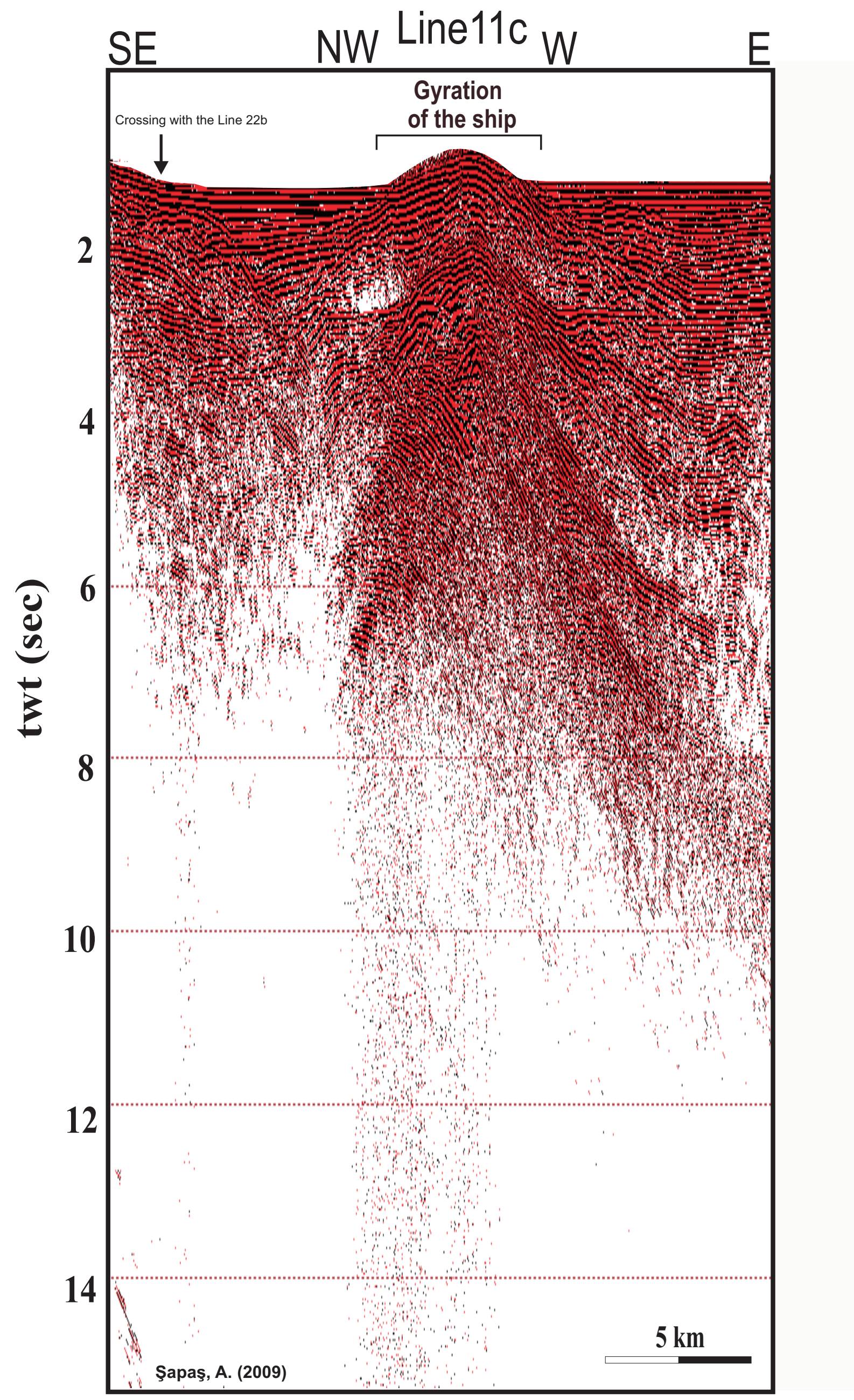


Figure A.2 : Tekirdağ Basin lines stack sections.

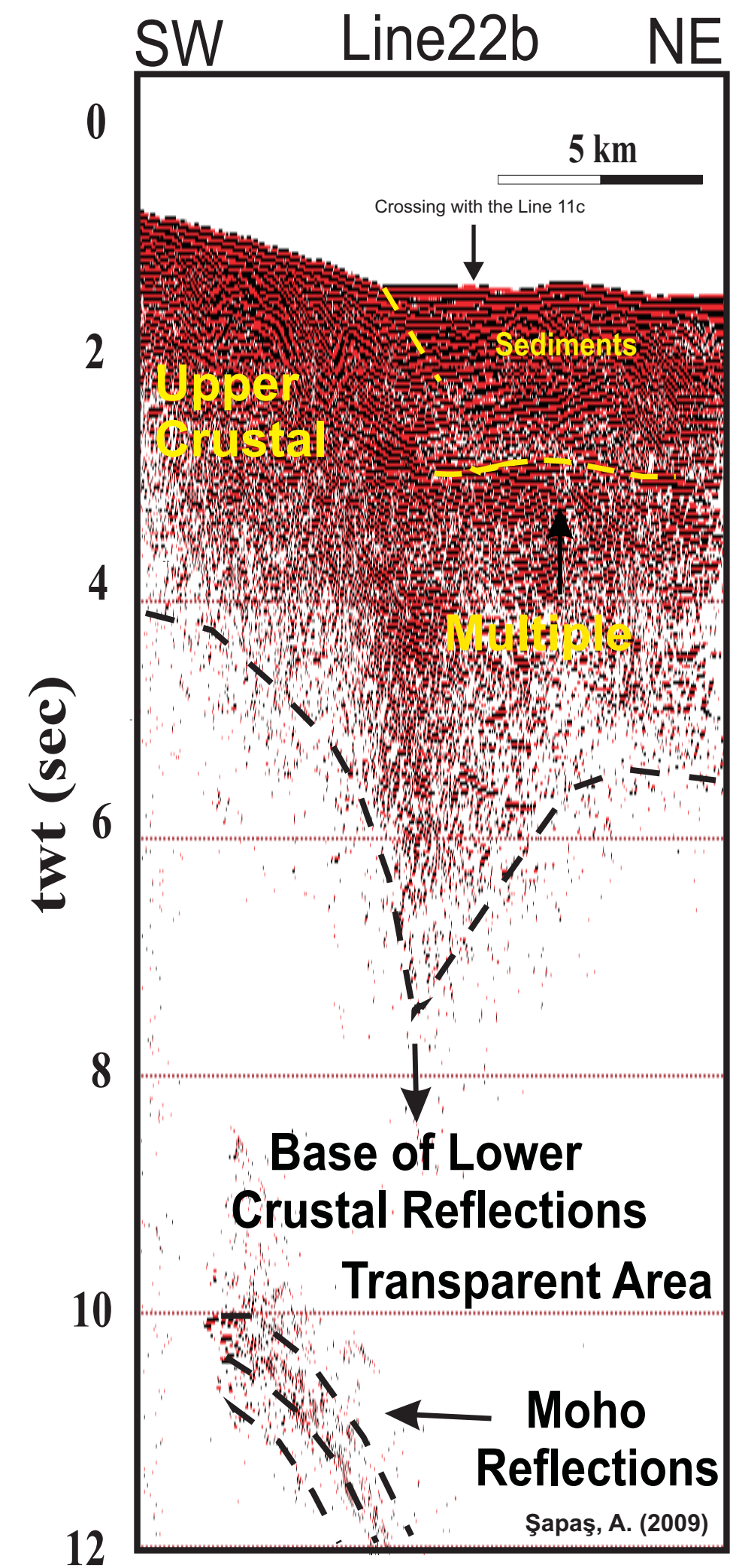
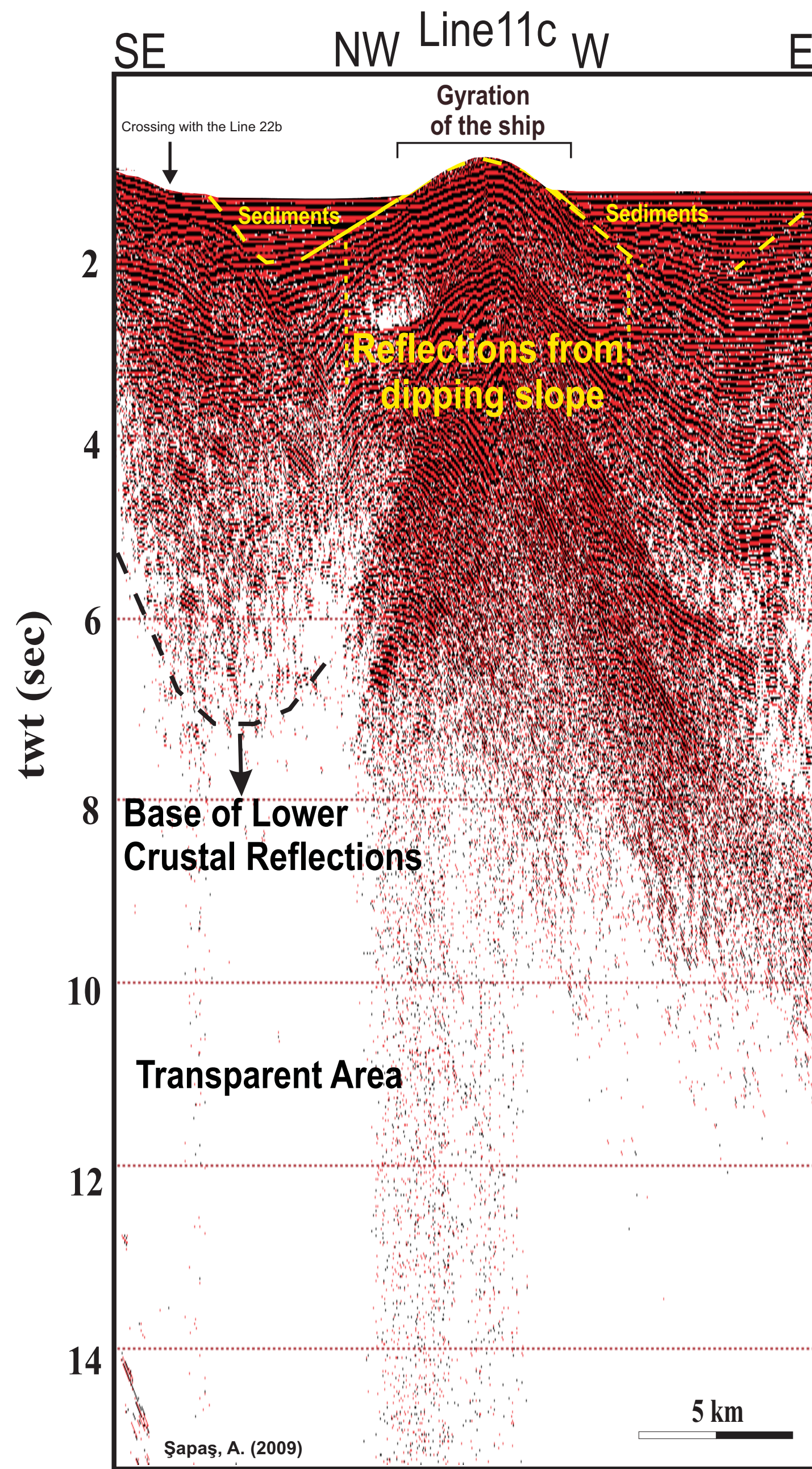


Figure A.3 : Tekirdağ Basin lines interpreted stack sections.

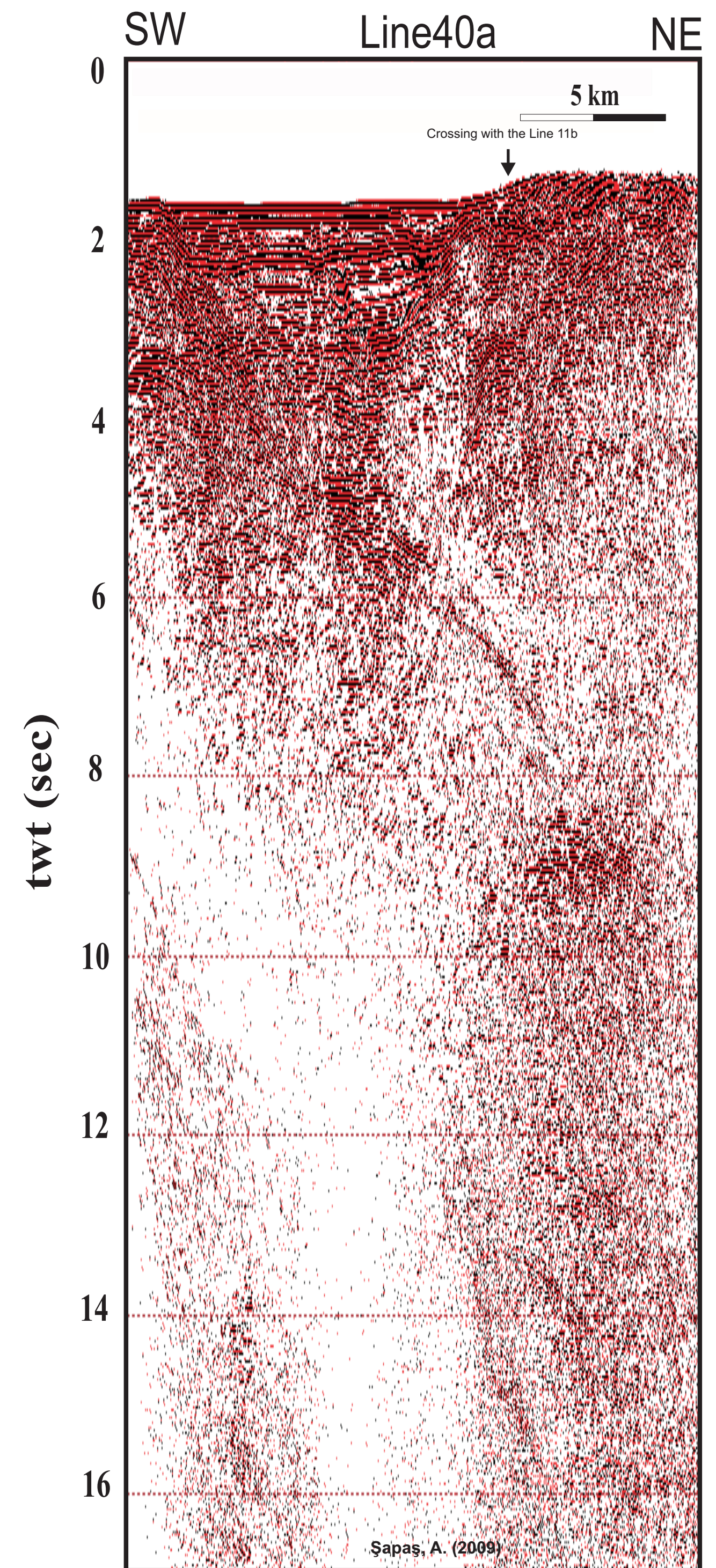
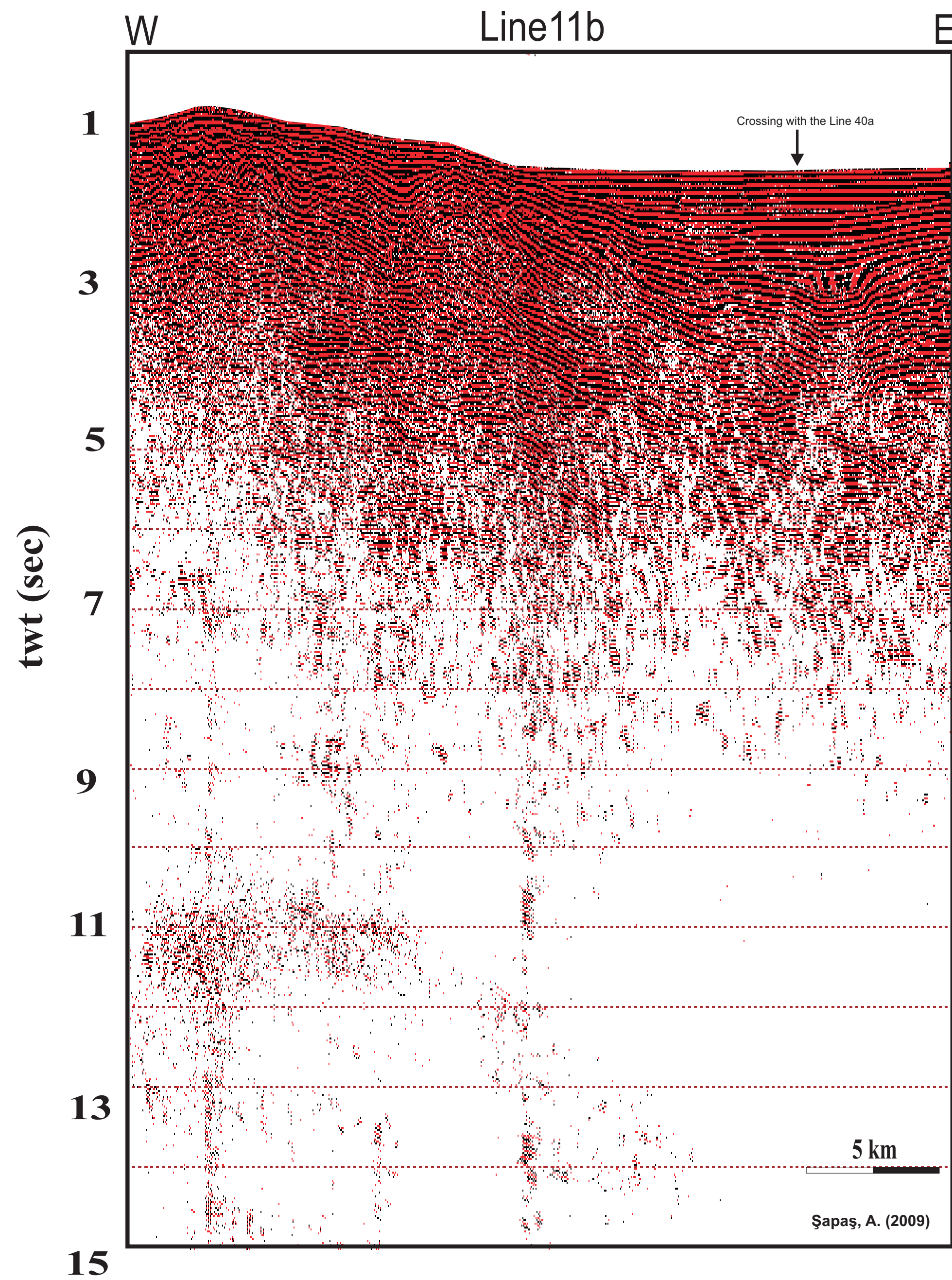


Figure A.4 : Central Basin lines stack sections.

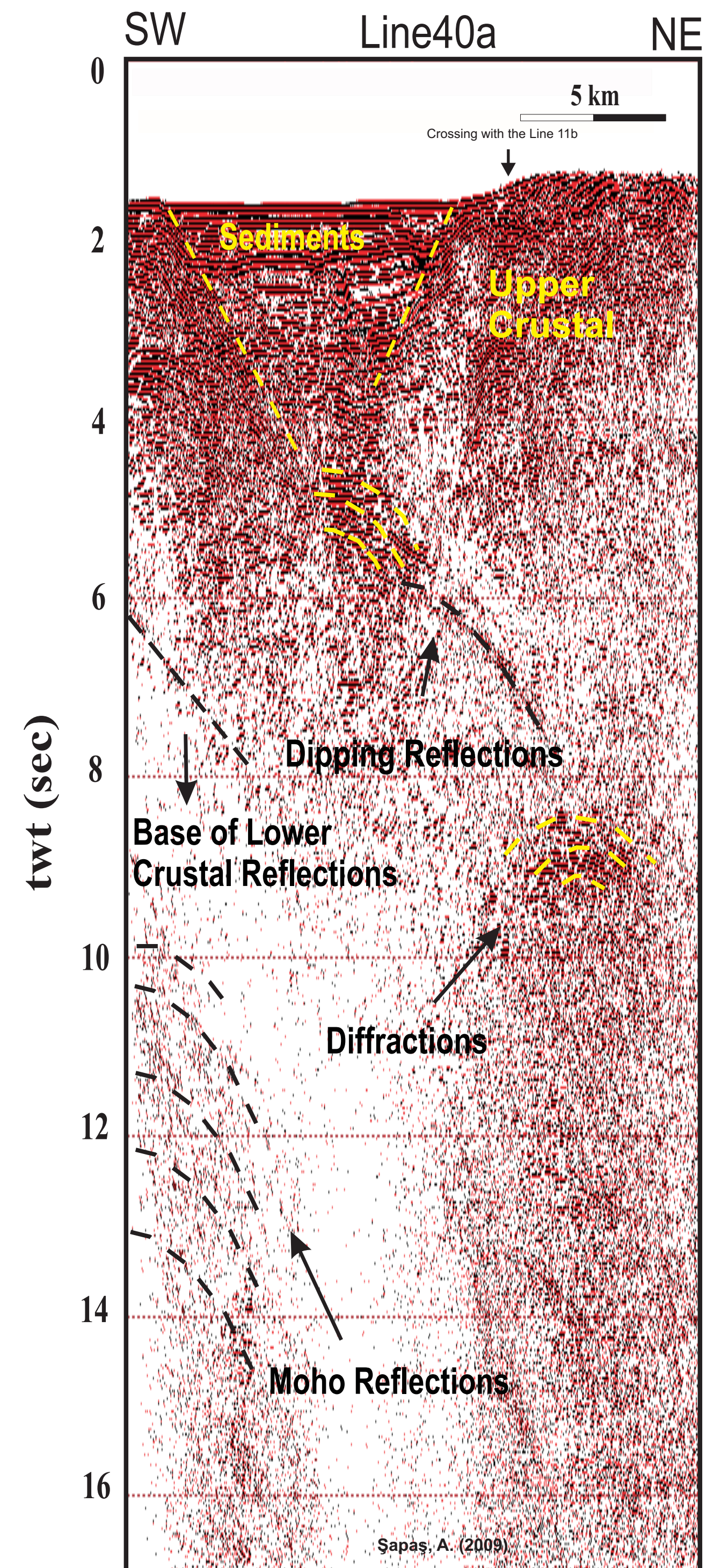
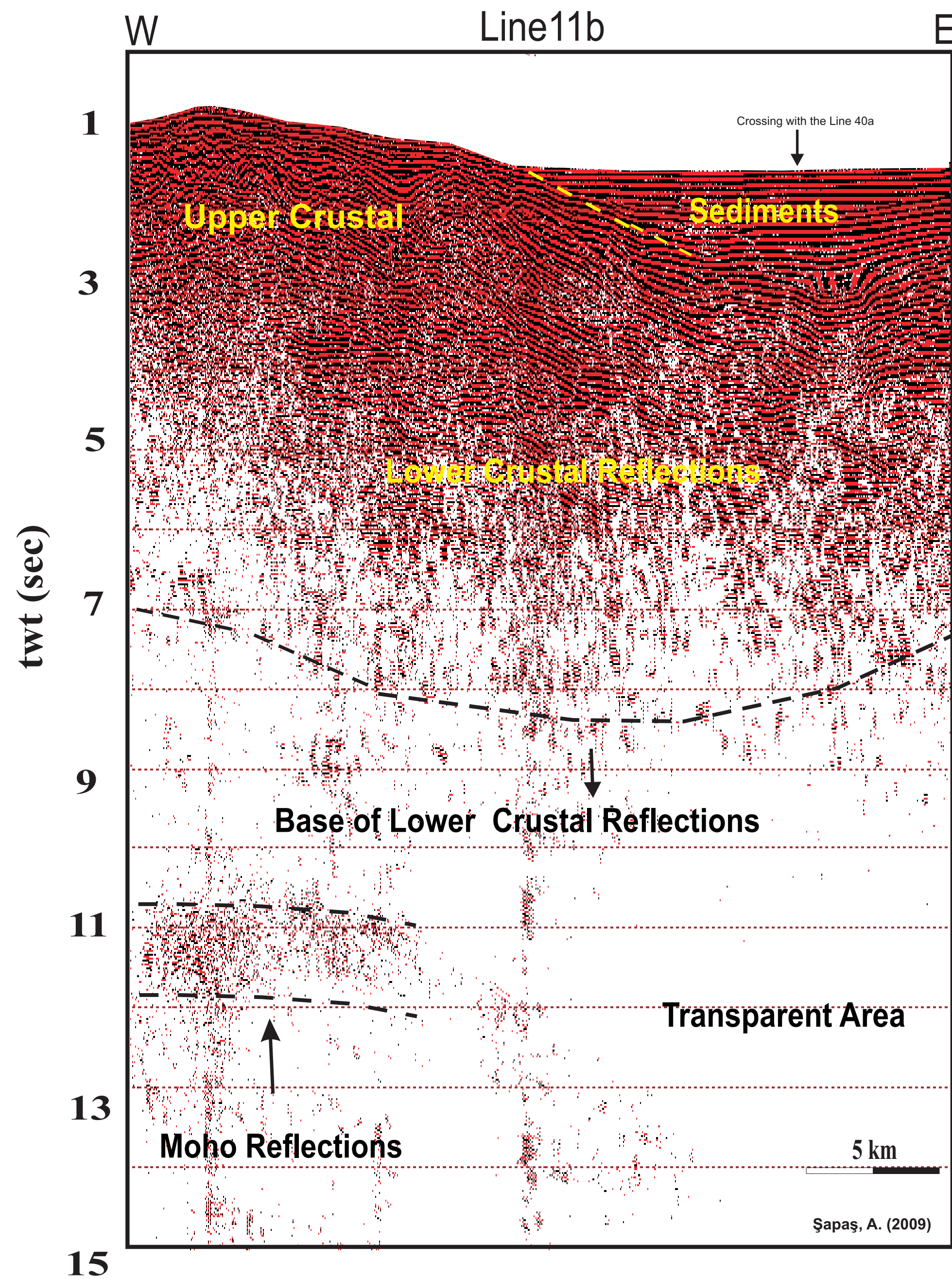


Figure A.5 : Central Basin lines interpreted stack sections.

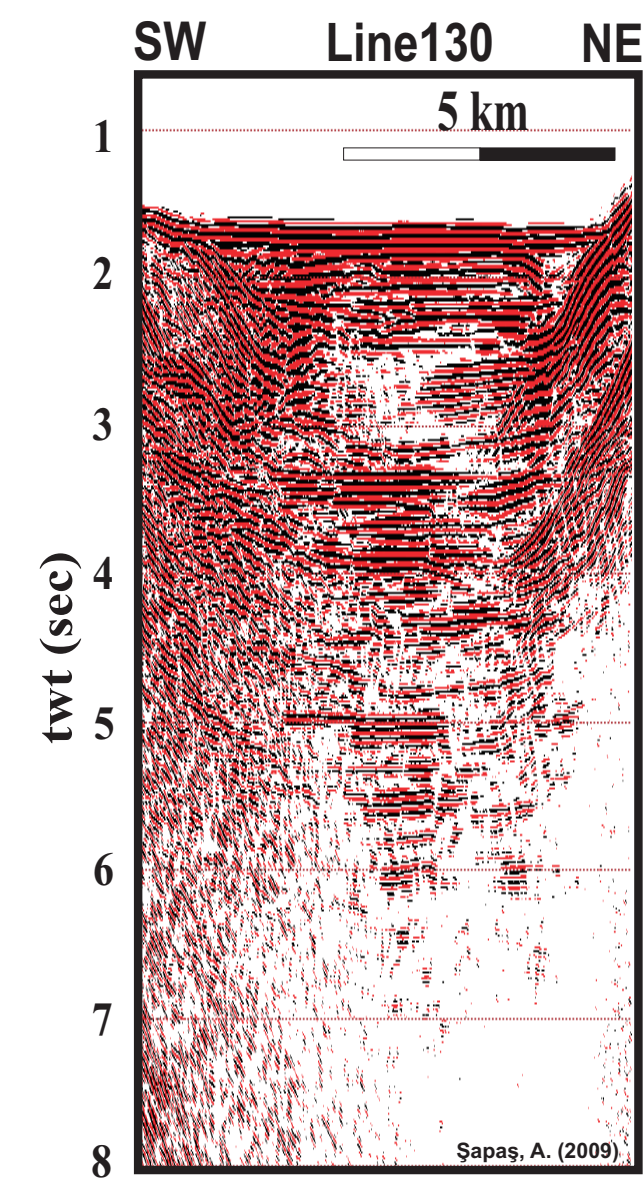
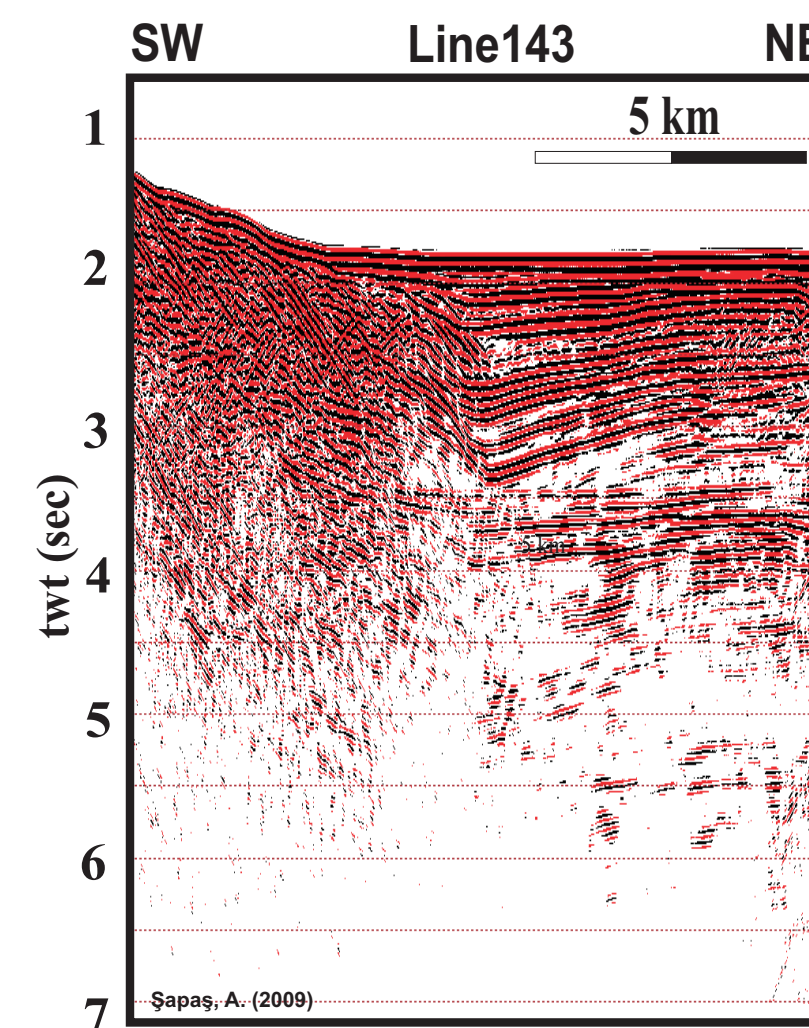
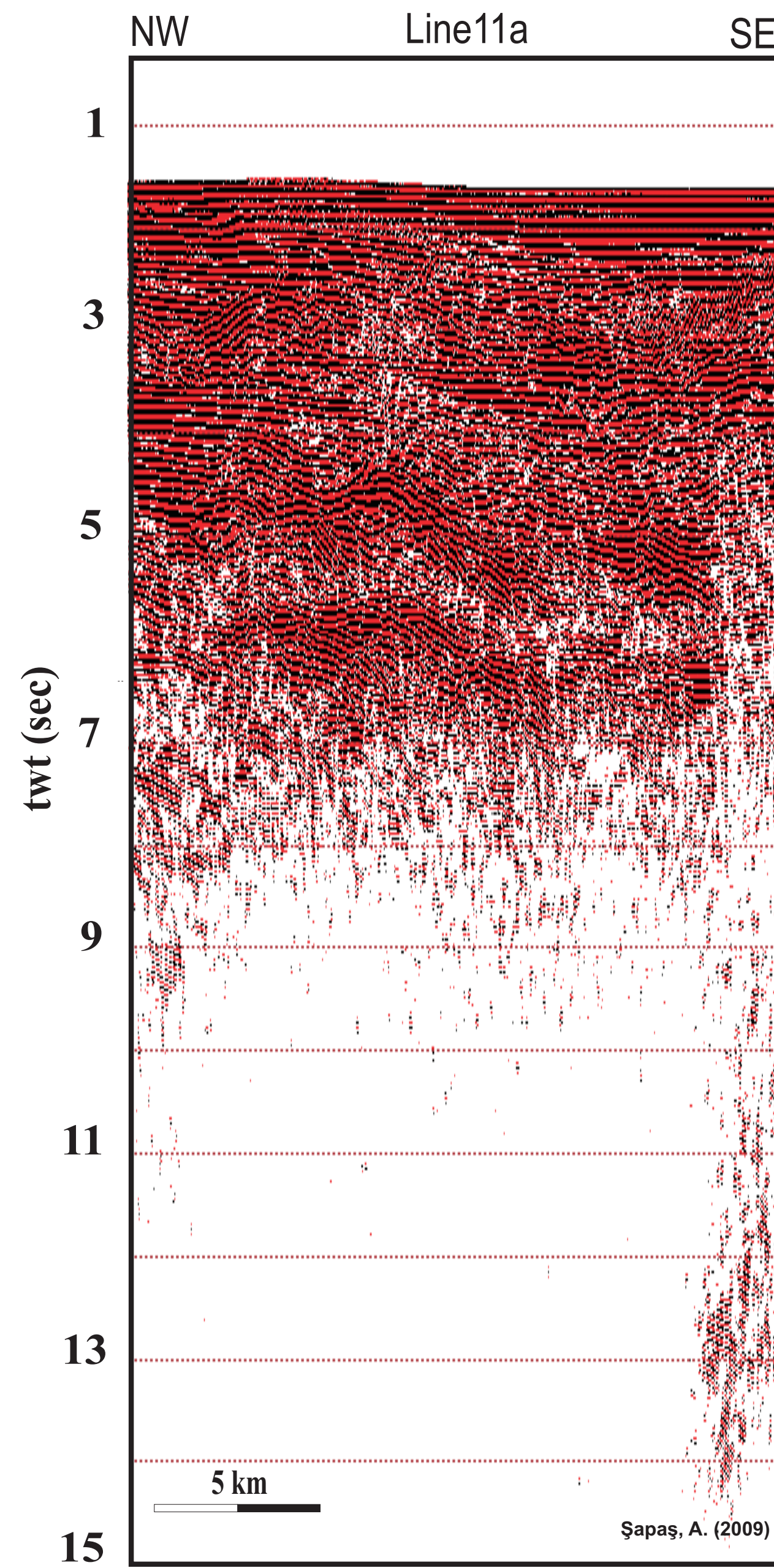


Figure A.6 : Çınarcık Basin lines stack sections.

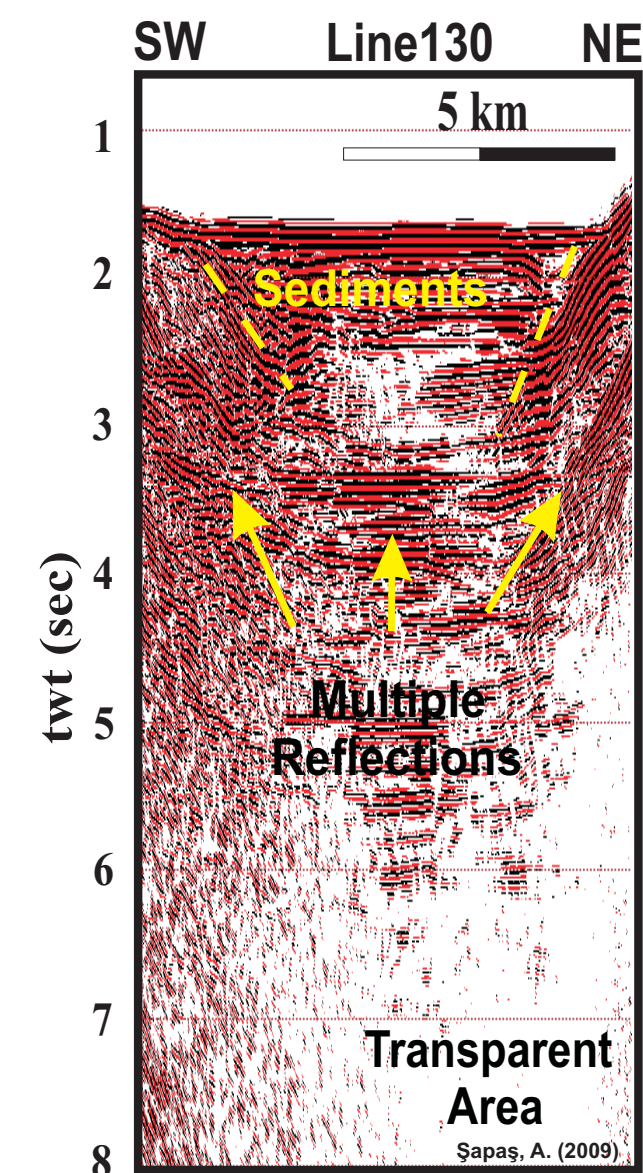
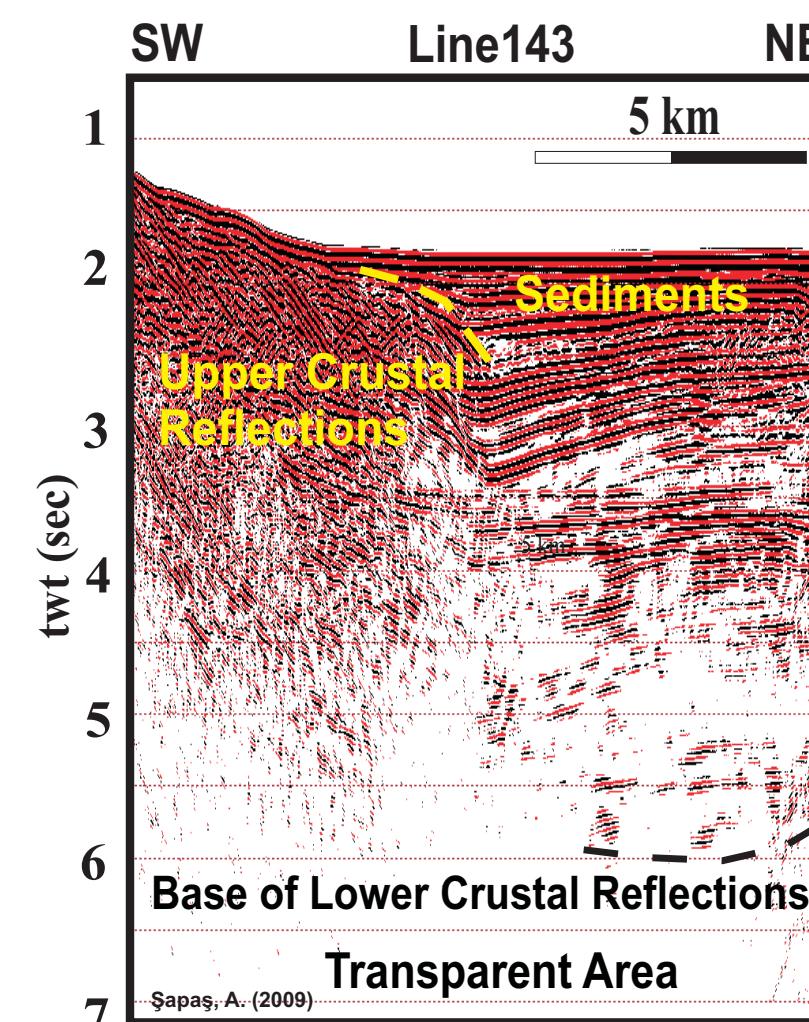
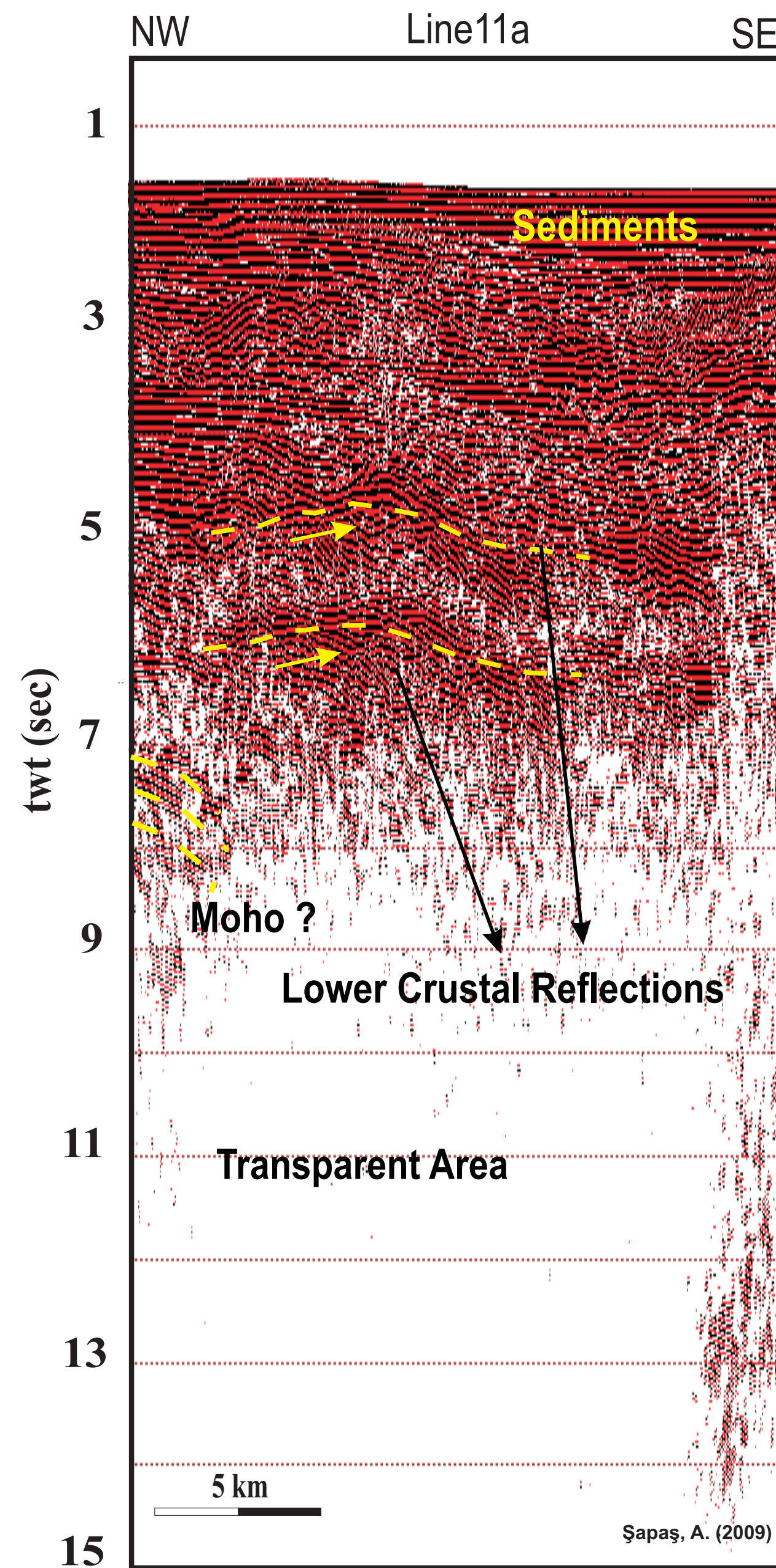


Figure A.7 : Çınarcık Basin lines interpreted stack sections.

APPENDIX B

Table B.1: List of studied earthquakes for SKS splitting analysis. (-) latitudes represent south direction, (-) longitudes represent west direction.

DATE	Lat (°)	Lon (°)	Depth (km)	Mag (Mw)	Region
1992/07/29	39.50	143.50	5.90	6.2	OFF EAST COAST OF HONSHU JAPAN
1996/06/17	-7.14	122.59	87.3	7.9	FLORES SEA
1996/11/02	-7.56	117.30	02.0	5.8	BALI SEA
1996/10/25	-17.38	-69.99	16.2	5.7	PERU-BOLIVIA BORDER REGION
1996/11/12	-14.99	-75.68	13.0	7.7	NEAR COAST OF PERU
1996/12/31	15.83	-92.97	19.5	6.4	MEXICO-GUATEMALA BORDER REGION
1996/07/06	21.97	142.83	41.0	6.2	MARIANA ISLAND REGION
1996/07/15	18.73	145.63	77.0	6.3	MARIANA ISLAND
1996/07/15	17.60	- 100.97	18.3	6.8	GUERRERO MEXICO
1996/07/20	13.86	12.67	10.1	5.9	MINDORO PHILIPPINE ISLAND
1996/09/21	-19.00	-67.53	24.3	5.7	CENTRAL BOLIVIA
1996/09/24	15.19	-61.44	47.0	5.7	LEEWARD ISLAND
1996/06/09	17.44	145.46	49.0	6.5	MARIANA ISLAND
1997/12/11	3.93	-75.79	78.0	6.3	COLOMBIA
1997/12/18	13.84	-88.74	82.0	6.0	EL SALVADOR
1997/09/02	3.85	-75.75	98.7	6.8	COLOMBIA
1997/07/10	-22.73	-70.89	33	5.9	NEAR COST OF NORTHERN CHILE
1997/10/05	-59.74	-29.20	74.0	6.3	SOUTH SANDWICH ISLAND REGION
1997/10/06	9.79	125.78	06.0	6.4	MINDANAO PHILIPPINE ISLAND
1997/10/28	-4.37	-76.68	12.0	7.2	NORTHERN PERU
1997/10/15	-30.93	-71.22	18.0	7.1	NEAR COAST OF CENTRAL CHILE
1997/11/09	13.85	-88.81	76.4	6.5	EL SALVADOR
1997/11/27	-13.74	-68.79	86.0	6.7	PERU – BOLIVIA BORDER REGION
1997/10/05	5.68	125.45	23.9	5.8	MINDANAO PHILIPPINE ISLAND
1997/11/15	43.81	145.02	61.0	6.1	HOKKAIDO JAPAN REGION

Table B.1 (Continued) : List of studied earthquakes for SKS splitting analysis. (-) latitudes represent south direction, (-) longitudes represent west direction.

DATE	Lat(°)	Lon(°)	Depth (km)	Mag(Mw)	Region
1997/12/22	-5.50	147.87	179.3	7.2	NEAR COAST OF NEW GUINEA PNG.
1997/01/23	-22.00	-65.72	276.2	7.1	SOUTHERN BOLIVIA
1997/02/19	4.56	-76.49	100.7	5.8	COLOMBIA
1997/03/23	30.98	-41.54	10.0	5.9	NORTHERN MID- ATLANTIC RIDGE
1998/04/03	-8.15	-74.24	165.0	6.6	PERU-BRASIL BORDER REGION
1998/05/23	8.14	123.73	658.0	6.0	MINDANAO PHILIPPINE ISLAND
1998/03/08	20.59	122.14	157.5	5.7	PHILIPPINE ISLAND REGION
1998/09/01	-58.2	-26.53	151.7	5.6	SOUTH SANDWICH ISLAND REGION
1998/09/28	-18.19	112.41	152	6.5	JAWA INDONESIA
1999/07/11	15.78	-88.33	10.0	6.7	HONDURAS
1999/10/05	-5.16	150.88	138.0	7.1	NEW BRITAIN REGION P.N.G
1999/04/05	-5.59	149.57	150.0	7.4	NEW BRITAIN REGION
1999/04/03	13.17	-87.63	38.40	6.0	HONDURAS
2000/01/20	56.62	-161.87	220.80	5.8	ALASKA PENINSULA
2000/04/23	-28.31	-62.99	608.5	7.0	SANTIAGO DEL ESTERO PROV. ARGENTINA
2000/04/29	-6.41	-77.06	124.6	5.7	NORTHERN PERU
2000/01/01	-60.72	153.67	10	6.0	WEST OF MACQUARIE ISLAND
2000/08/06	28.86	139.56	394.8	7.3	BONIN ISLANDS REGIONS
2000/12/12	5.77	-82.53	33.0	6.0	SOUTH PANAMA
2000/08/31	5.07	123.21	588.3	5.7	MINDANAO PHILIPPINE ISLANDS
2000/10/04	11.12	-62.56	110.3	6.1	WINWARD ISLANDS
2000/10/10	-6.28	154.63	100.0	5.6	SOLOMON ISLANDS
2000/10/14	23.56	141.83	137.5	5.5	VOLCANO ISLANDS REGION
2000/10/17	15.52	-92.07	100.5	5.8	MEXICO GUATEMALA BORDER REGION
2000/06/21	14.11	144.96	112.2	5.9	MARIANA ISLAND

Table B.1 (Continued) : List of studied earthquakes for SKS splitting analysis. (-) latitudes represent south direction, (-) longitudes represent west direction.

DATE	Lat(°)	Lon(°)	Depth (km)	Mag(Mw)	Region
2000/06/27	-7.10	125.91	496.1	5.8	BANDA SEA
2000/06/29	13.03	144.54	52.4	5.9	MARIANA ISLAND
2000/07/15	-7.03	128.93	217.7	5.9	BANDA SEA
2000/08/20	7.43	12.55	174.3	5.6	MINDANAO PHILIPPINE ISLANDS
2000/09/21	-55.71	110.62	560.9	5.5	JAVA SEA
2000/09/17	-5.36	146.77	228.0	5.9	EASTERN NEW GUINEA REGION
2000/10/10	-6.28	154.63	100.0	5.6	SOLOMON ISLANDS
2000/10/14	23.56	141.83	137.5	5.5	VOLCANO ISLANDS REGION
2000/10/17	15.52	-92.07	180.5	5.8	MEXICO GUATEMALA BORDER REGION
2000/04/03	0.27	122.05	187.0	5.4	MINAHASSA PENINSULA SULAVESSI
2000/04/23	-28.38	-62.94	609.8	6.1	SANTIAGO DEL ESTERO PROV. ARGENTINA
2000/04/23	-5.37	151.47	105.2	5.6	NEW BRITAIN REGION P.N.G.
2000/05/12	-23.55	-66.45	225.0	7.2	JUJUY PROVINCE ARGENTINA
2000/06/09	30.39	137.73	485.3	6.2	SOUTH OF HONSHU JAPAN
2000/06/14	-24.03	-66.75	196.5	5.7	SALTA PROVINCE ARGENTINA
2000/06/16	-33.38	-70.09	120.2	6.4	CHILE ARGENTINA BORDER REGION
2000/06/19	14.01	120.53	115.0	5.6	LUZON PHILIPPINE ISLAND
2000/07/08	-7.02	123.36	684.5	6.5	BANDA SEA
2000/01/28	-7.49	122.68	574.9	5.5	FLORES SEA
2000/02/15	17.68	145.40	521.5	5.8	MARIANA ISLAND
2000/02/26	9.41	-78.53	65.0	6.1	PANAMA
2000/03/03	7.32	128.49	141.9	6.3	BANDA SEA
2000/03/28	22.34	143.73	126.5	7.6	VOLCANO ISLAND REGION
2001/01/15	13.08	-88.58	74.6	5.8	EL SALVADOR
2001/02/24	-20.18	-68.69	115.9	5.8	CHILE BOLIVIA BORDER REGION

Table B.1 (Continued) : List of studied earthquakes for SKS splitting analysis. (-) latitudes represent south direction, (-) longitudes represent west direction.

DATE	Lat(°)	Lon(°)	Depth (km)	Mag(Mw)	Region
2001/02/16	-7.16	177.49	521.0	6.1	BALI SEA
2001/12/02	30.40	141.09	123.8	6.5	EASTERN HONSHU JAPAN
2001/12/02	-12.74	166.66	100.5	6.0	SANTA CRUZ ISLANDS
2001/11/05	-17.29	-179.25	564.1	6.3	FIJI ISLANDS REGION
2001/12/09	-0.00	122.87	156.3	6.0	MINAHASSA PENINSULA SULAWESI
2001/03/11	-25.37	-177.97	231.0	5.8	SOUTH OF FIJI ISLANDS
2001/03/14	0.45	121.89	109.4	5.9	MINAHASSA PENINSULA SULAWESI
2001/10/22	-20.91	-179.13	622.5	5.6	FIJI ISLANDS REGION
2001/06/16	-15.01	-173.39	33.0	5.7	TONGO ISLANDS
2001/12/28	-8.36	-74.22	160.6	6.0	PERU BRAZIL BORDER REGION
2001/06/29	-19.55	-66.25	273.9	6.1	SOUTHERN BOLIVIA
2001/06/19	-22.74	-67.88	146.6	5.9	CHILE BOLVIA BORDER REGION
2001/07/03	21.64	142.98	290.0	6.5	MARIANA ISLANDS REGION
2002/01/30	18.23	-95.69	105.4	5.5	VERACRUZ MEXICO
2002/01/16	15.50	-93.13	80.20	6.4	NEAR COAST OF CHIAPAS MEXICO
2002/01/31	-12.73	169.48	659.8	5.7	SANTA CRUZ ISLAND REGION
2002/07/31	8.12	-82.58	33.0	5.9	PANAMA COSTA RICA BORDER REGION
2002/08/02	29.32	139.04	424.5	6.2	SOUTH OF HONSHU JAPAN
2002/08/02	29.28	138.97	426.1	6.3	JAPAN
2002/09/24	-31.41	-68.94	117.3	6.4	SAN JUAN PROVINCE ARGENTINA
2002/09/29	-6.27	146.38	118.6	5.4	EASTERN NEW GUINEA REGION
2002/10/03	-7.42	11.77	315.2	6.2	BALI SEA
2002/10/12	-8.30	-71.74	534.3	6.9	WESTERN BRAZIL
2002/10/12	-8.26	-71.53	535.9	6.8	WESTERN BRAZIL

Table B.1 (Continued) : List of studied earthquakes for SKS splitting analysis. (-) latitudes represent south direction, (-) longitudes represent west direction.

DATE	Lat(°)	Lon(°)	Depth (km)	Mag(Mw)	Region
2002/11/12	-56.5	-27.46	117.0	6.1	SOUTH SANDWICH ISLANDS REGION
2002/11/29	-28.82	-63.01	595.2	5.3	SANTIAGO DEL ESTERO PROV. ARGENTINA
2002/12/21	4.97	123.12	596.3	5.4	CELEBES SEA
2003/01/07	-33.59	-69.76	110.7	6.0	CHILE ARGENTINA BORDER REGION
2003/02/01	16.59	-92.78	205.2	5.5	CHIAPAS MEXICO
2003/04/27	-8.14	-71.51	545.7	5.9	WESTERN BRAZIL
2003/05/16	18.71	-100.93	116.8	4.9	GUERRERO MEXICO
2003/05/18	-31.28	-68.66	115.4	5.5	SAN JUAN PROVINCE ARGENTINA
2003/05/24	-14.52	-71.44	142.6	5.4	CENTRAL PERU
2003/05/26	6.80	123.71	559.7	6.8	MINDANAO PHILIPPINE ISLANDS
2003/05/27	15.24	-91.55	200.0	4.7	MEXICO GUATEMALA REGION
2003/06/12	-5.99	154.76	184.7	6.2	SOLOMON ISLANDS
2003/06/20	-7.5	-71.62	553.0	6.7	WESTERN BRAZIL
2003/06/21	-7.58	127.78	165.5	5.9	BANDA SEA
2003/06/24	18.33	145.4	400.0	4.9	MARIANA ISLANDS
2003/07/15	-2.6	68.38	10.0	7.6	CARLSBERG RIDGE
2003/07/21	-5.51	148.96	190.1	6.3	NEW BRITAIN REGION
2003/07/21	18.88	-100.74	133.3	4.9	MEXICO
2003/07/08	-6.97	-71.80	517.5	5.2	WESTERN BRAZIL
2003/07/08	17.52	-94.51	139.1	4.6	CHIAPAS MEXICO
2003/08/04	-60.53	-43.41	10.0	7.5	SCOTIA SEA
2003/08/16	-4.59	151.77	156.6	5.3	NEW BRITAIN REGION
2003/08/21	-45.18	167.12	33.0	7.0	SOUTH ISLAND NEW ZEALAND
2003/08/25	14.07	-91.05	116.9	6.0	GUATEMALA
2003/08/28	-7.28	126.08	412.0	5.6	BANDA SEA
2003/09/11	15.26	-91.66	179.7	4.6	MEXICO GUATEMALA BORDER REGION

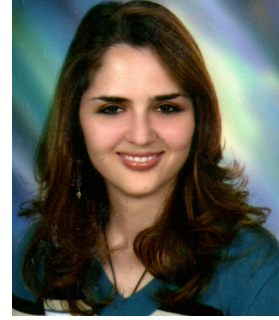
Table B.1 (Continued) : List of studied earthquakes for SKS splitting analysis. (-) latitudes represent south direction, (-) longitudes represent west direction.

DATE	Lat(°)	Lon(°)	Depth (km)	Mag(Mw)	Region
2003/09/17	-21.41	-68.05	127.3	6.1	CHILE BOLIVIA BORDER REGION
2003/11/11	22.32	143.25	101.0	5.9	VOLCANO ISLANDS REGION
2003/12/25	18.41	-68.67	141.1	5.0	MONA PASSAGE
2003/12/28	-9.71	-71.17	562.8	4.9	PERU BRAZIL BORDER REGION
2004/01/13	-22.65	-63.41	532.7	5.1	SALTA PROVINCE ARGENTINA
2004/01/29	6.31	126.87	222.6	5.7	MINDANAO PHILIPPINE ISLANDS
2004/02/04	-26.05	-63.31	560.3	4.9	SANTIAGO DEL ESTERO PROV. ARGENTINA
2004/02/06	18.51	-102.45	100.8	4.8	MICHOACAN MEXICO
2004/04/14	71.09	-7.52	10.0	6.0	JAN MAYEN ISLAND REGION
2004/02/21	-58.43	-14.96	10.0	6.6	SOUTHWESTERN ATLANTIC OCEAN
2004/02/24	35.14	-4.0	0.00	6.4	STRAIT OF GIBRALTAR
2004/02/26	-18.17	66.42	10.0	6.3	MAURITIUS- REUNION REGION
2004/06/10	55.68	160.0	188.6	6.9	KAMCHATKA
2004/06/28	54.80	-134.25	20.0	6.0	QUEEN CHARLOTTE ISLANDS REGION
2004/06/29	-51.60	139.62	10.0	6.4	SOUTH OF AUSTRALIA
2004/07/01	-50.6	162.88	10.0	6.2	AUCKLAND ISLANDS REGION
2004/07/19	49.68	-126.94	22.0	6.3	VANCOUVER ISLANDS REGION
2004/08/07	51.75	-166.31	8.0	6.0	SOUTH OF ALEUTION ISLANDS
2004/09/28	-52.52	28.02	10.0	6.4	SOUTH OF AFRICA
2004/11/02	49.28	-128.77	10.0	6.6	VANCOUVER ISLANDS REGION
2004/12/23	-49.31	161.35	10.0	8.1	NORTH OF MACQUARIE ISLAND

Table B.1 (Continued) : List of studied earthquakes for SKS splitting analysis. (-) latitudes represent south direction, (-) longitudes represent west direction.

DATE	Lat(°)	Lon(°)	Depth (km)	Mag(Mw)	Region
2005/02/16	-35.70	-16.34	10.0	6.4	SOUTHERN MID-ATLANTIC RIDGE
2005/02/16	-36.32	-16.56	10.0	6.6	SOUTHERN MID-ATLANTIC RIDGE
2005/03/06	84.94	99.15	10.0	6.3	NORTH OF SEVERNAYA ZEMLYA
2005/03/28	2.09	97.11	30.0	8.7	NORTHERN SUMATERA INDENOSIA
2005/05/18	-56.41	-26.86	102.2	6.0	SOUTH SANDWICH ISLANDS REGOIN
2005/07/04	-42.28	42.37	10.0	6.3	PRINCE EDWARD ISLANDS REGION
2005/07/25	71.08	-7.45	10.0	5.5	JAN MAYEN ISLANDS REGION
2005/10/29	-45.27	96.96	10.0	6.5	SOUTH INDIAN RIDGE
2005/12/05	-6.22	29.83	22.0	6.8	LAKE TANGANYIKA REGION
2006/01/02	-60.93	-21.58	10.0	7.4	SOUTHWESTERN ATLANTIC OCEAN
2006/07/30	72.17	0.84	10.0	4.9	NORWEGIAN SEA
2006/08/20	-61.03	-34.37	10.0	7.0	SCOTIA SEA
2006/09/06	-55.37	-28.98	10.0	6.8	SOUTH SANDWICH ISLANDS REGION

CURRICULUM VITA



Candidate's full name: Aslıhan Şapaş

Place and date of birth: İstanbul, 1977

Permanent Address: İ.T.U.

Universities and Colleges attended:

2001-..... – Ph.D., at İ.T.U. Faculty of Mines, Department of Geophysical Engineering

1999-2001—M.Sc., at İ.T.U. Faculty of Mines, Department of Geophysical Engineering

1995-1999-- Bc.S., at İ.T.U. Faculty of Mines, Department of Geophysical Engineering

1991-1995 -- Maçka Anatolian Technical High School, Computer Department

Publications:

- **Şapaş, A.** and Boztepe-Güney, A., 2009. SKS splitting in the Isparta Angle, the Southwestern Turkey: Anisotropic Complexity in Mantle, *Journal of Earth System Science*, **118**, 71-80.
- **Şapaş, A.**, and Boztepe-Güney, A., 2006. The analysis of SKS splitting in Isparta, *17th International Geophysical Congress*, 14-17 November 2006, Ankara, Turkey.
- **Şapaş, A.**, Boztepe-Güney, A., 2005, The analysis of SKS splitting in Western Turkey, *International Earth Sciences Colloquium on the Aegean Regions*, Abstracts Book , p.262., Dokuz Eylul University, 4-7 October 2005, İzmir, Turkey.
- **Şapaş, A.**, and Boztepe Güney, A., 2004. The analysis of SKS splitting in Ankara, Central Turkey, *16th International Geophysical Congress*, 7-10 December 2004, Ankara, Turkey.
- Demirbağ, E, Düşünür, D., **Şapaş, A.** and Sarıkavak, K. 2003. Investigation of the Active Tectonism in the Central Marmara Basin by Geophysical

Means. *International Workshop on the North Anatolian, East Anatolian and Dead Sea Fault Systems: Recent Progress in Tectonics and Paleoseismology and Field Training Course in Paleoseismology*, p.32, Middle East Technical University (METU), 31 August - 12 September 2003, Ankara, Turkey.

- **Şapaş, A.**, Yolsal, S. and Boztepe Güney, A. , 2003. Investigation of SKS Splitting in the Upper Mantle Beneath the Isparta Region. *International Workshop on the North Anatolian, East Anatolian and Dead Sea Fault Systems: Recent Progress in Tectonics and Paleoseismology and Field Training Course in Paleoseismology*, p.161, Middle East Technical University (METU), 31 August - 12 September 2003, Ankara, Turkey.